

Important Notice

This copy may be used only for the purposes of research and private study, and any use of the copy for a purpose other than research or private study may require the authorization of the copyright owner of the work in question. Responsibility regarding questions of copyright that may arise in the use of this copy is assumed by the recipient.

THE UNIVERSITY OF CALGARY

Seismic Polarization Filtering:
Noise Reduction and Off-Line Imaging

by

Ye Zheng

A THESIS

SUBMITTED TO THE FACULTY OF GRADUATE STUDIES
IN PARTIAL FULFILMENT OF THE REQUIREMENTS FOR THE
DEGREE OF MASTER OF SCIENCE

DEPARTMENT OF GEOLOGY AND GEOPHYSICS

CALGARY, ALBERTA

SEPTEMBER, 1995

©Ye Zheng 1995

THE UNIVERSITY OF CALGARY
FACULTY OF GRADUATE STUDIES

The undersigned certify that they have read, and recommend to the Faculty of Graduate Studies for acceptance, a thesis entitled "Seismic Polarization Filtering: Noise Reduction and Off-Line Imaging" submitted by Ye Zheng in partial fulfilment of the requirements for the degree of Master of Science.



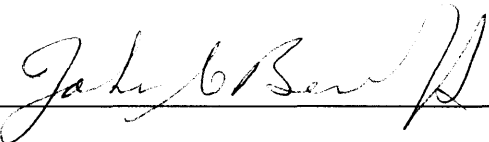
Supervisor, Dr. R.R. Stewart

Department of Geology and Geophysics



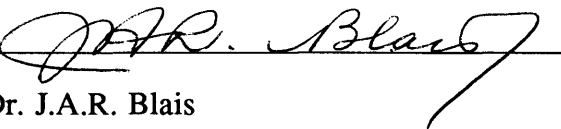
Dr. D.C. Lawton

Department of Geology and Geophysics



Dr. J.C. Bancroft

Department of Geology and Geophysics



Dr. J.A.R. Blais

Department of Geomatics Engineering

September 21, 1995

Date

ABSTRACT

The polarization direction of a P-wave is generally in the propagation direction of the seismic wave. We can distinguish the propagation direction by measuring the polarization direction. In this thesis, the noise effect on polarization direction is studied. Computer code for the polarization filter was developed. Numerical and physical modeling data were used to separate in-line and off-line energy by the polarization filter. The results indicate that it is possible to build an off-line image from three-component seismic data, if the data have a reasonable signal-to-noise (S/N) ratio. If S/N ratio is too low, some techniques like common-mid-point (CMP) stacking can be used to enhance signal before polarization filtering. The polarization filter is applied to the field data from Rumsey area of central Alberta to reject the off-line energy and enhance in-line energy.

ACKNOWLEDGEMENTS

I would like to express my special thanks to Dr. Robert R. Stewart for his many positive contributions, helpful discussion and supervision during the past four years. I also want to thank all the CREWES staff for computer software and hardware supporting and physical modeling experiment. Thanks to Shaowu Wang for his assistance with physical modeling and other help. Thanks also to Gulf Canada Resources Ltd. for providing the Rumsey seismic data and associated geological information. I am grateful to Veritas Seismic Ltd. for allowing use of its software resources and to Mr. Lee H. Hunt for proof reading.

Finally I want to thank the CREWES Project of The University of Calgary for giving me the chance to study in this area and for providing much appreciated financial support.

Table of Contents

Approval Page.....	ii
Abstract.....	iii
Acknowledgements.....	iv
Table of Contents.....	v
List of figures.....	vii
List of tables.....	x

Chapter 1

Introduction	1
1.1 Polarization of seismic waves	1
1.2 Brief review of polarization processing	1
1.3 Objectives of this thesis	3

Chapter 2

Polarization filtering	5
2.1 Introduction.....	5
2.2 Polarization ellipse and covariance matrix	6
2.3 Flinn's method	9
2.4 Montalbetti and Kanasewich's method	10
2.5 Some examples of synthetic data	11
2.6 Direct least squares (DLS) method	15
2.7 Application of polarization filter to field data with ground roll	18

Chapter 3

The effect of noise on polarization direction	24
-----------------------------------------------------	----

3.1 Introduction	24
3.2 Direction perturbation of noise	24
3.3 Limitation of single station polarization processing	29
Chapter 4	
Directional filtering	36
4.1 Introduction	36
4.2 The method	36
4.3 Application to a simple synthetic example	40
Chapter 5	
Off-line imaging	58
5.1 Introduction	58
5.2 Synthetic modeling data	59
5.3 Physical modeling data	62
5.4 Field data of Rumsey area	64
5.5 Polarization processing procedures	66
Chapter 6	
Conclusions	91
Chapter 7	
Future work	93
References	97

LIST OF FIGURES

2.1 Relationship between directions of eigenvector and the vector of displacement	12
2.2 Polarization filter test for removing random noise	13
2.3 Bandpass filter test for removing random noise	13
2.4 Polarization filter test for removing circularly polarized noise with the same frequency of the signal	14
2.5 Bandpass filter test for removing circularly polarized noise with the same frequency of the signal	14
2.6 A shot record (vertical component) for testing ground roll reduction	20
2.7 A shot record (radial component) for testing ground roll reduction	21
2.8 Polarization filtered shot record (vertical component)	22
2.9 Polarization filtered shot record (radial component)	23
3.1 Projection of data to the coordinate correspondent to the axes of the ellipse of the particle motion trajectory	25
3.2 The effects of signal-to-noise ratio on the polarization direction	30
3.3 The effects of circularly polarized noise on the polarization direction of a rectilinearly polarized signal	31
3.4 The change of polarization direction caused by a rectilinear noise(1)	32
3.5 The change of polarization direction caused by a rectilinear noise(2)	33
3.6 The change of polarization direction caused by a rectilinear noise(3)	34
3.7 The change of polarization direction caused by a circular noise	35
4.1 The diagram to illustrate stacking	37

4.2 A fault model for numerical modeling	40
4.3 The geometry of the numerical modeling	41
4.4 The diagram for calculating the distance from the fault to the line	42
4.5 The definition of wave direction	43
4.6 The vertical component of a shot record of the synthetic data	45
4.7 The transverse component of a shot record of the synthetic data	45
4.8 The stacked section of the vertical component of the synthetic data	46
4.9 The stacked section of the transverse component of the synthetic data	46
4.10 The hodogram of the reflection from the fault plane (1)	47
4.11 The hodogram of the reflection from the flat layer (1)	47
4.12 The hodogram of the reflection from the fault plane (2)	48
4.13 The hodogram of the reflection from the flat layer (2)	48
4.14 The hodogram of the reflection from the fault plane measured on the stacked sections	49
4.15 The hodogram of the reflection from the flat layer measured on the stacked sections	49
4.16 Pre-stack direction filtered section (75° - 85°)	50
4.17 Pre-stack direction filtered section (85° - 95°)	50
4.18 Pre-stack direction filtered section (95° - 105°)	51
4.19 Pre-stack direction filtered section (105° - 115°)	51
4.20 Pre-stack direction filtered section (115° - 125°)	52
4.21 Pre-stack direction filtered section (125° - 130°)	52
4.22 Pre-stack direction filtered section (130° - 140°)	53
4.23 Pre-stack direction filtered section (140° - 145°)	53
4.24 Post stack direction filtered section (75° - 85°)	54
4.25 Post stack direction filtered section (85° - 95°)	54

4.26 Post stack direction filtered section (95° - 105°)55
4.27 Post stack direction filtered section (105° - 115°)55
4.28 Post stack direction filtered section (115° - 125°)56
4.29 Post stack direction filtered section (125° - 130°)56
4.30 Post stack direction filtered section (130° - 140°)57
4.31 Post stack direction filtered section (140° - 145°)57
5.1 Single layer reef model for numerical modeling59
5.2 Two shot of the vertical component of the synthetic data67
5.3 Two shot of the transverse component of the synthetic data67
5.4 Migrated section of the vertical component68
5.5 The in-line energy enhanced migrated section69
5.6 The off-line enhanced migrated section70
5.7 The two-layer synthetic model71
5.8 The off-line enhanced migrated section from the two-layer model72
5.9 The physical model73
5.10 A vertical component shot record of the physical modeling74
5.11 A transverse component shot record of the physical modeling74
5.12 The conventionally processed vertical component stacked section of the physical modeling data75
5.13 The conventionally processed transverse component stacked section of the physical modeling data75
5.14 Polarization filtered section (50° - 85°)76
5.15 Polarization filtered section (85° - 95°)76
5.16 Polarization filtered section (95° - 105°)77
5.17 Polarization filtered section (105° - 150°)77

5.18 The location of the field seismic line and the tied well	78
5.19 The Leduc structure map of the Rich D3A Oil Pool	79
5.20 The vertical component of a shot record of the field data	80
5.21 The transverse component of a shot record of the field data	81
5.22 The synthetic seismogram and sonic log	82
5.23 The stacked section of the vertical component data	83
5.24 The stacked section of the transverse component data	84
5.25 The enlarged stacked section of the vertical component data and synthetic seismogram	85
5.26 The polarization filtered section (20° - 160°)	86
5.27 The polarization filtered section (20° - 160°)	87
5.28 The polarization filtered section (80° - 100°)	88
5.29 Flow chart: prestack polarization filtering	89
5.30 Flow chart: post stack polarization filtering	90
7.1 A shot record from the Foothills area (vertical component)	94
7.2 A shot record from the Foothills area (radial component)	95
7.3 A shot record from the Foothills area (transverse component)	96

LIST OF TABLES

4.1 Comparison of pre-stack and post stack polarization filtering	44
-------------------------------------------------------------------------	----

Chapter 1: Introduction

1.1 Polarization of seismic waves

Seismic waves can be described in terms of their polarization mode. A compressional wave (P wave) is a rectilinearly polarized wave. A plot of the particle motion (a hodogram) is a line and the direction of the line is parallel to the direction of the wave propagation for the typical P wave. The shear wave (S wave) is another kind of rectilinearly polarized wave. The hodogram of the particle motion is also a line, but the line is perpendicular to the wave propagation direction. Another kind of wave, often met in exploration seismic recording, is called ground roll. Ground roll can be a major source of noise especially at near offsets. Ground roll is a surface wave which travels along or near the surface of the ground (Sheriff, 1984). It arises because of the coupling of compressional waves and shear waves (SV) that propagate along a free surface (Yilmaz, 1987). It has different polarization properties than those of P and S waves. Ground roll is an elliptically polarized wave with retrograde particle motion. Its major axis of motion is in the vertical direction.

2-D seismic recordings contain not only the reflections from points directly beneath the line, but also from areas on the sides of the line: we have both in-line and off-line energy. The existence of the off-line energy (French, 1974; Hospers, 1985) may result in the misinterpretation of conventional processed seismic data. If we can develop an algorithm to determine the direction of the incoming waves and to pass the waves from a specific direction, we could enhance the in-line energy and reject the off-line energy. This may improve the quality of the conventional section. The use of three component (3-C) seismic recordings makes this possible. Furthermore, we would like to take advantage of the recorded off-line energy to get the image of the off-line reflectors (Stewart and Marchisio, 1991; Ebrum et al, 1989). This means we can perhaps develop a partial 3-D image from a 2-D seismic line.

1.2 Brief review of polarization processing

Because of the difference in polarization properties for different waves, it is possible to design a filter to reduce one type of seismic wave and to enhance another kind

of seismic wave. Flinn (1965) described a method to estimate the polarization properties of a seismic signal. The outline of the method is to: select a time window of multicomponent seismic data; construct a covariance matrix in the time domain from the data; solve the eigenvalue problem to get the eigenvalues and the eigenvector associated with the major eigenvalue; design two filter factors from the eigenvalue and the eigenvector and then to apply them on the raw data. A covariance matrix is defined as following:

$$\mathbf{S} = \begin{bmatrix} \text{Var}(1,1) & \text{Cov}(1,2) & \text{Cov}(1,3) \\ \text{Cov}(2,1) & \text{Var}(2,2) & \text{Cov}(2,3) \\ \text{Cov}(3,1) & \text{Cov}(3,2) & \text{Var}(3,3) \end{bmatrix}, \quad (1.1)$$

where $\text{Var}(j,j) = \frac{1}{M} \sum_{i=1}^M (V_j(t_i) - v_j)^2$,

$$\text{Cov}(j,k) = \frac{1}{M} \sum_{i=1}^M (V_j(t_i) - v_j)(V_k(t_i) - v_k),$$

$V_j(t)$, ($j=1,2,3$) is 3-component seismic data; v_j is the expected value of $V_j(t)$; M is the number of samples of the time window.

Montalbetti and Kanasewich (1970) and Kanasewich (1981) developed an algorithm based on Flinn's (1965) method with some modification of the filter factors. This filter was applied to remote earthquake data. The filter is effective on distinguishing different teleseismic phases.

A polarization filter can be designed in the frequency domain. One could transform the time series (either the whole trace or a section of the data) into the frequency domain and then construct a covariance matrix with a specific frequency range. Filter factors are made of the eigenvalues of the matrix and the eigenvector associated with the major eigenvalue. These factors can be applied to the raw data similarly to the time domain procedures. Other authors have treated this topic (Samson and Olson, 1980; 1981; Bataille and Chiu, 1991). They design the filter as a combination of polarization filter and bandpass (or f-k) filter. Samson and Olson (1980; 1981) treated the data set from different locations as multichannel data (it could be all vertical component from multilocations). They defined the multichannel data as an N-dimensional vector and

construct the covariance matrix of the N-dimensional vector. This method can reduce noise for any kind of seismic data set, not only for a three component data set. The assumption in this method is that the noise level at different locations is the same. It is necessary to normalize the noise before polarization processing. Bataille and Chiu (1991) described a polarization analysis algorithm in the frequency domain. The advantage of the frequency-domain analysis is that it is possible to separate waves from different directions simultaneously.

Jurkevics (1988) designed a polarization filter for three-component array data. The covariance matrix for each sensor is the same as the Flinn (1965) and Kanasewich (1981) covariance matrix. An average matrix \mathbf{S} is used for polarization estimation:

$$\mathbf{S} = \frac{1}{M} \sum_{m=1}^M \mathbf{S}_m, \quad (1.2)$$

where \mathbf{S}_m is the covariance matrix for sensor m and M is the total number of three-component sensors. In order to carry out the covariance averaging, it is necessary to time-align the computation windows according to phase velocities of coherent wavefronts across the array. The misalignment must be less than $T/5$, where T is the period of signal, to ensure constructive phase superposition. Bandpass filtering is used on the data before the construction of the covariance matrix.

There are some other types of polarization processing as mentioned in the papers of Lucas (1989) and Cho and Spencer (1992). Lucas (1989) describes the single station and geophone array polarization analysis. Cho and Spencer (1992) developed a new algorithm for estimating the moveout velocities and polarization states in mixed wavefields recorded on multicomponent array data in the presence of random noise. Lucas (1989) and Cho and Spencer (1992) both applied their techniques to numerical and physical modeling data to separate the seismic waves with different polarization modes and velocities. The array analysis techniques described by Lucas (1989) and Cho and Spencer (1992) work in the frequency domain.

1.3 Objectives of this thesis

There are three principal goals of this thesis:

- 1) To develop a practical polarization filter for enhancing the waves with a certain propagation direction and to suppress others;
- 2) To construct off-line images;
- 3) To improve the in-line section.

Three types of datasets will be used in this thesis: synthetic data, physical modeling data and field data. The synthetic data used in Chapters 2 and 3 were generated using a ray tracing computer code that I designed. The synthetic data used in Chapters 4 and 5 were created from the SIERRA seismic package. The physical modeling was conducted in the physical modeling lab of the Department of Geology and Geophysics, The University of Calgary. The field data were provided by Gulf Canada, acquired in the central Alberta in 1988.

All numerical modeling and processing were conducted on a Sun workstation. ITA seismic processing software was used to process the data. Matlab was used to display the seismic traces of the simple synthetic modeling data and the hodogram of the seismic data in a given window (Chapters 3 and 4). The field data were processed in the Sage system at Veritas Seismic Ltd. and the ITA system at The University of Calgary.

Chapter 2: Polarization filtering

2.1 Introduction

P waves and S waves have been used effectively in exploration seismology. Both waves are linearly polarized (Kanasewich, 1981). The particle trajectory of particle motion of a P wave is along the direction of the wave propagation. The trajectory of an S wave is perpendicular to the direction of the wave propagation. Meanwhile, a seismic source may generate other kinds of waves, for example, ground roll. Ground roll is one type of surface wave that arises because of the coupling of compressional waves and shear waves (SV) that propagate along the free surface (Yilmaz, 1987). Ground roll is elliptically polarized with retrograde motion. Moreover, seismic recordings are often contaminated by noise which makes the detection and interpretation of small seismic events difficult (Kanasewich, 1981). This noise can be divided into mechanical and electrical noise. The former includes the vibration of equipment, vehicles and wind. The latter can be caused by power lines and other electronic instruments. The polarization difference between the signal and noise provides the possibility of using a polarization filtering technique to separate them.

If there are three-component seismic recordings, a polarization filter can be designed to enhance the signal-to-noise (S/N) ratio by taking advantage of the polarization properties. This is another approach to improve the quality of seismic recording. A polarization filter can be designed to enhance rectilinearly polarized waves and to attenuate other energy. Or, if we are interested in surface waves, a polarization filter also can be designed to enhance this type of wave and to reject body waves.

As mentioned previously, Samson and Olson's (1980; 1981) method could be applied to single-component multilocation data to enhance the S/N ratio with the condition of normalizing the noise level on all traces before polarization processing.

A polarization filter may under some circumstances be also used for detecting the direction of impinging seismic waves. It is sometimes important to distinguish in-line energy and off-line energy. The existence of the off-line energy (French, 1974; Hospers,

1985) may result in the misinterpretation of the seismic data using conventional analysis. Moreover, it is not always true that the seismic line is just over the geology we are interested in. Therefore, the off-line energy may be of interest. Three-component recording provides the possibility of using off-line energy to construct images not directly below the line (Ebrom et al, 1989; Stewart and Marchisio, 1991).

In addition, the polarization filter can be used to separate P-waves and S-waves, or to enhance Rayleigh waves. Generally speaking, if the two waves have different polarization properties, an appropriate polarization filter can be designed to separate them or to enhance one and to attenuate the another.

2.2 Polarization ellipse and covariance matrix

We express the observed seismic data as being composed of a rectilinearly polarized signal and noise as below (Bataille and Chiu, 1991):

$$\vec{V}(t) = u(t) \vec{p} + \vec{n}(t) , \quad (2.1)$$

where, $\vec{V}(t) = [V_1(t), V_2(t), V_3(t)]^T$ is the seismic data vector recorded at a three-component receiver, $u(t)$ is a scalar series of time t , \vec{p} is a unit vector, indicating the polarized direction of wave $u(t)$, $\vec{n}(t) = [n_1(t), n_2(t), n_3(t)]^T$ is the noise, T refers to the transpose, indices 1 to 3 refer to the Cartesian coordinate in the order of vertical, radial and transverse, respectively.

We assume that the signal $u(t)\vec{p}$ and the noise $\vec{n}(t) = [n_1(t), n_2(t), n_3(t)]^T$ are not correlated and that the expectation value (average) of the noise is zero. The correlation of the signal and the noise is:

$$\Phi_{un_i} = \int_{t_1}^{t_2} u(t)n_i(t+\tau) dt = 0 \quad \text{for time delay } \tau \text{ } i=1,2,3. \quad (2.2.1)$$

The expectation of the noise is:

$$S_{n_i} = \frac{1}{t_2 - t_1} \int_{t_1}^{t_2} n_i(t) dt = 0 \quad i=1,2,3, \quad (2.2.2)$$

where t_1, t_2 are the ends of the time window.

To eliminate the effect of the DC term (offset bias), we subtract the expectation of the observed data from equation (2.1). Because of the zero mean of the noise, all bias is contributed by signal $u(t)\vec{p}$. Now, we have

$$\vec{V}(t) - \vec{v} = (u(t) - \mu) \vec{p} + \vec{n}(t), \quad (2.3)$$

where \vec{v} is the expectation of the observed data and μ is the expectation of the signal in a given window. Thus:

$$\vec{v} = \mu \vec{p}. \quad (2.4)$$

With these assumptions, we can construct the covariance matrix \mathbf{S} of the observed data over a time window $M\Delta t$ as following, where M is the number of samples in the time window and Δt is the sampling interval. From equation 2.1, we get:

$$\begin{aligned} \mathbf{S} &= \sum_{i=1}^M (\vec{V}(t_i) - \vec{v})(\vec{V}(t_i) - \vec{v})^T \\ &= \sum_{i=1}^M ((u(t_i) - \mu) \vec{p} + \vec{n}(t_i)) \cdot ((u(t_i) - \mu) \vec{p} + \vec{n}(t_i))^T. \end{aligned} \quad (2.5)$$

With some manipulation and substituting equations (2.2.1) and (2.2.2) into equation (2.5)

$$\mathbf{S} = U\vec{p}\vec{p}^T + \mathbf{N}, \quad (2.6)$$

$$\mathbf{S} = \begin{bmatrix} \text{Var}(1,1) & \text{Cov}(1,2) & \text{Cov}(1,3) \\ \text{Cov}(2,1) & \text{Var}(2,2) & \text{Cov}(2,3) \\ \text{Cov}(3,1) & \text{Cov}(3,2) & \text{Var}(3,3) \end{bmatrix}, \quad (2.7)$$

where $\text{Var}(j,j) = \frac{1}{M} \sum_{i=1}^M (V_j(t_i) - v_j)^2$,

$$\text{Cov}(j,k) = \frac{1}{M} \sum_{i=1}^M (V_j(t_i) - v_j)(V_k(t_i) - v_k),$$

v_j is the expected value of $V_j(t)$,

$$U = \frac{1}{M} \sum_{i=1}^M (u(t_i) - \mu)^2,$$

$$\mu = \frac{1}{M} \sum_{i=1}^M u(t_i).$$

\mathbf{N} is the covariance matrix of noise $\vec{n}(t)$,

$$\mathbf{N} = \begin{bmatrix} N_{11} & N_{12} & N_{13} \\ N_{21} & N_{22} & N_{23} \\ N_{31} & N_{32} & N_{33} \end{bmatrix},$$

where

$$N_{ij} = \frac{1}{M} \sum_{k=1}^M n_i(t_k)n_j(t_k).$$

Now we try to get the direction vector from equation (2.6). Because \vec{p} is a unit vector with $\vec{p}^T \vec{p} = 1$, we can rewrite (2.6) as:

$$(\mathbf{S} - \mathbf{N}) \cdot \vec{p} = U \cdot \vec{p}. \quad (2.8)$$

This is an eigenvalue problem. U is an eigenvalue of matrix $(\mathbf{S} - \mathbf{N})$ and \vec{p} is the associated eigenvector. We do not know the covariance matrix of the noise \mathbf{N} . To overcome this problem we substitute \mathbf{S} for $(\mathbf{S} - \mathbf{N})$ and assume the eigenvalues and eigenvectors of \mathbf{S} are close to those of $(\mathbf{S} - \mathbf{N})$. If the S/N value is not too low, this approximation is reasonable. However, even if the noise is spherically polarized

(isotropic), the direction of the principal eigenvector of \mathbf{S} is not exactly equal to that of $(\mathbf{S} - \mathbf{N})$. Under some circumstances, however, we can still use the eigenvalues and the principal eigenvector to process the signal contaminated by noise for separating the signal and noise and approximately determining the polarization direction of the signal. Some examples of synthetic data will be given later.

The matrix \mathbf{S} has at least one non-zero eigenvalue and all eigenvalues must be non-negative, because \mathbf{S} is symmetric and \mathbf{S} are non-negative definite.

2.3 Flinn's method

Assume $\lambda_1, \lambda_2, \lambda_3$ are the three eigenvalues of \mathbf{S} and that there is the following relation between the eigenvalues:

$$\lambda_1 \geq \lambda_2 \geq \lambda_3 > 0$$

and \vec{e}_1 is the eigenvector associated with λ_1 .

Flinn (1965) defined the first filter factor:

$$G_1 = 1 - \lambda_2 / \lambda_1. \quad (2.9)$$

G_1 , varying between 0 and 1, indicates the rectilinearity of the particle trajectory. If G_1 is close to 1, the particle motion is rectilinear polarized in very high degree. If G_1 is close to 0, it means the wave has very low degree of rectilinearity. This is a scalar factor applied to all three components to reduce the amplitude caused by non-rectilinearly polarized noise from the observed data.

Using the direction vector \vec{p} of the raw data and the principal eigenvector \vec{e}_1 , the second factor is defined as:

$$G_2 = |\vec{p} \cdot \vec{e}_1|. \quad (2.10)$$

If the direction vector of the raw data has the same direction of the major axis of the polarization ellipse, G_2 reaches its maximum, 1, and if the direction of \vec{p} is

perpendicular to the direction of \vec{e}_1 , G_2 equals zero. It is also a scale factor and is the same for the three components. The product of G_1 and G_2 was applied to the raw data.

2.4 Montalbetti and Kanasewich's method

Montalbetti and Kanasewich (1970); Kanasewich (1981) defined the first filter factor G_1 the same way as in Flinn's (1965) definition. However, Montalbetti and Kanasewich (1970) used a different way to define the second filter factor. Supposing $\vec{e}_1 = (E_1, E_2, E_3)^T$, They used the component of the major eigenvector as a weight applied to the associated component of the raw data. The output of the filter is:

$$X'_i = G_1 (E_i X_i) \quad i=1,2,3, \quad (2.11)$$

where, X_i is the i -th component of the raw data and X'_i is the correspondent output.

For better output and avoiding spikes on the output data, a smoothing function was applied to the filter factors G_1 and E_i . It is defined as following:

$$A_j^* = \frac{1}{2M+1} \sum_{k=j-M}^{j+M} A_k, \quad (2.12)$$

where, A_k is a filter factor calculated from equation (2.9) or a component of the major eigenvector of the polarization ellipse. $2M+1$ is the length of the smoothing window. Usually, it is one half of the window for calculating the covariance matrix as mentioned by Montalbetti and Kanasewich (1970).

In fact, the smoothing function averages the data in a window and then outputs the average to another array on the correspondent midpoint of the window. Then it moves the window one sample downward and repeats the above procedure.

Finally, the output of Montalbetti and Kanasewich's polarization filter is:

$$X'_i = G_1^* E_i^* X_i, \quad (2.13)$$

where, G_1^* and E_i^* are smoothed G_1 and E_i by equation 2.12.

2.5 Some examples of synthetic data

Before applying the polarization filter to synthetic data, let's modify the second filter factor for a better physical understanding.

Within a time window, the polarization ellipse is shown in Figure 2.1. The major axis of the ellipse is \vec{e}_1 from the eigenanalysis of the covariance matrix. At the midpoint of the window, the vector of particle displacement is \vec{V} , which is usually not parallel to \vec{e}_1 . Assuming \vec{V} is composed of the linear polarized signal and spherically polarized noise, the direction of the linear polarized signal should be close to the direction of the major axis of the polarization ellipse (usually \vec{V} and \vec{e}_1 are not parallel as long as there is some noise on the recording. We will discuss this problem later). Now we can divide \vec{V} into two vectors, \vec{V}_n and \vec{V}_s . \vec{V}_s is parallel to \vec{e}_1 and \vec{V}_n is perpendicular to \vec{e}_1 . We could say that \vec{V}_n is caused by non-rectilinearly polarized noise and \vec{V}_s is mainly caused by signal. Therefore, the second filter factor is a vector, as defined as:

$$\vec{G}_2 = |\vec{V}_s| \vec{e}_1 = |\vec{V} \cdot \vec{e}_1| \vec{e}_1. \quad (2.14)$$

The function of \vec{G}_2 is to reject the noise \vec{V}_n by projecting the displacement vector \vec{V} to the direction of eigenvector \vec{e}_1 , which we consider is the polarization direction of the rectilinear signal.

We apply the factors to the mid-point of the time window. Finally, the filtered data at the mid-point of the time window, with respect to the original coordinate system, is:

$$\vec{V}' = G_1 \vec{G}_2 = (1 - \frac{\lambda_2}{\lambda_1}) |\vec{V} \cdot \vec{e}_1| \vec{e}_1. \quad (2.15)$$

Then the window is moved downward one time point, and the above procedure is repeated. After the window is moved from the beginning to end of the recording, the filtering process is completed. This filter is a point-by-point non-linear filter.

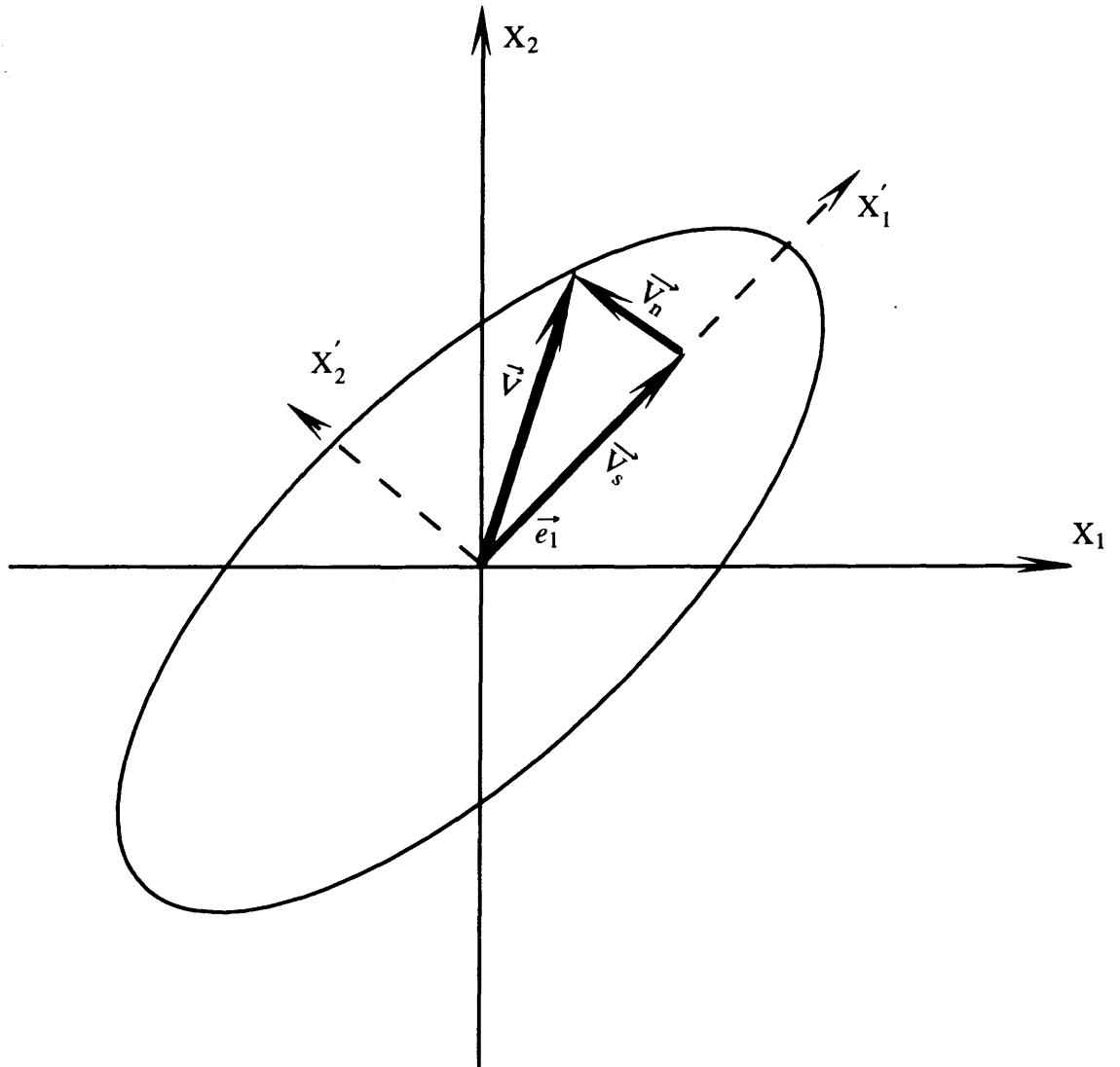


FIGURE 2.1. Shows the relationship between the direction of the eigenvector \vec{e}_1 , trajectory of the particle over the time window $N\Delta t$, and the vector \vec{V} of displacement at the mid-point of the time window. \vec{V} can be divided into two vectors, \vec{V}_s and \vec{V}_n . We assume that \vec{V}_s is mainly caused by signal and \vec{V}_n is caused by noise.

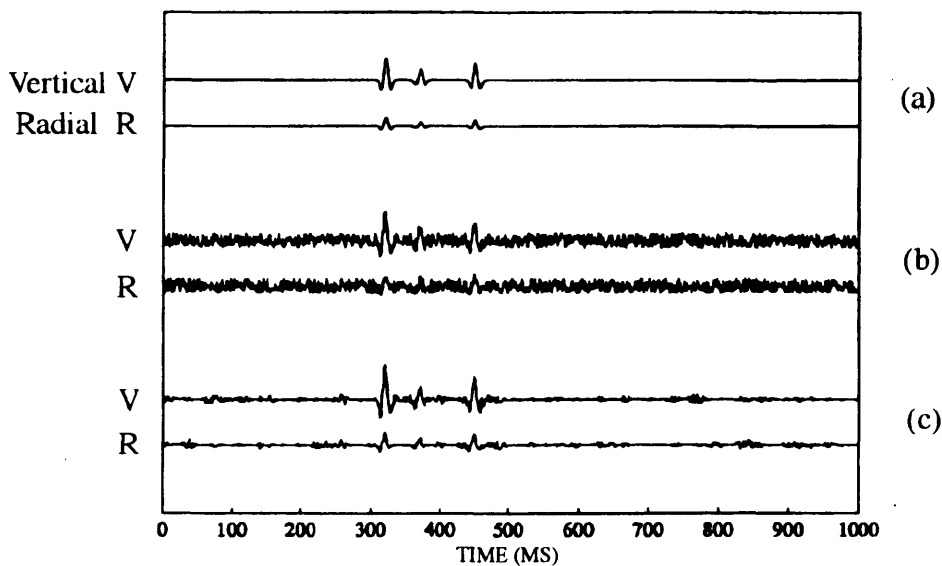


FIGURE 2.2. Polarization filter test for removing random noise: (a) Pure signal of three wavelets centered at time 320, 370 and 420 ms with amplitude of 1.0, 0.5 and 0.8, respectively. (b) Random noise with amplitude of 0.3 is added to the signal. (c) Polarization filtered data. The S/N ratio is improved.

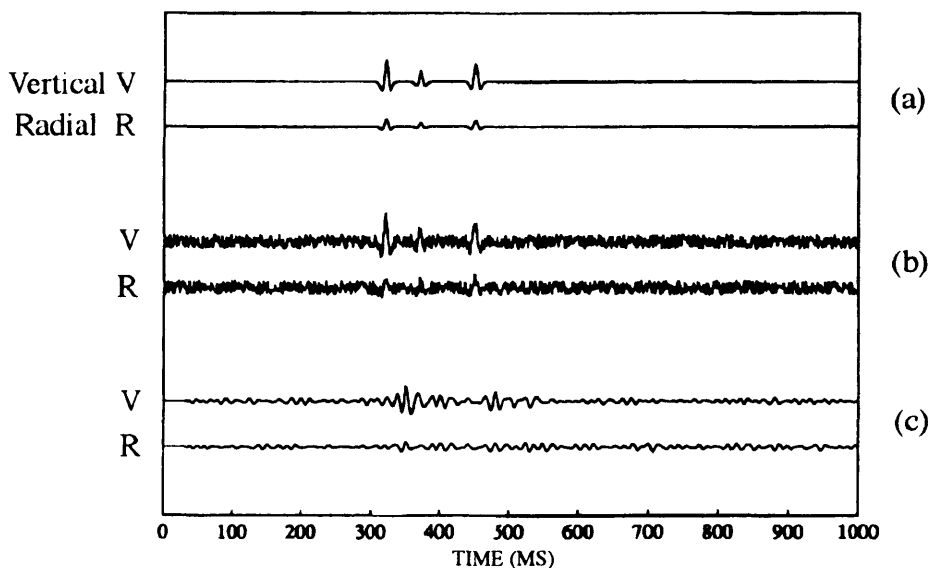


FIGURE 2.3. Bandpass filter test for removing random noise: (a) and (b) are the same as (a) and (b) of Figure. 2.2. (c) Bandpass filtered only data. There is still some noise left and the wavelets are distorted.

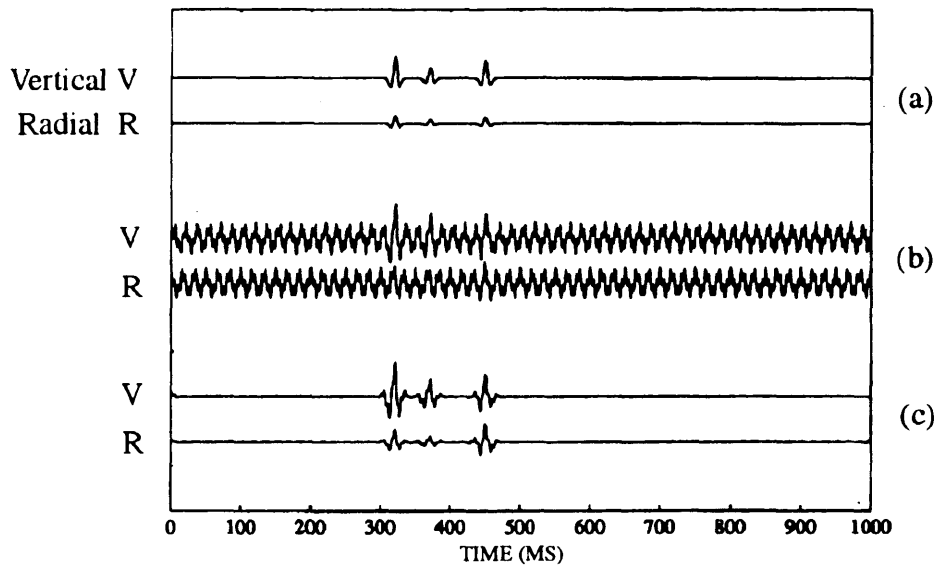


FIGURE 2.4. Polarization filter test for removing circularly polarized noise with the same frequency of signal: (a) Same as (a) of Figure. 2.2. (b) 60 and 200 Hz circularly polarized noise with the amplitude of 0.4 and 0.3, respectively, are added to the pure signal. (c) Output of the polarization filter is very close to the pure signal.

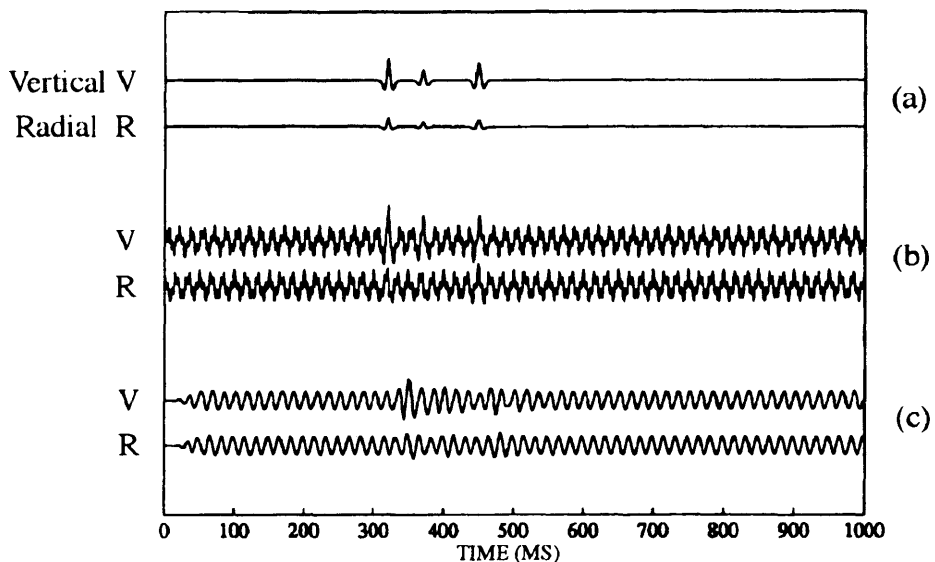


FIGURE 2.5. Bandpass filter test for removing circularly polarized noise with the same frequency of signal: (a) and (b) are the same as the (a) and (b) of Figure. 2.4. (c) Bandpass filtered data of (b). The 60 Hz noise remained. It is hard to distinguish signal from (c).

Varies types of synthetic data are used to test the polarization filter. For simplicity, I will just discuss 2-D data.

A Ricker wavelet (Sheriff, 1984) is used to simulate the real seismic wavelet. It is a zero-phase wavelet and similar to the wavelet of vibroseis data. The centre frequency of the wavelet is 60 Hz and three wavelets used have amplitudes of 1, 0.5, and 0.8 respectively. The wavelets are centered at the time of 320, 370 and 450 ms, respectively. Random noise is added to the signal and the polarization filter is applied to the noise contaminated signal to see how the filter works.

Figure 2.2 shows random noise, with the amplitude of 0.3, added to the signal. (a) is the pure signal and (b) is the noise contaminated signal. It is hard to distinguish the second wavelet in (b), because of the noise. After the data of (b) passed the polarization filter, the S/N ratio is improved and we can see the signal clearly. The same data is input to a bandpass filter (40 - 80 Hz) and the result is shown in Figure 2.3. It is clear that the result of polarization filter is better than bandpass filter in this case. The first and the second wavelets of the bandpass filtered data are joined together. Some noise remains in the bandpass filtered data, since the random noise has pretty wide frequency range and some of the frequency component are within the band passed through the filter.

Let's test an important property of the polarization filter. The signal is the same as that in Figure 2.2 (a), but 60 Hz circularly polarized noise is added to the data (Figure 2.4 (a)). We also added 200 Hz circularly polarized noise in the data. The polarization filter works very well in this case (Figure 2.4(c)). The output is almost the same as the input (Figure 2.4 (a)). A bandpass filter (40 - 80 Hz) is also applied to the data. It is expected that only the 200 Hz circularly polarized noise is eliminated and the 60 Hz noise is still on the traces (Figure 2.5).

2.6 Direct least squares (DLS) method

The basis of polarization analysis, discussed so far, is the eigenvalue problem of the covariance matrix of the observed data. The purpose of the processing is to find the polarization ellipse which best fits to the data within a time or a frequency domain in the sense of least squares. The eigenvalues of the covariance matrix are related to the length of semi-axes of the polarization ellipse and the eigenvectors are related to the direction of

the semi-axes. This is a good method to solve this problem. However, if we try to solve the eigenvalue problem directly, it takes much time. The direct least-squares method (DiSiena et al., 1984) is another method to get the formula for the direction of the ellipse which is a straight forward method to get the polarization direction of seismic waves. Actually, the final results are the same as what we get from the solution of the eigenvalue problem, and least-squares computations can be done sequentially.

The DLS method for 2-D data follows. With the same assumptions as the covariance method, we have a seismic data set $\overline{V}(t) = (V_1(t), V_2(t))^T$ which contains seismic signal as well as noise. Within a time window, we extract some data from $\overline{V}(t)$ as $\overline{u}(t) = (u_1(t), u_2(t))^T$, $t=j-L, j+L$, where j is the midpoint of the selected window and $2L+1$ is the length of the window. The geometrical centre of hodogram is:

$$x_0 = \frac{1}{2L+1} \sum_{t=j-L}^{j+L} u_1(t),$$

$$y_0 = \frac{1}{2L+1} \sum_{t=j-L}^{j+L} u_2(t).$$
(2.16)

Assuming there is a line through the centre of the hodogram (x_0, y_0) with the direction cosine $(\cos \theta, \sin \theta)$. We can project the displacement vector to the line and sum up the squares of the projection:

$$A(\theta) = \sum_{t=j-L}^{j+L} ((u_1(t)-x_0)\cos \theta + (u_2(t)-y_0)\sin \theta)^2.$$
(2.17)

If the line has the same direction as the major axis of the polarization ellipse, $A(\theta)$ receives its maximum. If the line has the same direction of the minor axis of the ellipse, $A(\theta)$ receives its minimum value. To get the direction of the line making $A(\theta)$ maximum or minimum, let:

$$\frac{dA(\theta)}{d\theta} = 2 \sum_{t=j-L}^{j+L} (-(u_1(t)-x_0) \sin \theta + (u_2(t)-y_0) \cos \theta) ((u_1(t)-x_0) \cos \theta + (u_2(t)-y_0) \sin \theta)$$

$$= 0. \quad (2.18)$$

After a few mathematical manipulations, we get (Davis et al., 1981):

$$\tan 2\theta = \frac{2\Psi_{12}}{\Psi_{22} - \Psi_{11}}, \quad (2.19)$$

$$\text{where, } \Psi_{11} = \sum_{t=j-L}^{j+L} (u_1(t)-x_0)^2,$$

$$\Psi_{22} = \sum_{t=j-L}^{j+L} (u_2(t)-y_0)^2,$$

$$\Psi_{12} = \sum_{t=j-L}^{j+L} (u_1(t)-x_0)(u_2(t)-y_0).$$

It obvious from equation 2.19 that if $\frac{dA(\theta)}{d\theta}$ is 0, $\frac{dA(\theta+\frac{\pi}{2})}{d\theta}$ and $\frac{dA(\theta\pm\pi)}{d\theta}$ are also 0.

After we get θ from equation (2.19), we should compare $A(\theta)$ and $A(\theta+\frac{\pi}{2})$. The direction associated with the larger A is the direction of the major axis of the ellipse, and the smaller correspondents to the minor axis.

Assuming that $A_1=A(\theta)$ is greater than $A_2=A(\theta+\frac{\pi}{2})$, we define the first filter factor as:

$$G_1 = 1 - A_2/A_1. \quad (2.20)$$

G_1 varies between 0 and 1. For a rectilinear wave, the hodogram should be a line. Therefore the projection of the displacement vector on the line perpendicular to the hodogram line is 0. At this time, G_1 receives its maximum, 1. For a circular polarized wave, the projection of the displacement vector in any direction will same. Therefore, A_1 equals A_2 . At this time, G_1 is 0. G_1 here works in the same way as that in equation (2.9).

The direction vector of the major axis of the ellipse is $\vec{e}_1 = (\cos \theta, \sin \theta)^T$, so the second filter factor is:

$$\vec{G}_2 = |\vec{u}(j) \cdot \vec{e}_1| \vec{e}_1 = g (\cos \theta, \sin \theta)^T, \quad (2.21)$$

where, $g = |u_1(j)\cos \theta + u_2(j)\sin \theta|$.

Because \vec{e}_1 is the direction vector of the major axis of the polarization ellipse, which is the same as the normalized eigenvector associated with the major eigenvalue of the covariance matrix, \vec{G}_2 here plays the same role as that in the equation (2.14).

The output of the filter is:

$$\vec{u} = G_1 \vec{G}_2 = (1-A_2/A_1) g (\cos \theta, \sin \theta)^T. \quad (2.22)$$

Of course, some smoothing function, like equation (2.12), can be applied to the filter factors before they go to equation (2.22).

For 3-D data, we can follow the similar procedures as 2-D. We can project the seismic data to a line and sum up the squares of the projection. The line with the maximum value of the sum of the projection is the major axis of the polarization ellipsoid. Another way we can do is to find a plane with the maximum sum of the projection and then work on that plane.

2.7 Application of polarization filter to field data with ground roll

Although this is not a successful case, I would like to share the experience with people who are interested in this topic. The CREWES project of The University of Calgary conducted a low-frequency survey at the Blackfoot Field, Alberta in 1995. The 4 km line has 200 stations at 20 m interval. At each station, there are a number of types of geophones, from 2 Hz to 10 Hz, 3-component and single-component. A shot record is shown in Figure 2.6 (vertical component) and Figure 2.7 (radial component) recorded by 10 Hz 3-C geophones (Litton 1033). On the record, we can see strong ground roll at near offsets. The polarization filter was applied to the data. The output is shown in Figure 2.8 (vertical component) and Figure 2.9 (radial component). On the filtered record, the coherent signals are improved a little bit at farther offsets. However, the ground roll at the near offsets still remains on the filtered record. The polarization filter did not help

reduce ground roll very much in this case. The reason is that the ground roll is stronger than the signal in this record. If the S/N ratio of a dataset is too low, the polarization and the rectilinearity of the data are effected to a high degree by the noise. Therefore, it is difficult to separate signal and noise by the polarization filter. We will discuss this issue in Chapter 3 in detail. In our previous discussion of synthetic ground roll removal, the polarization filter did a good job in that case. Polarization filtering worked in that situation because the signal is stronger than the noise (refer to Figure 2.4).

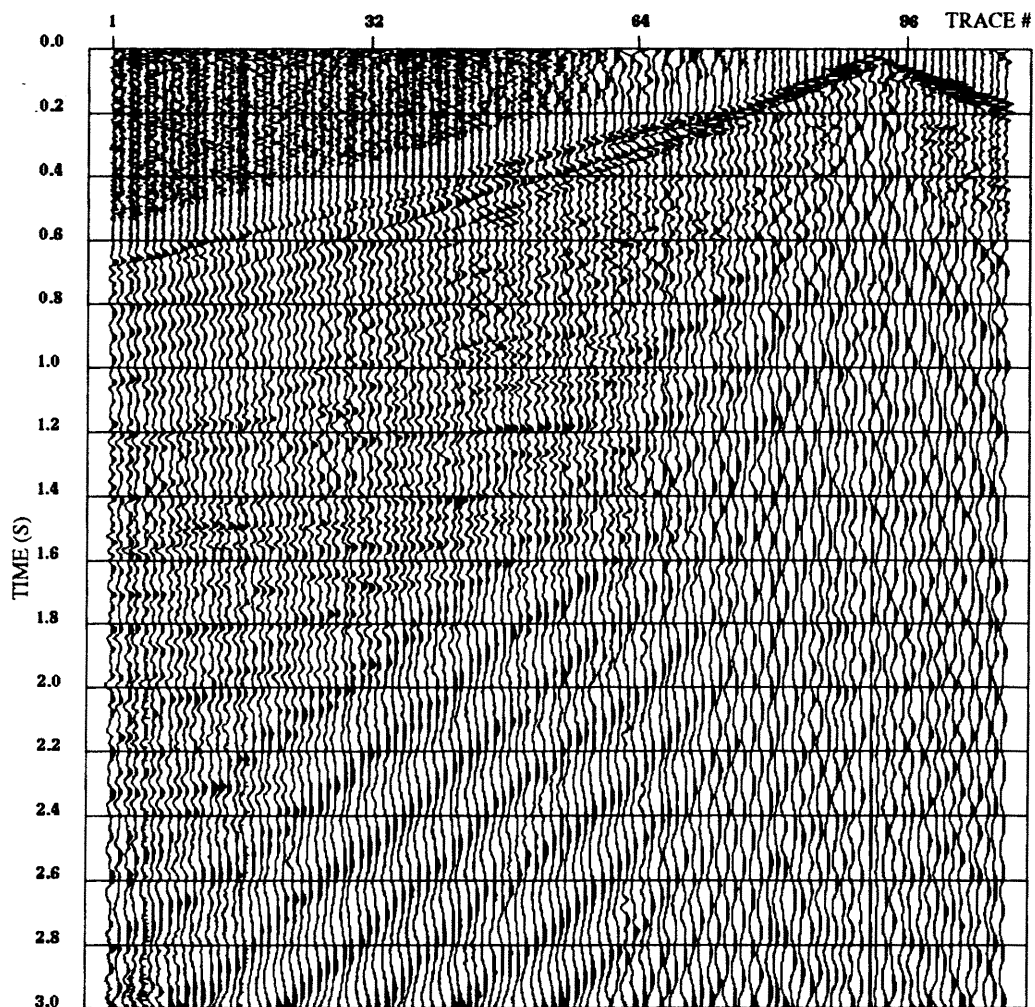


FIGURE 2.6 The vertical component of a shot record (10 Hz geophone) across the Blackfoot field of Southern Alberta.

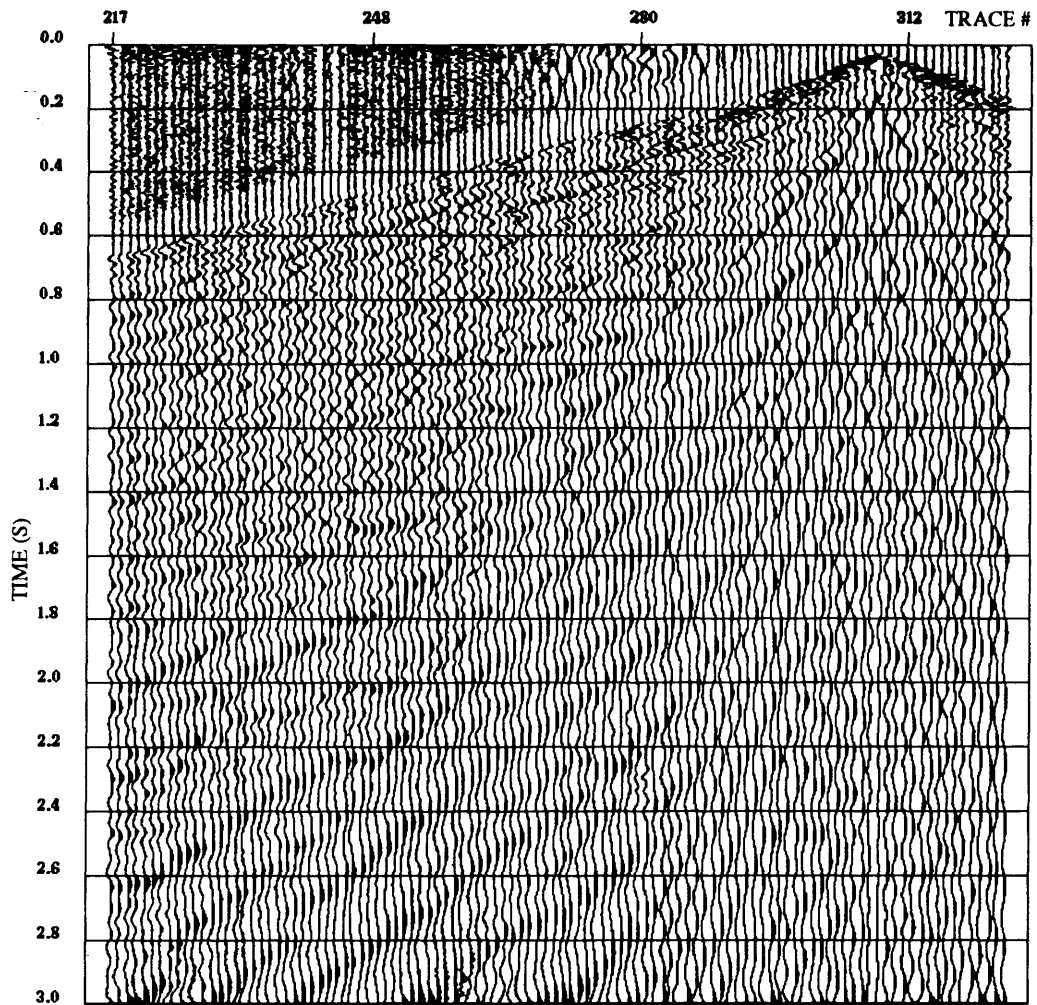


FIGURE 2.7 The radial component of a shot record (10 Hz geophone) across the Blackfoot field of Southern Alberta.

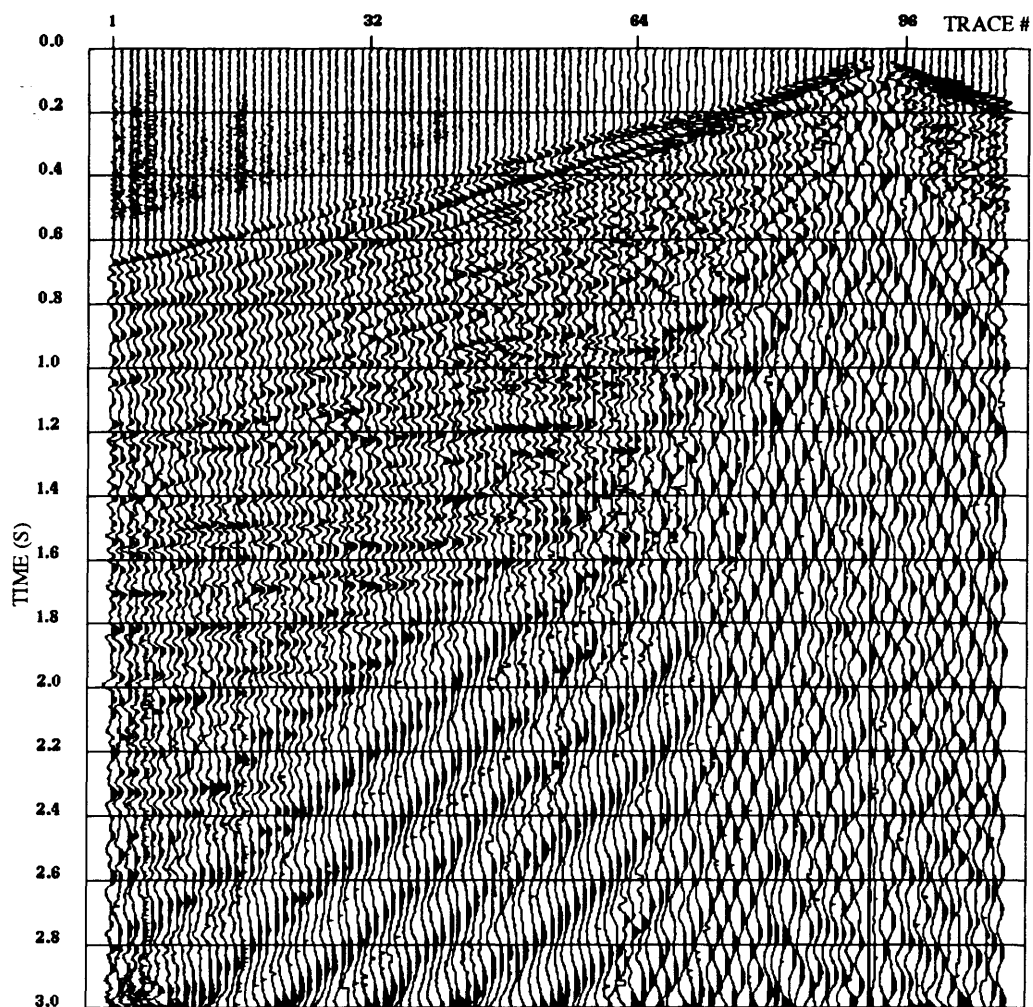


FIGURE 2.8 The vertical component of the output of the polarization filter. The S/N ratio is improved a little bit at the far offsets, but the ground roll is still on the record. The polarization filter does not perform well on the low S/N ratio data.

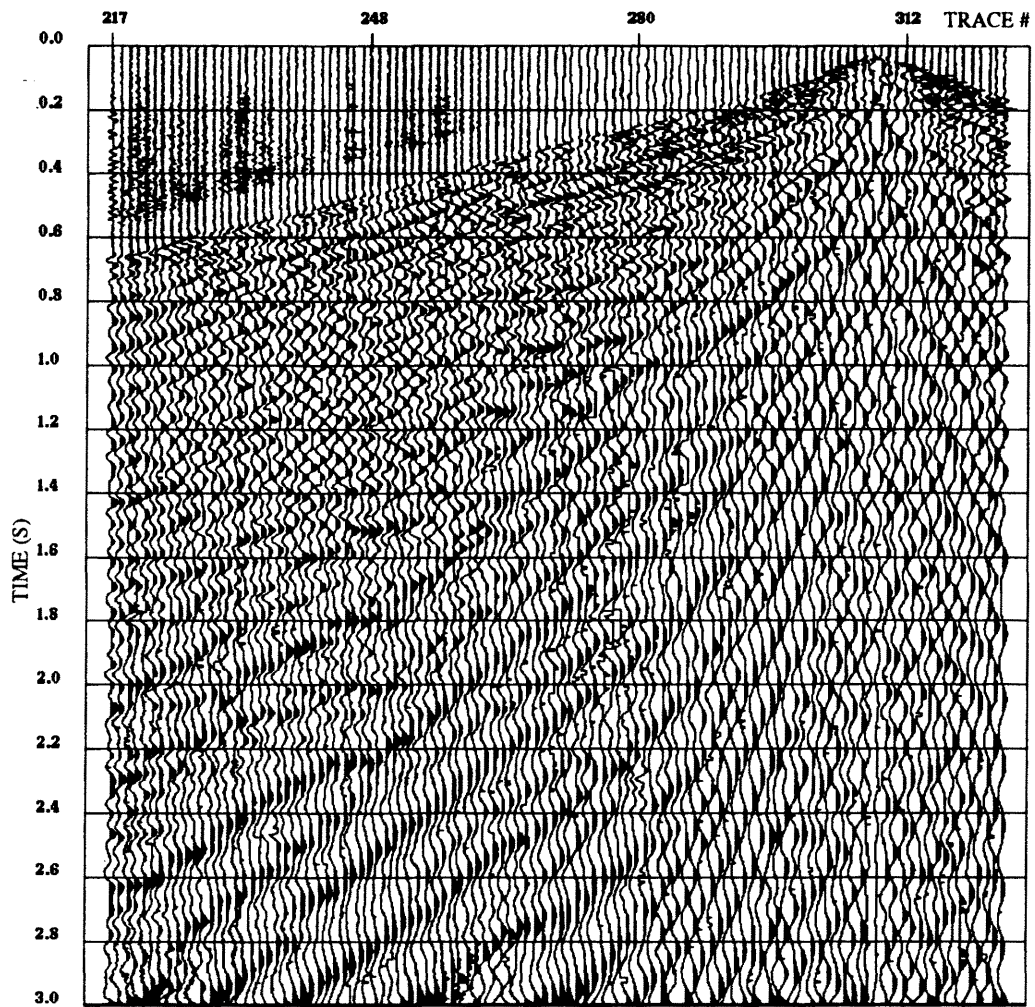


FIGURE 2.9 The radial component of the output of the polarization filter. The ground roll at the near offsets was not reduced by the polarization filter.

Chapter 3: The effect of noise on polarization direction

3.1 Introduction

As mentioned in the previous chapter, when a rectilinear polarized signal is contaminated by noise, the polarization direction of the observed data is usually not the same as the polarization direction of the rectilinear signal. This is the case even if the noise is another rectilinear polarized wave with a different direction. People may think that the polarization direction won't be changed if the noise is circularly polarized. However, the fact is different.

3.2 Direction perturbation of noise

Generally, when a rectilinearly polarized signal is contaminated by noise, regardless of what polarization property the noise has, its polarization direction will be changed. Let's discuss this in two-dimensions.

At first, let us reiterate some words from Gal'perin's (1984). "... in the case of interference of two linearly-polarized oscillations with an identical period, but with arbitrary phases, amplitudes and directions of arrival we may always find two mutually-perpendicular directions in which oscillations take place with a phase difference of 90°." Now let us derive the formula for searching for the mutually-perpendicular directions.

After Gal'perin (1984) , if we have a rectilinear signal \vec{X} where

$$\vec{X} = \begin{pmatrix} X_1 \\ X_2 \end{pmatrix} = \begin{pmatrix} A \sin \omega t \\ B \sin \omega t \end{pmatrix}, \quad (3.1)$$

and noise \vec{Y} given by

$$\vec{Y} = \begin{pmatrix} Y_1 \\ Y_2 \end{pmatrix} = \begin{pmatrix} C \sin(\omega t + \beta) \\ D \sin(\omega t + \gamma) \end{pmatrix}, \quad (3.2)$$

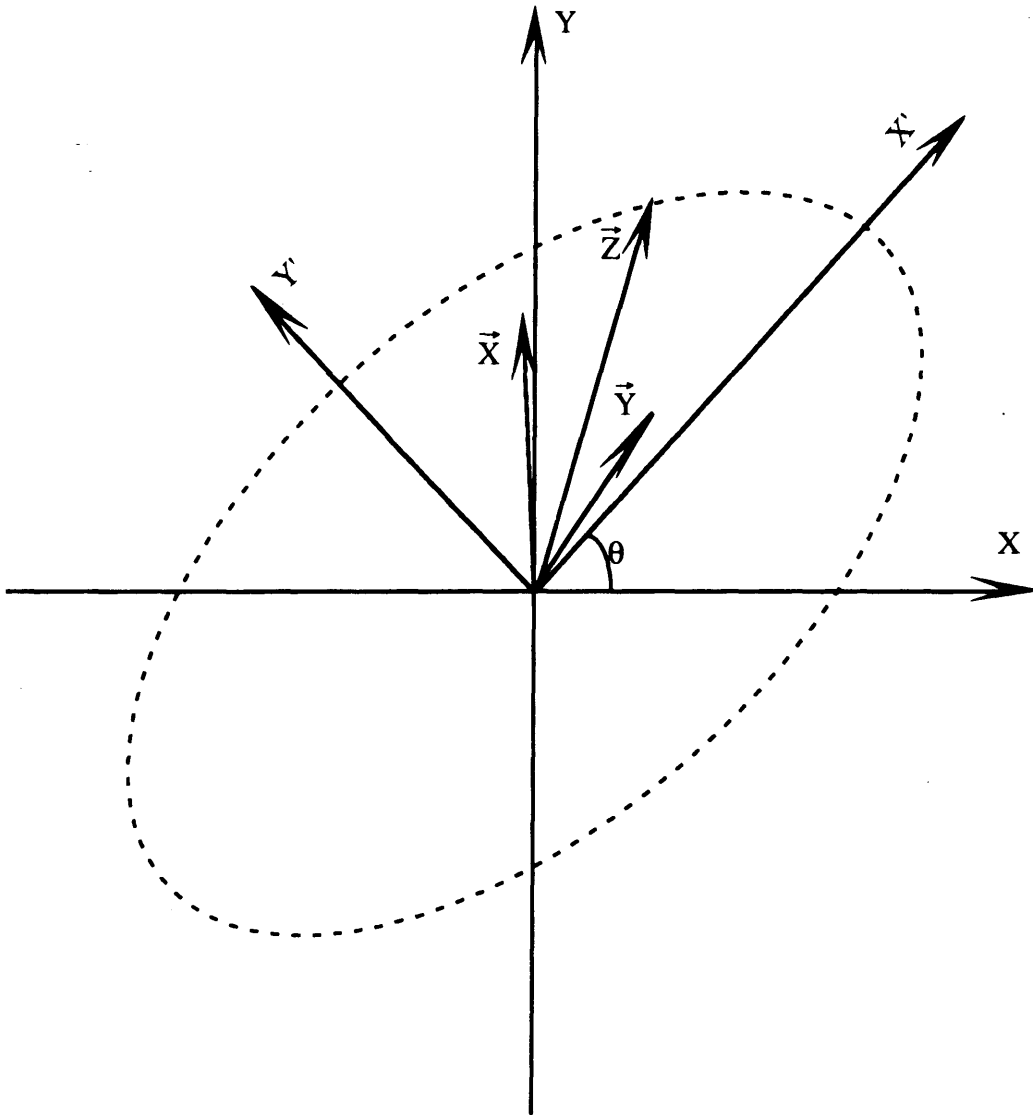


FIGURE 3.1. Projection of data to the coordinate correspondent to the axes of the ellipse of the particle motion trajectory. X-Y are the original coordinate of the data. X' and Y' are the axes of the ellipse. $\vec{Z} = \vec{X} + \vec{Y}$.

the observed data \vec{Z} will be:

$$\vec{Z} = \vec{X} + \vec{Y} = \begin{pmatrix} A\sin\omega t + C\sin(\omega t + \beta) \\ B\sin\omega t + D\sin(\omega t + \gamma) \end{pmatrix}. \quad (3.3)$$

The trajectory of \vec{Z} will be an ellipse. Supposing X' and Y' are the axes of the ellipse (Figure 3.1). The projection of \vec{Z} on X' and Y' are:

$$\begin{aligned} C_{\eta}\sin(\omega t + \eta) &= A\cos\theta\sin\omega t + C\cos\theta\sin(\omega t + \beta) + \\ &+ B\sin\theta\sin\omega t + D\sin\theta\sin(\omega t + \gamma), \\ C_{\xi}\sin(\omega t + \xi) &= -A\sin\theta\sin\omega t - C\sin\theta\sin(\omega t + \beta) + \\ &+ B\cos\theta\sin\omega t + D\cos\theta\sin(\omega t + \gamma), \end{aligned} \quad (3.4)$$

where, C_{η} is the amplitude of the component of \vec{Z} on the axis of X' ,
 C_{ξ} is the amplitude of the component of \vec{Z} on the axis of Y' ,
 θ is the angle between the axes of X and X' ,
 η and ξ are the phase change when we project \vec{Z} from the original coordinates X - Y to new coordinates X' - Y' .

when $\omega t = 0$:

$$\begin{aligned} C_{\eta}\sin\eta &= C\cos\theta\sin\beta + D\sin\theta\sin\gamma, \\ C_{\xi}\sin\xi &= -C\sin\theta\sin\beta + D\cos\theta\sin\gamma, \end{aligned} \quad (3.5)$$

when $\omega t = \frac{\pi}{2}$:

$$\begin{aligned} C_{\eta}\cos\eta &= A\cos\theta + C\cos\theta\cos\beta + B\sin\theta + D\sin\theta\cos\gamma, \\ C_{\xi}\cos\xi &= -A\sin\theta - C\sin\theta\cos\beta + B\cos\theta + D\cos\theta\cos\gamma. \end{aligned} \quad (3.6)$$

So we get:

$$\tan\eta = \frac{C\cos\theta\sin\beta + D\sin\theta\sin\gamma}{A'\cos\theta + B'\sin\theta}, \quad (3.7)$$

$$\cot\xi = \frac{A'\sin\theta - B'\cos\theta}{C\sin\theta\sin\beta - D\cos\theta\sin\gamma},$$

where, $A' = A + C\cos\beta$,

$$B' = B + D\cos\gamma.$$

Because X' and Y' are on the axes of the trajectory ellipsoid, so the phase difference of the two components on X' and Y' is $\frac{\pi}{2}$, that is:

$$\tan\eta = -\cot\xi. \quad (3.8)$$

Combining and simplifying equations 3.7 and 3.8, we get:

$$\tan 2\theta = 2 \frac{A'B' + CD\sin\beta\sin\gamma}{A'^2 - B'^2 + C^2\sin^2\beta - D^2\sin^2\gamma}, \quad (3.9)$$

which gives us the direction of the axes of the ellipse has been found.

The direction of the trajectory for signal \vec{X} is:

$$\tan\theta' = \frac{B}{A},$$

or

$$\tan 2\theta' = 2 \frac{AB}{A^2 - B^2}. \quad (3.10)$$

Usually, $\theta' \neq \theta$.

Let's discuss two specific cases.

CASE I: when $\beta = \gamma = 0$, the noise \vec{Y} is another rectilinear wave.

$$\tan 2\theta = 2 \frac{(A+C)(B+D)}{(A+C)^2 - (B+D)^2} = \frac{2 \frac{B+D}{A+C}}{1 - \left(\frac{B+D}{A+C}\right)^2} = \frac{2 \tan \theta}{1 - \tan^2 \theta}. \quad (3.11)$$

So: $\tan \theta = \frac{B+D}{A+C}$.

When either A or $B \gg C$ and D , or $\frac{A}{B} = \frac{C}{D}$, $\theta = \theta'$. This means, when the S/N ratio is high or the noise has the same direction as the signal, we can get an accurate direction of signal \vec{X} from the observed data \vec{Z} . Otherwise the calculated direction will not be the accurate direction of signal \vec{X} .

CASE II: when $C=D=1$, $\beta-\gamma = \frac{\pi}{2}$, the noise \vec{Y} is a circularly polarized wave with an amplitude of 1.

$$\tan 2\theta = 2 \frac{AB - A \sin \beta + B \cos \beta}{A^2 - B^2 + 2A \cos \beta + 2B \sin \beta}. \quad (3.12)$$

The direction varies with the phase difference β . For a more specific case, when the rectilinear signal is a normal incident wave, $B = 0$. Equation (3.12) becomes:

$$\tan 2\theta = -2 \frac{\sin \beta}{A + 2 \cos \beta}. \quad (3.13)$$

Figure 3.2 and Figure 3.3 show the direction perturbation variation with S/N ratio A (we have supposed the amplitude of the noise is 1) and the phase difference between the vertical components of the signal and noise. Only when β is 0 or π , can we get the exact direction of the rectilinear signal \vec{X} from the observed data. The perturbations due to a circularly polarized signal are significant. The maximum perturbation is 20° for the S/N ratio of 3, and 12° for 5.

In summary, if the observed data contains noise, the polarization direction is not the same as the polarization direction of the rectilinear signal in the data, unless the S/N ratio is so high that the noise is negligible.

Synthetic data are used to verify the above results. In Figure 3.4, we can see when there are two rectilinear waves from different directions with no phase difference between them, the superposition of these two waves is still a rectilinearly polarized wave, but the polarization direction is changed. When there are two rectilinear waves from different directions with a phase difference, then generally the superposition of these two waves is an elliptically polarized wave (Figure 3.5 and 3.6). The phase difference is 30° in Figure 3.5 and 210° in Figure 3.6. In Figure 3.7 the signal and noise have the same dominant frequency of 30 Hz. The S/N ratio is 2. The signal is a normally incident P wave. The noise is a circularly polarized with the phase difference (β) of 45° from the signal on the vertical component. The trajectory of the combined data of the signal and noise is an ellipse. There is an angle of 10° between the major axis of the ellipse and the direction of the signal.

3.3 Limitation of single station polarization processing

The direction perturbation caused by noise makes the detection of the polarization direction difficult. Generally speaking, we cannot get the exact polarization direction from the observed data. If the S/N ratio of the data is sufficiently high, satisfactory results can still be achieved. A lot of data does not have sufficient signal quality, but there are some techniques that can increase the S/N ratio without changing the polarization properties of the wave. Such processes can be applied before polarization analysis.

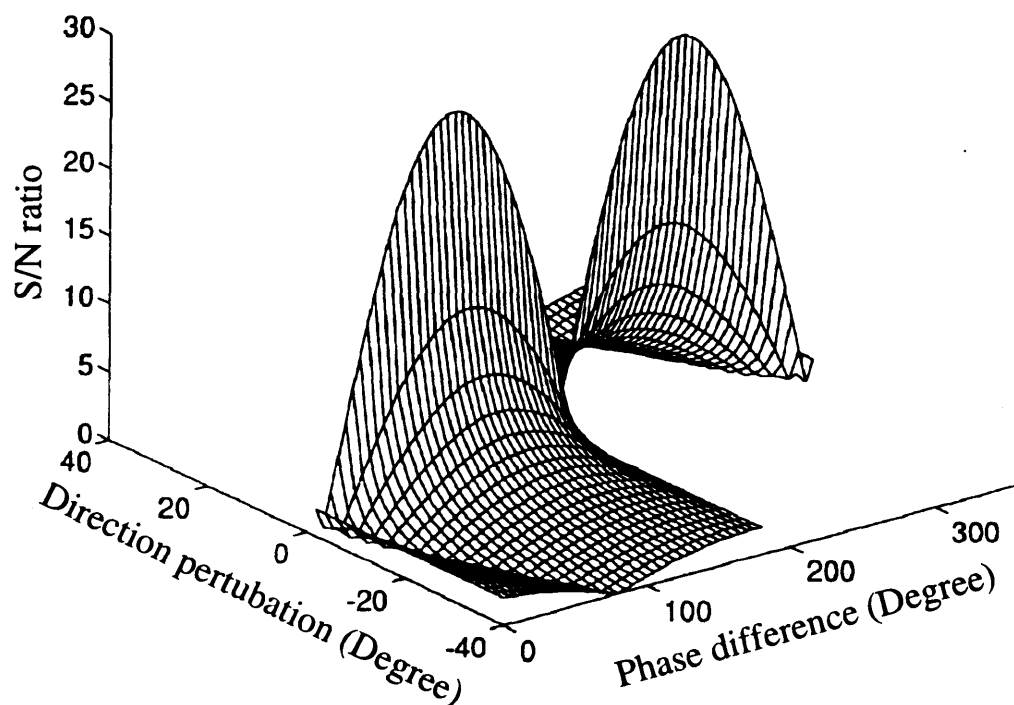


FIGURE 3.2 This figure shows how the S/N ratio effects the polarization direction of a rectilinearly polarized signal contaminated by a circularly polarized noise. The 'phase difference' in the figure is the β in the equation 3.13. When the S/N ratio is large enough, the error of detecting polarization direction could be neglected.

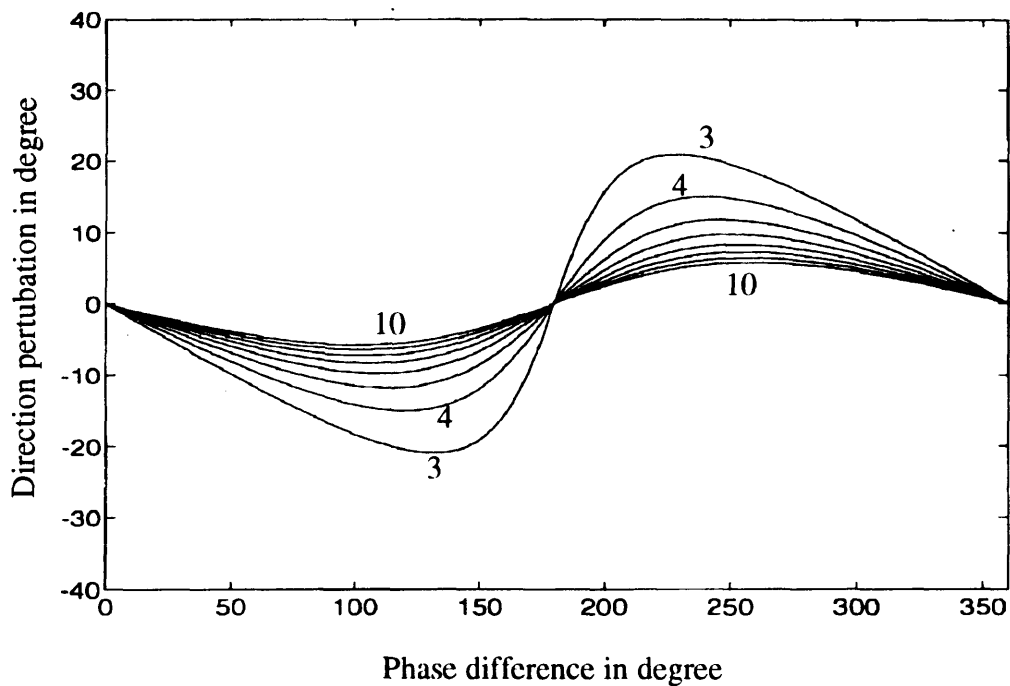


FIGURE 3.3 This plot shows how circularly polarized noise effects the polarization direction of a rectilinearly polarized signal. The numbers in the figure indicate the S/N ratio for different curves. The 'phase difference' in the figure is β from Equation 3.13. When the S/N ratio is 3, the maximum direction perturbation is about 20° . If the S/N ratio is greater than 5, the direction error will be less than 10° . When β equals 0° or 180° , the direction perturbation is 0, regardless of the S/N ratio.

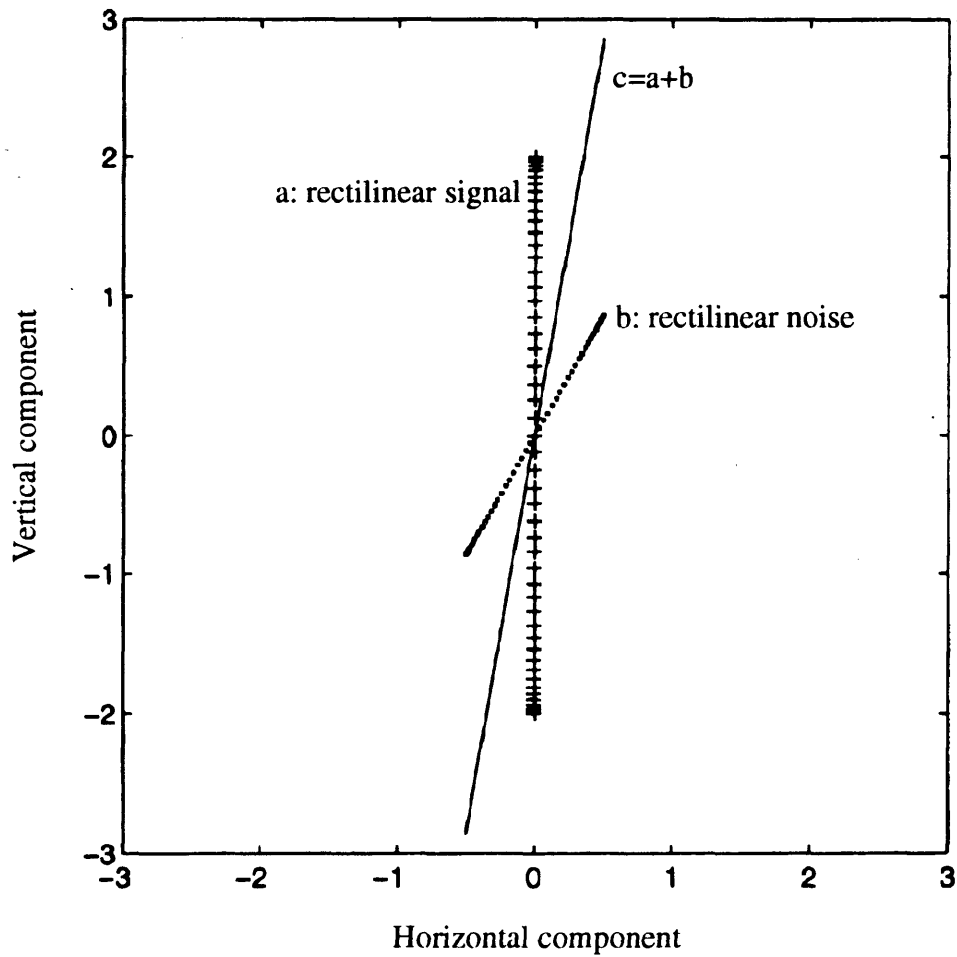


FIGURE 3.4 When there are two rectilinear harmonic waves from different directions, the summation of these two waves could be a rectilinear wave, if the phases of the two individual waves are the same. Here wave $a = 2.0 \cos(2\pi ft)$, $b = \cos(2\pi ft)$, $f=30$ Hz. Wave a comes vertically up, while wave b comes with an angle of 30° with the vertical direction. The summation of these two waves is wave c . We can see wave c is still a rectilinearly polarized wave.

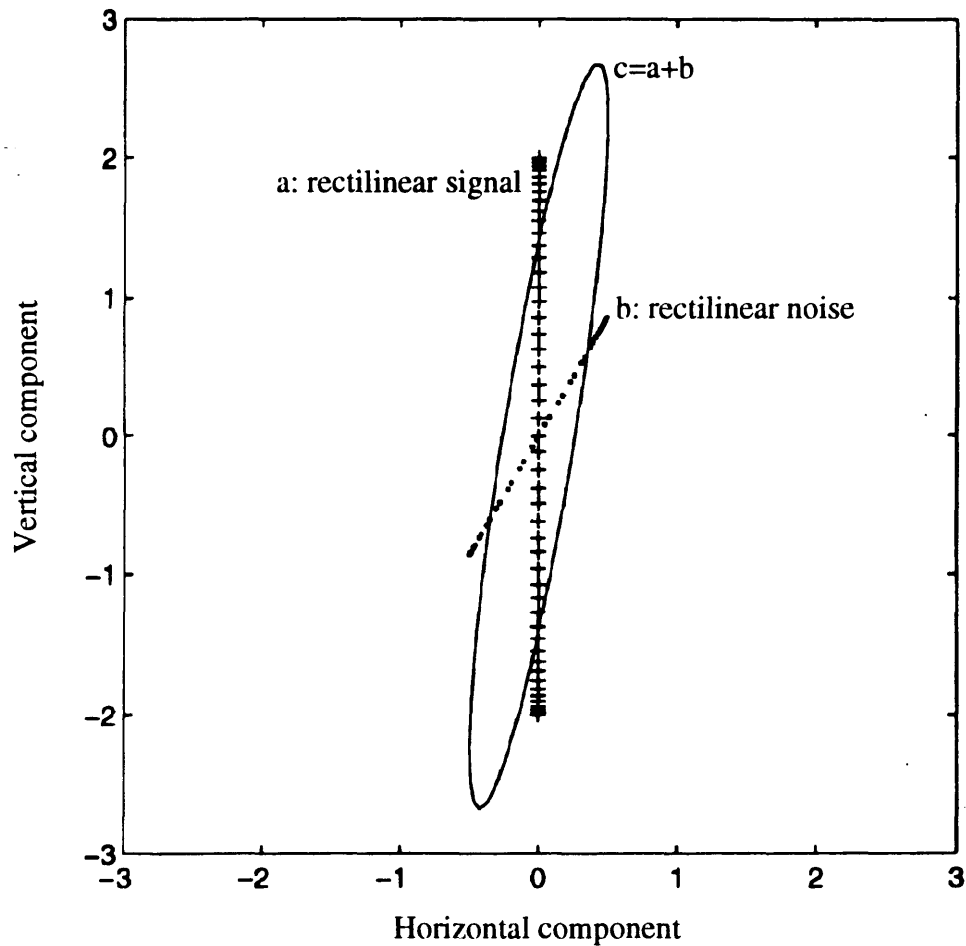


FIGURE 3.5 When two rectilinear waves come from different directions and there is a phase difference between these two waves, the summation of these two waves is an elliptically polarized wave, in general. Here wave $a = 2.0 \cos(2\pi ft)$ in vertical direction, and wave $b = \cos(2\pi ft - \pi/6)$ coming with an angle of 30° between the vertical direction, $f=30$ Hz. The summation of these two waves is wave c . It is an elliptically polarized wave.

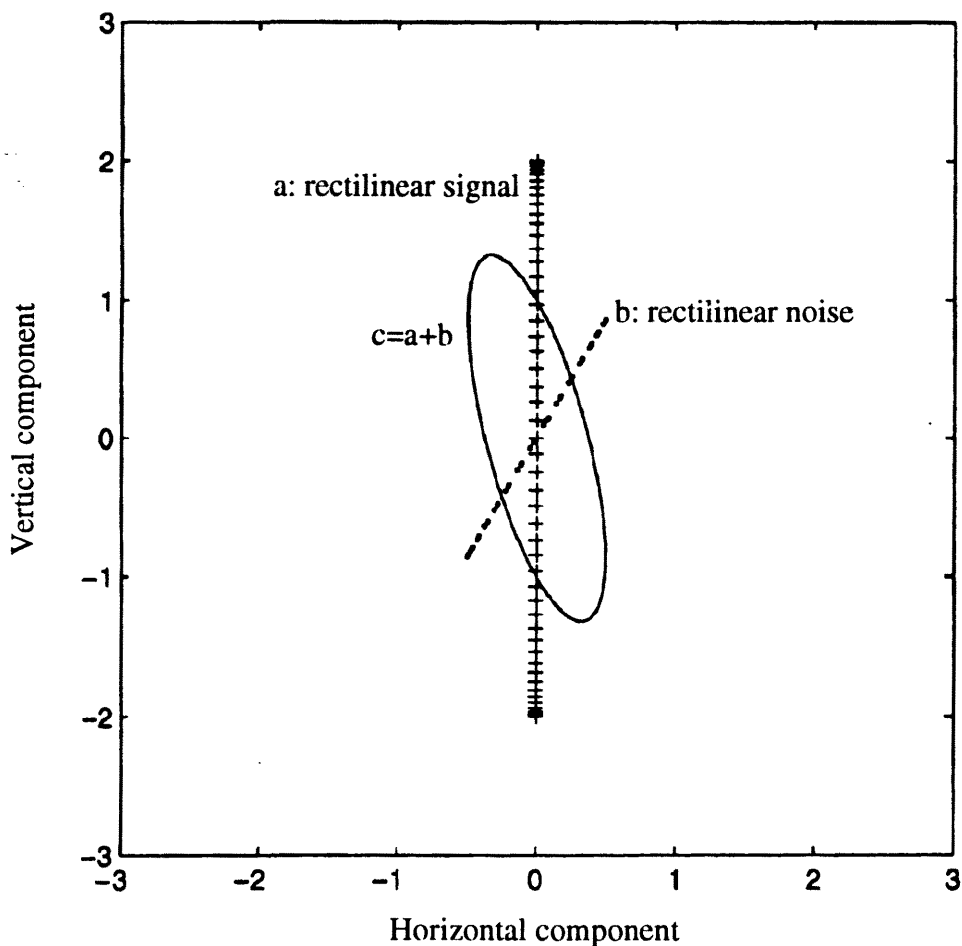


FIGURE 3.6 When two rectilinear waves come from different directions and there is a phase difference between these two waves, the summation of these two waves is an elliptically polarized wave. Here wave $a = 2.0 \cos(2\pi ft)$ and wave $b = \cos(2\pi ft - 7\pi/6)$. Here the phase difference is 210° rather than 30° in Figure 3.5. We can see the superposition of these two waves is an elliptically polarized wave and the major axis of the ellipse is not between the directions of wave a and b .

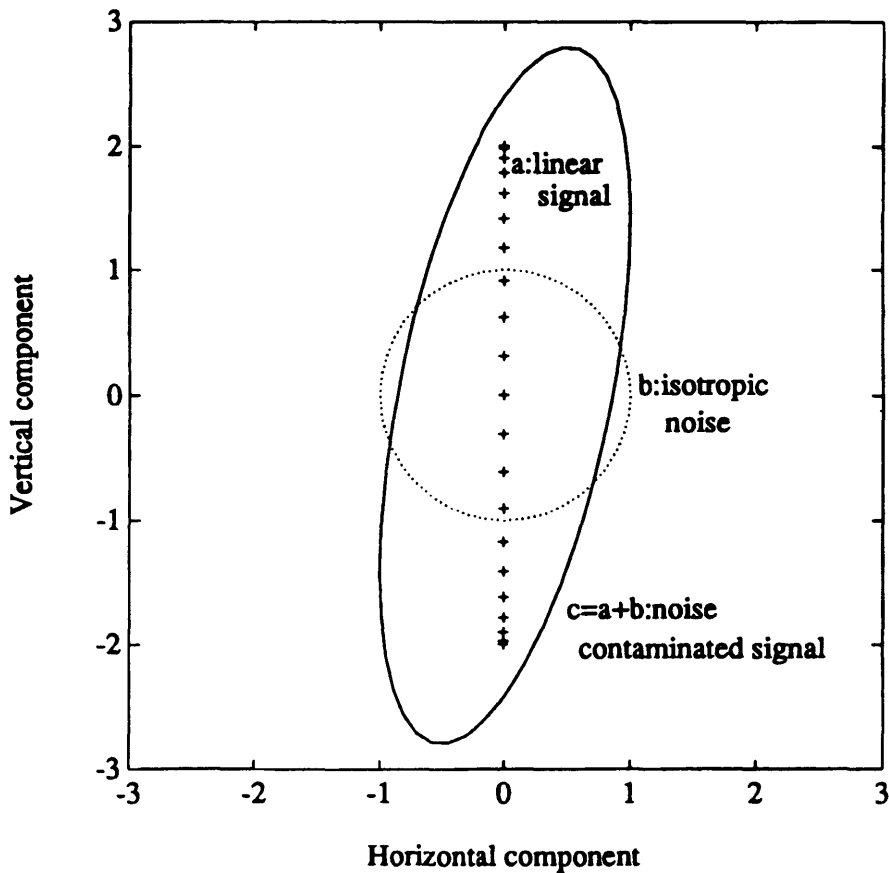


FIGURE 3.7. When a rectilinear wave is contaminated by circularly polarized noise, the direction of the major axis of the trajectory is usually not the same as the direction of rectilinear wave. Here, a is a normal incident, rectilinear polarized signal, b is a circularly polarized noise, the S/N ratio is 2 in terms of amplitude. The hodogram (solid ellipse) of the combination c of signal a and noise b shows c has the different polarization direction from the signal a and the difference is around 10° .

Chapter 4: Directional filtering

4.1 Introduction

Off-line energy may lead to the misinterpretation of conventional processed seismic data. We expect to develop an algorithm to determine the direction of the incoming waves and to pass the waves from a specific direction using 3-component seismic data. This may improve the quality of the conventional section by rejecting off-line energy. Furthermore, we would like to take advantage of the recorded off-line energy to get the image of the off-line reflectors (Ebrom et al, 1989; Stewart and Marchisio, 1991) to build a partial 3-D image from a 2-D seismic line.

4.2 The method

As mentioned in Chapter 2, we can get the polarization direction from 3-C seismic data with a reasonably high S/N ratio. For low S/N ratio data, some processes can be used to enhance S/N ratio before polarization filtering. For the commonly used P wave in petroleum exploration, its polarization direction is the same as its propagation direction. Therefore, for a certain type of waves, we can design a directional filter when we measure the polarization direction of the seismic waves. If we want to pass the waves within a certain range of directions, the directional filter factor is defined as following:

$$G_3 = \begin{cases} 1, & \text{if } \theta_0 - \varphi \leq \theta \leq \theta_0 + \varphi \\ 0, & \text{if } \theta \leq \theta_0 - \varphi \text{ or } \theta \geq \theta_0 + \varphi \end{cases} \quad (4.1)$$

where, θ_0 is the midpoint of the direction window. φ is the half-length of the window. Of course some tapering functions, such as cosine function, can be applied on the direction window. Combined with the factors of polarization filter described in Chapter 2, the output of the filter for passing the waves of the direction within the window of $\theta_0 - \varphi \leq \theta \leq \theta_0 + \varphi$ is:

$$\vec{u} = G_1 \vec{G}_2 G_3 = (1 - A_2/A_1) g G_3 (\cos \theta, \sin \theta)^T, \quad (4.2.1)$$

For rejecting the waves of the direction within the window, the output of the filter is:

$$\vec{u} = G_1 \vec{G}_2 (1-G_3) = (1-A_2/A_1) g (1-G_3) (\cos \theta, \sin \theta)^T. \quad (4.2.2)$$

For the definitions of G_1 , \vec{G}_2 , A_1 and A_2 , please see Chapter 2.

As discussed in Chapter 3, noise can change the polarization direction of seismic waves. When S/N ratio of the raw data is low, the change could be significant. In this case, the polarization direction we get from the methods described in Chapter 2 may be useless. Some techniques of enhancing S/N ratio should be applied before polarization processing. The critical point for these enhancement is that any processing before polarization filtering should not change the property of the signal's polarization direction.

Common-mid-point (CMP) stacking is a typical method to enhance signal-to-noise (S/N) ratio in seismic data processing. The CMP recording technique uses redundant recording to improve the S/N ratio. Theoretically, the data are improved by a factor of \sqrt{N} , where N is the stacking fold. CMP stacking also attenuates coherent noise such as multiples, guided waves and ground roll. This is because primary reflections and coherent noise usually have different stacking velocities (Mayne, 1962; Yilmaz, 1987).

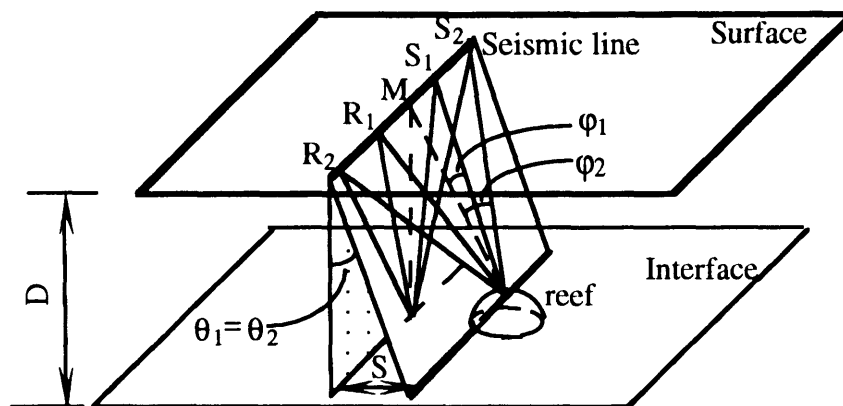


FIGURE 4.1 Stacking diagram: the reef is S away from the seismic line laterally. The receivers can record the reflections both from the flat interface and the reef.

Referring to Figure 4.1, there are two shot-receiver pairs (S_1 - R_1 and S_2 - R_2). They have same CMP location M . There is an off-line scatterer (reef) at the depth of D and lateral distance of S away from the seismic line. The medium velocity is V . After NMO correction, the reflection from the reef will be coherent. The stacking velocity is somewhat different from the medium velocity in this case. Generally speaking, the

stacking velocity for off-line reflection is different from that for flat interfaces, but the difference is small if the offset S of the reef is small. Therefore, we can use the velocity of the flat interface at the depth of the reef to stack the reef reflection. The vertical component V_1 of the amplitude of the reef reflection P_1 on the first pair of shot-receiver is:

$$V_1 = P_1 \cos \varphi_1 \cos \theta_1, \quad (4.3)$$

where, θ_1 is the angle between the vertical plane through the seismic line and the plane through the ray-path from the reef. φ_1 is the angle between the vertical plane perpendicular to the seismic line and the ray-path from the reef (see Figure 4.1).

The transverse component T_1 of the first pair shot-receiver is:

$$T_1 = P_1 \cos \varphi_1 \sin \theta_1, \quad (4.4)$$

For a second pair of shot and receivers, the vertical component V_2 and transverse component T_2 are:

$$V_2 = P_2 \cos \varphi_2 \cos \theta_2, \quad (4.5)$$

$$T_2 = P_2 \cos \varphi_2 \sin \theta_2, \quad (4.6)$$

where, P_2 is the reef reflection on the second pair of shot-receiver. θ_2 is the angle between the vertical plane through the seismic line and the ray-path from the reef. φ_2 is the angle between the vertical plane perpendicular to the seismic line and the ray-path from the reef.

It is clear that:

$$\theta_1 = \theta_2. \quad (4.7)$$

Therefore, on the stacked section, the vertical component V is:

$$\begin{aligned} V &= V_1 + V_2 = P_1 \cos \varphi_1 \cos \theta_1 + P_2 \cos \varphi_2 \cos \theta_2, \\ &= (P_1 \cos \varphi_1 + P_2 \cos \varphi_2) \cos \theta_1. \end{aligned} \quad (4.8)$$

The transverse component T is:

$$\begin{aligned} T &= T_1 + T_2 = P_1 \cos \varphi_1 \sin \theta_1 + P_2 \cos \varphi_2 \sin \theta_2 , \\ &= (P_1 \cos \varphi_1 + P_2 \cos \varphi_2) \sin \theta_1 . \end{aligned} \quad (4.9)$$

The direction of the reflection from the reef measured on the stacked section, θ , will be:

$$\tan \theta = \frac{(P_1 \cos \varphi_1 + P_2 \cos \varphi_2) \sin \theta_1}{(P_1 \cos \varphi_1 + P_2 \cos \varphi_2) \cos \theta_1} = \tan \theta_1 . \quad (4.10)$$

The direction of the reflection from the reef measured on the stacked section remains unchanged with respect to the unstacked data. It is very important that we can use the CMP stacking technique to enhance the S/N ratio for determining the direction of seismic waves. As we mentioned in the previous chapter, we may be unable to get the correct directions of seismic waves if the data have a high noise level. Some S/N ratio enhancement must be applied without changing the wave direction information before we do polarization analysis. From the above, we can say that it is safe to apply polarization filtering post stack, because stacking does not affect the directional angles of the wave propagation direction. Here we did not consider the NMO stretch effect. As a result of NMO correction, traces are stretched in a time varying manner, which causes their frequency content to shift toward to low end of the spectrum. Frequency distortion increases at shallow times and large offsets (Yilmaz, 1987). To eliminate NMO stretch smearing, we can apply a proper mute before stacking. For deeper times and small offsets, NMO stretch is usually negligible.

The free surface effect is another factor that can change the polarization direction of seismic waves. The net particle motion at surface is the vector sum of the motions associated with the incident P-wave, reflected P-wave and reflected S-wave, and in general is neither vertical nor parallel to the direction of the incident wave (Eaton, 1989). In physical modeling data, the free surface effect is complicated and perhaps lessened because the receiver sensor is relatively big. The diameter of the sensor is almost 1 cm. If the scale factor is 10,000, it will be equivalent to 100 m in field. Thus the receiver may

be have somewhat like an elastic interface. However future research should investigate this problem further.

4.3 Application to a simple synthetic example

A numerical model is used to test the directional filter and to compare the pre- and post stack directional filtering (Figure 4.2). This model is composed of a layer of 500 m thick and a half space. The P wave velocity is 2000 m/s for the top layer and 2700 m/s for the half space. There is a fault with 45° dip angle. We laid out a seismic line in the strike direction of the fault. The lateral distance from the seismic line to the hanging wall is 150 m. The line is 1000 m long. There are total 51 stations with 20 m spacing. A total of 11 shots are recorded by all stations except the station on the shot point. The shot interval is 100 m (Figure 4.3). The synthetic dataset is generated by the SIERRA seismic package using ray tracing method.

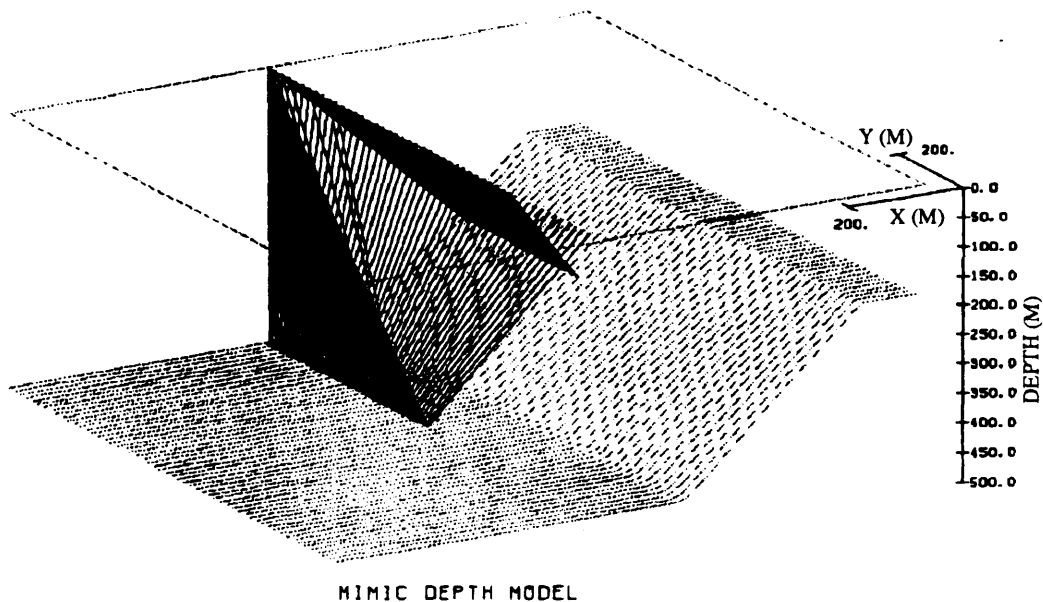


FIGURE 4.2 The model used for generating numerical modeling data. The ray-paths show the reflections from the flat layer beneath the seismic line and from the fault plane at the right side of the seismic line.

A shot record of the synthetic data is shown in Figures 4.6 and 4.7. On the vertical component, we can see two reflection events. One is from the flat layer and another is from the fault plane. The reflection from the flat layer comes later than that

from the fault plane, because the distance from the seismic line to the flat layer is further than the distance from the seismic line to the fault plane. The distance from the seismic line to the flat layer is 500 m. The distance from the seismic line to the fault plane is about 460 m (Figure 4.4). Only the reflection from the fault plane is on the transverse component. Here we only generated P waves at the shot points. For the vertical reflection the displacement of the surface is exactly vertical. Therefore, the projection on the horizontal direction is zero.

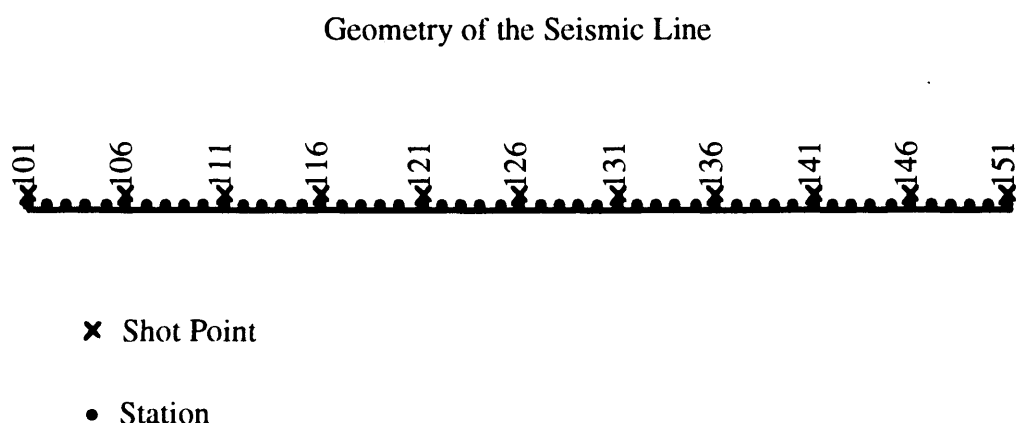


FIGURE 4.3 The geometry of the numerical modeling. 51 geophones were laid out on the line with the spacing of 10 m. There are totally 11 shots and the shot interval is 50 m.

First of all, we use conventional processing techniques (refraction statics, deconvolution, velocity analysis and NMO correction, automatic statics, stacking) to process both vertical and transverse component separately. The stacked section of the vertical component is shown in Figure 4.8. From the section, we can see two events at the time of 0.46 s and 0.5 s, respectively. The top one is from the fault plane and it is expected for us to see this reflection on the transverse stack. The second event is from the flat layer and it should not show up on the stacked section of the transverse component. Figure 4.9 is the stacked section of the transverse component. Only one reflection is on the section. It is from the fault plane on the right side of the seismic line.

Now let us check the polarization direction for both reflections from the flat layer underneath the seismic line and the fault plane on the right side of the seismic line and

compare the polarization directions with the wave propagation directions. At first, we measure the polarization direction on shot records. We take record 3 for the measurement. The shot point is 111 (Figure 4.3). The raw record is shown in Figures 4.6 and 4.7.

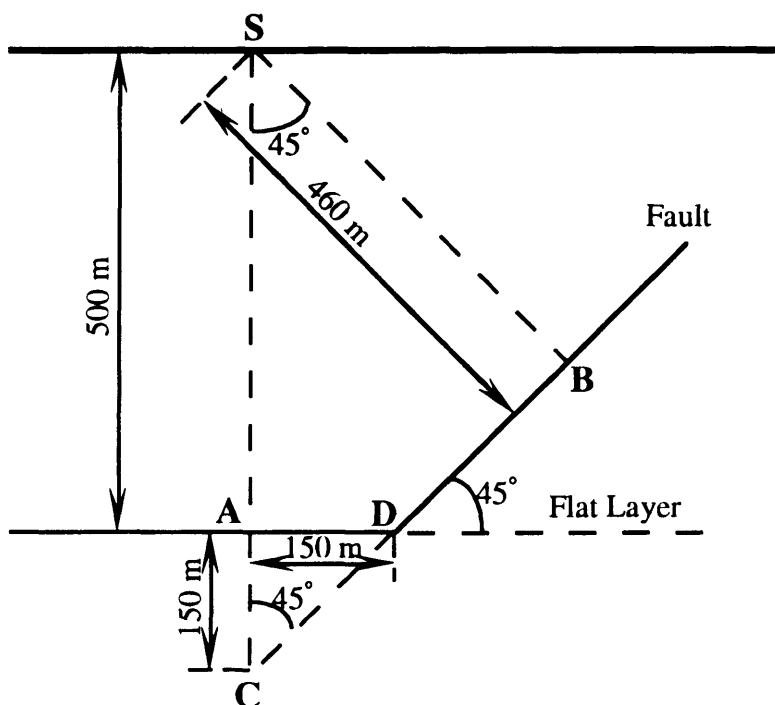


FIGURE 4.4 The distance from the source to the fault $SB = SC \cos 45^\circ$.

Before we measure the polarization direction, we define the direction of 90° as vertically up, 0° as horizontally from left to right and 180° as horizontally from right to left (Figure 4.5). Referring to Figure 4.4, we know that the wave propagation direction of the reflection from the flat layer is 90° and the direction of the reflection from the fault plane is 135° . We take trace 10 which is located at station 110. The offset is 10 m. The width of the window we used to measure the polarization direction is 30 ms. The hodograms of the wave taken from windows 444 - 474 ms and 484 - 514 ms are shown in Figures 4.10 and 4.11, representing the reflections from the fault plane and the flat layer, respectively. When the window is at 444 - 474 ms, the polarization direction is 135° , which indicates the direction of the seismic wave from the fault plane. When the window is at 484 - 514 ms, the polarization direction is 90° , which indicates the direction of the reflection from the flat layer.

Additional hodograms are shown in Figures 4.12 and 4.13. The windows are 505 - 535 ms and 545 - 575 ms on trace 35 of record 3. These hodograms also indicate the polarization direction is 135° for the reflection from the fault plane and 90° for that from the flat layer.

Now let us look at the polarization direction on stacked sections to see if there is any change caused by the processing procedure. Figures 4.14 and 4.15 are the hodograms windowed at 440 - 470 ms and 485 - 515 ms on trace 40 of the stacked sections (Figures 4.8 and 4.9). The polarization direction does not change after processing. However the processing did change a polarization feature - the rectilinearity (Equation 2.7). On the shot records, the rectilinearity is 1. The hodogram of the shot record is a straight line. On the stacked sections, the rectilinearity is slightly less than 1. The hodograms of the stacked data are very thin ellipses. This change is caused by deconvolution. To make the process of deconvolution stable, it is necessary to add some white noise into the seismic data. For an ideal deconvolution, the operator is infinite. In practice, we only can use a finite operator. The truncation of the operator can also cause some noise. We can see these decon-added noise on the stacked sections. On the deep part of the stacked sections (Figures 4.8 and 4.9), the traces are wavy instead of straight lines on the shot record (Figures 4.6 and 4.7).

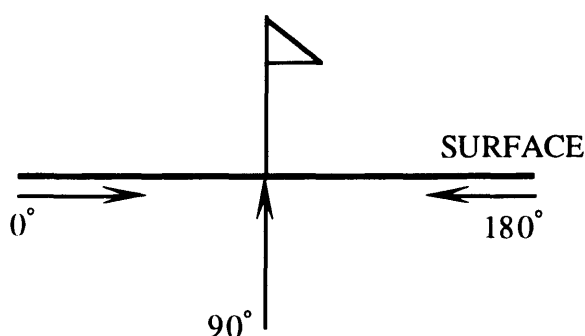


FIGURE 4.5 The definition of direction.

We applied the directional filter before and after stacking to compare the effects of the different sequences. Figures 4.16 to 4.23 are the stacked sections with pre-stack directional filtering in different direction windows. While Figures 4.24 to 4.31 show the

stacked sections with post stack directional filtering in different direction windows. For most of the sections, the width of the window is 10° . The window scans from the central angle of 80° to 142.5° by a 10° increment. We can see that the reflections from the flat layer and from the fault plane are separated by the window $85^\circ - 95^\circ$ and $130^\circ - 140^\circ$ (Figures 4.17, 4.22, 4.25 and 4.30). And the wave propagation directions are represented by the direction of the window. On other sections, we can not see any coherence because the windows for these sections do not cover the direction of the reflection wave propagation.

For the different sequences, (1) directional filtering then stacking, and (2) stacking then directional filtering, both did very good job and the results from the two sequences are identical. This indicates that the directional filter can be applied before or after stacking and that stacking does not change the polarization direction. Table 4.1 outlines the results of these two sequences.

TABLE 4.1. Comparison of pre-stack and post stack polarization filtering.

DIRECTION WINDOW	PRE-STACK		POST STACK	
	# OF EVENTS	FIGURE	# OF EVENTS	FIGURE
$75^\circ - 85^\circ$	No	4.16	No	4.24
$85^\circ - 95^\circ$	One at 0.5 s	4.17	One at 0.5 s	4.25
$95^\circ - 105^\circ$	No	4.18	No	4.26
$105^\circ - 115^\circ$	No	4.19	No	4.27
$115^\circ - 125^\circ$	No	4.20	No	4.28
$125^\circ - 130^\circ$	No	4.21	No	4.29
$130^\circ - 140^\circ$	One at 0.46 s	4.22	One at 0.46 s	4.30
$140^\circ - 145^\circ$	No	4.23	No	4.31

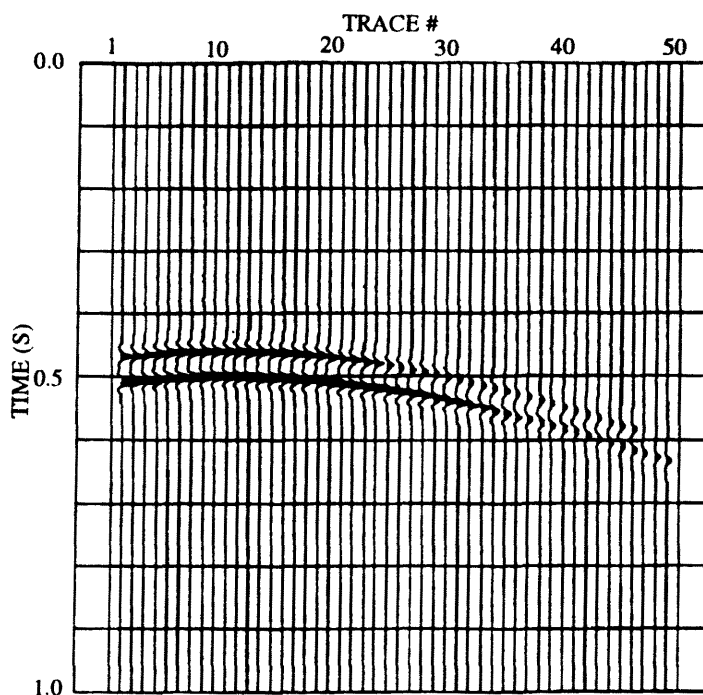


FIGURE 4.6 The vertical component of a shot record of the synthetic data (generated by SIERRA). The earlier event is from the fault plane and the later is from the flat layer.

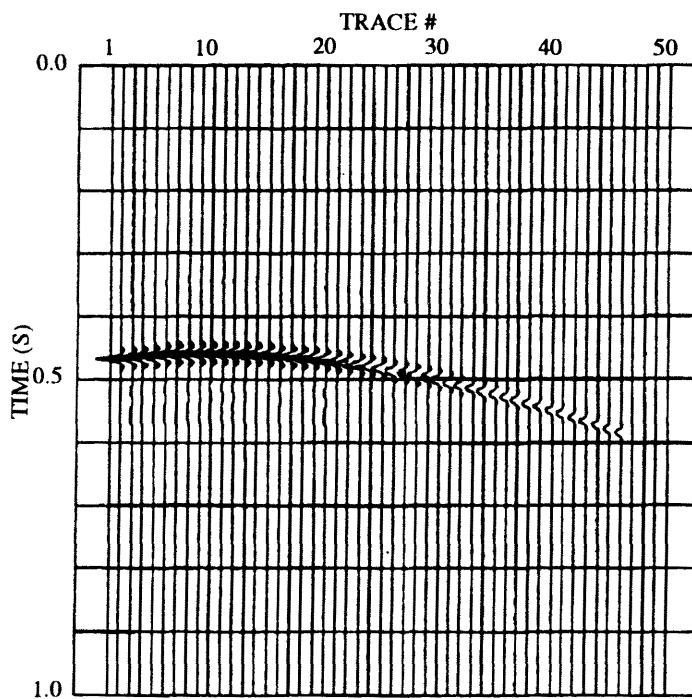


FIGURE 4.7 The transverse component of a shot record of the synthetic data. Only the reflection from the fault plane appears on the transverse component.

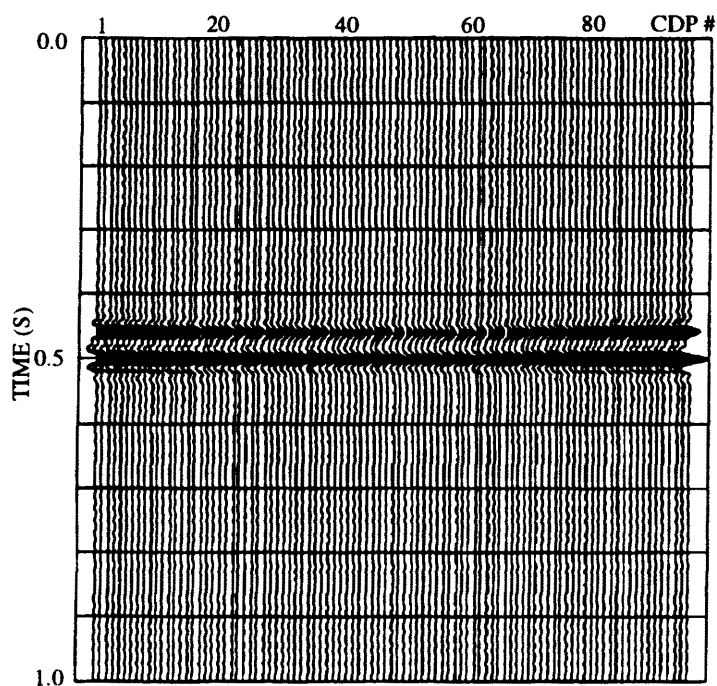


FIGURE 4.8 The stacked section of the vertical component of the synthetic data. There are two events at the time of 0.46 s and 0.5 s. The top one is from the fault plane and the second event is from the flat layer

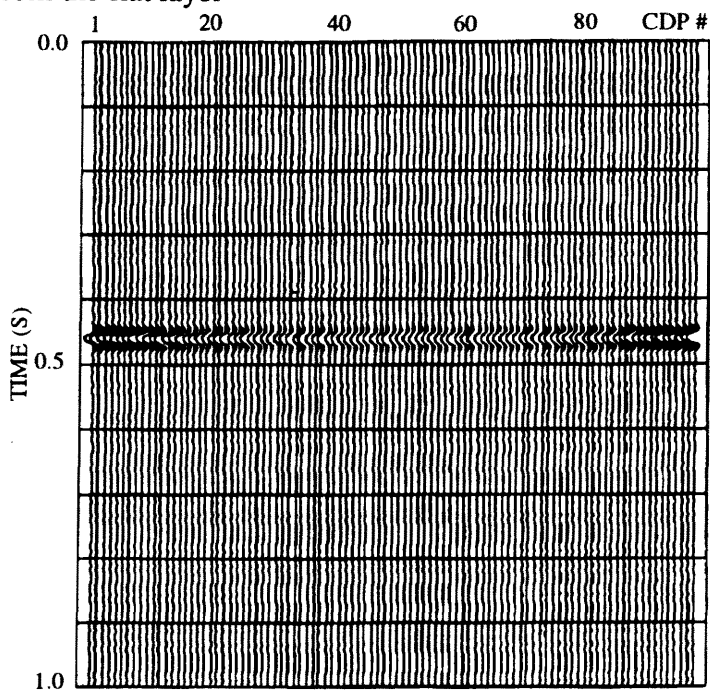


FIGURE 4.9 The stacked section of the transverse component. Only the reflection from the fault plane is on the section.

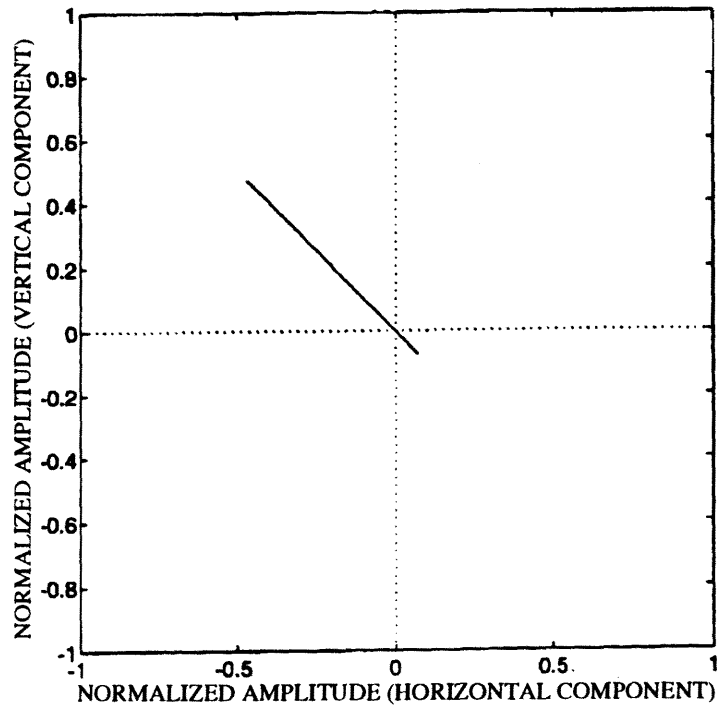


FIGURE 4.10 The hodogram of the reflection from the fault. The polarization direction is 135° . The width of the window is 30 ms from 444 to 474 ms, on trace 10 of record 3.

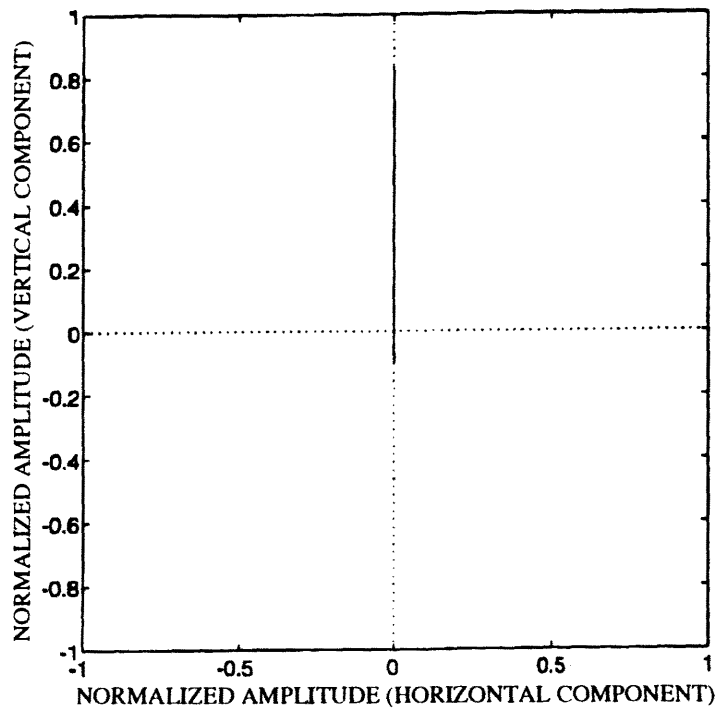


FIGURE 4.11 The hodogram of the reflection from the flat layer. The polarization direction is 90° . The window is from 484 to 514 ms on trace 10 of record 3.

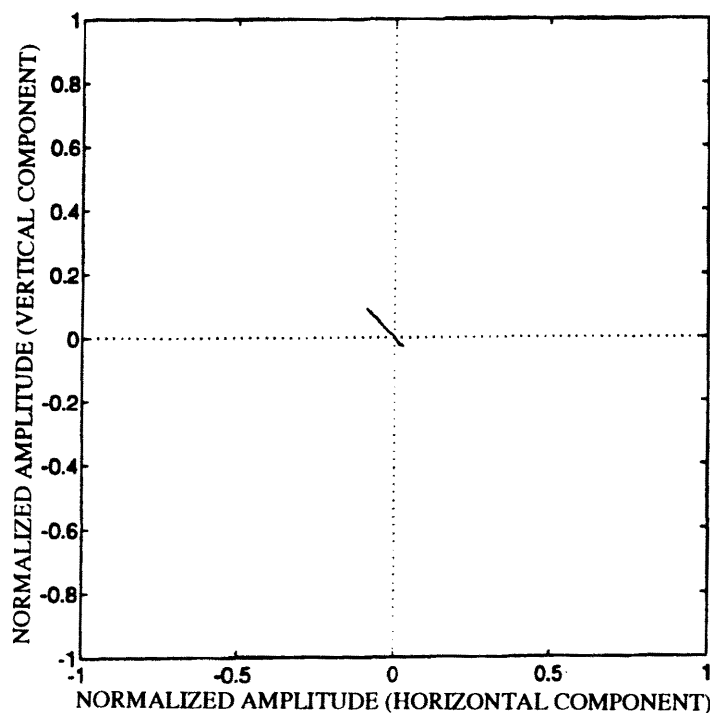


FIGURE 4.12 The hodogram from 505 to 535 ms on trace 35 of record 3, which indicates the wave propagation direction of the reflection from the fault plane is 135° .

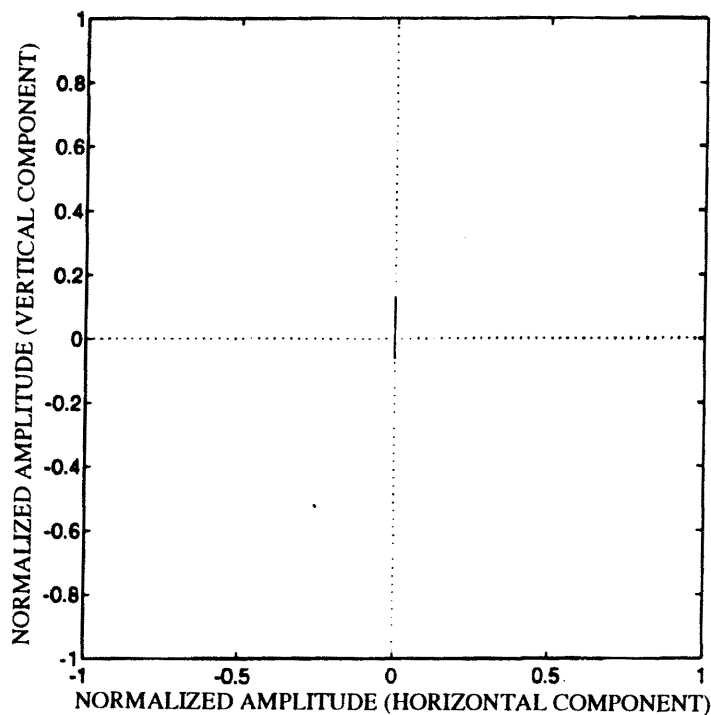


FIGURE 4.13 The hodogram from 545 to 575 ms on trace 35 of record 3, indicating the wave propagation direction of the flat layer reflection is 90° .

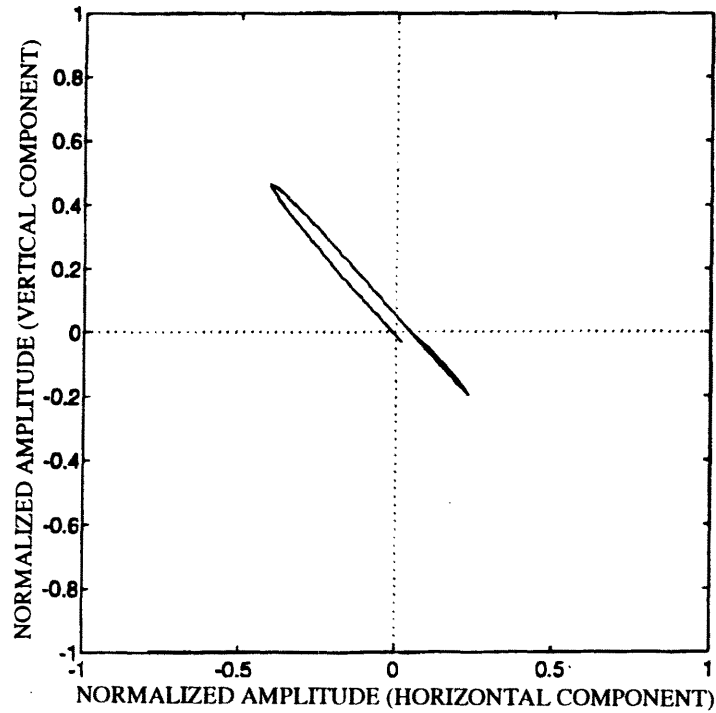


FIGURE 4.14 The hodogram of the stacked sections windowed at 440 - 470 ms on trace 40. The polarization direction is 135° , but the rectilinearity is less than 1.

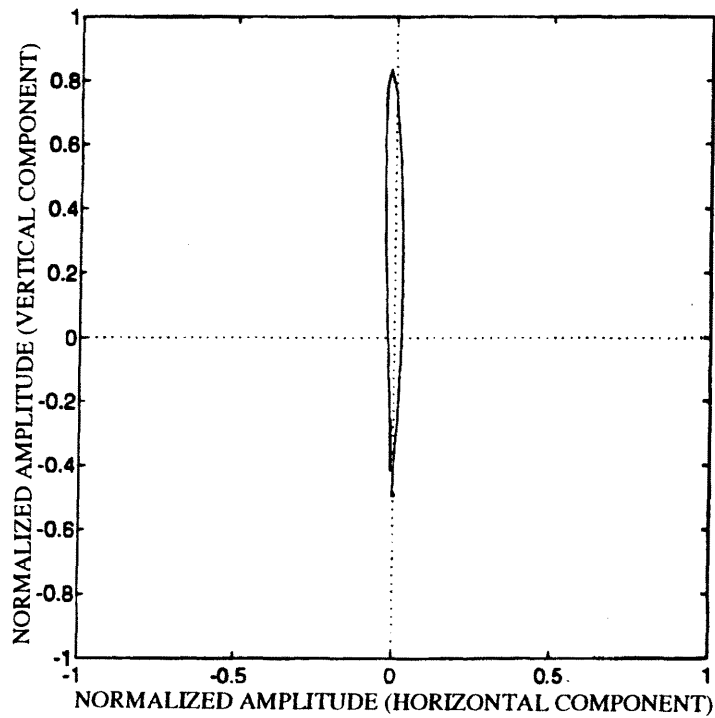


FIGURE 4.15 The hodogram of the stacked sections windowed at 485 - 515 ms on trace 40. The polarization direction is 90° and the rectilinearity is less than 1.

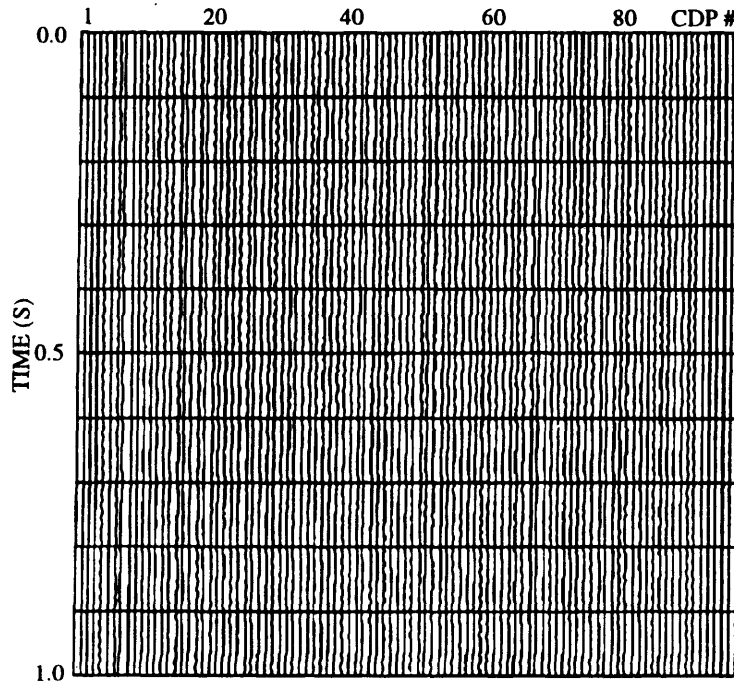


FIGURE 4.16 Pre-stack directional filtered stacked section. The direction window is $75^{\circ} - 85^{\circ}$. There is no signal on the section.

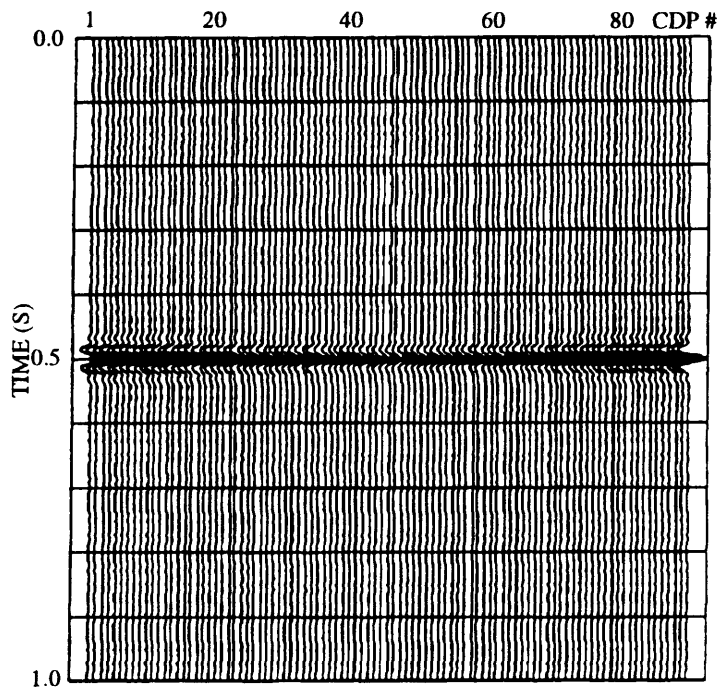


FIGURE 4.17 Pre-stack directional filtered stacked section. The direction window is $85^{\circ} - 95^{\circ}$. There is one event at 0.5 s on the section. It is from the flat layer.

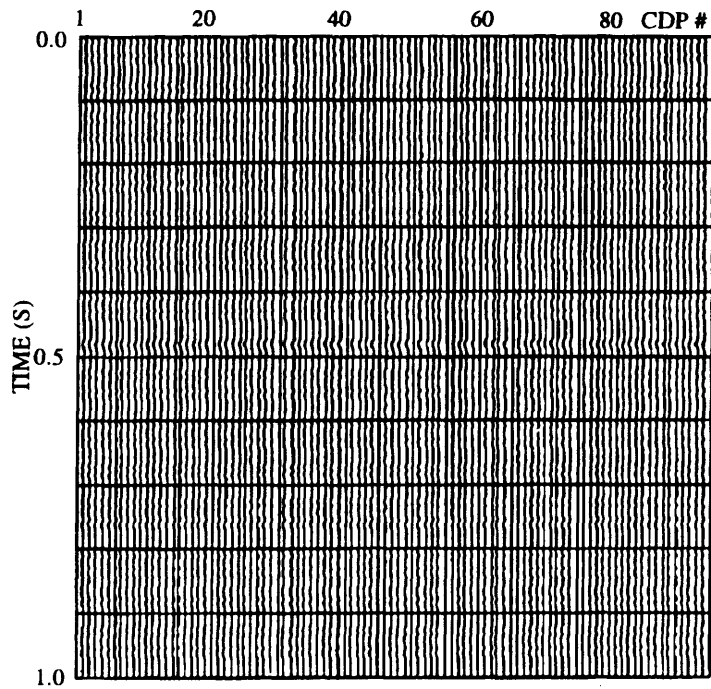


FIGURE 4.18 Pre-stack directional filtered stacked section. The direction window is $95^{\circ} - 105^{\circ}$. There is little signal on the section.

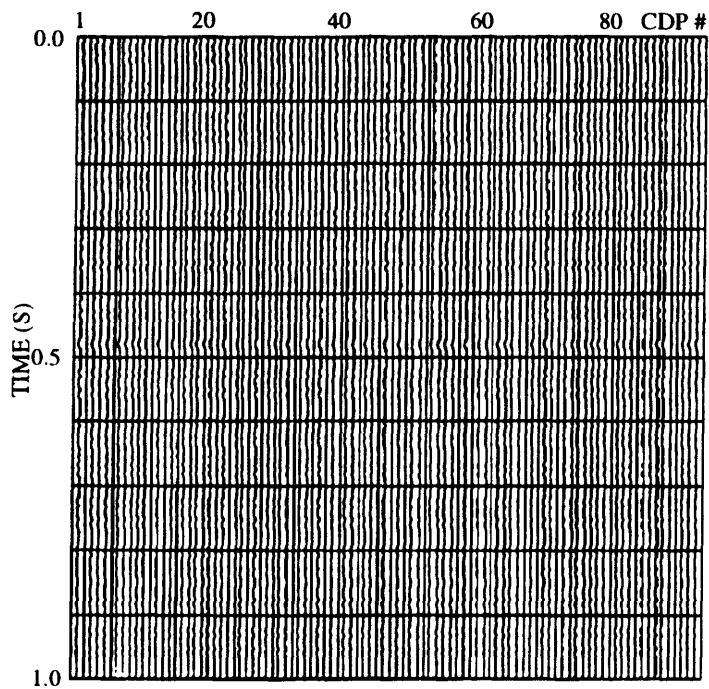


FIGURE 4.19 Pre-stack directional filtered stacked section. The direction window is $105^{\circ} - 115^{\circ}$. There is little signal on the section.

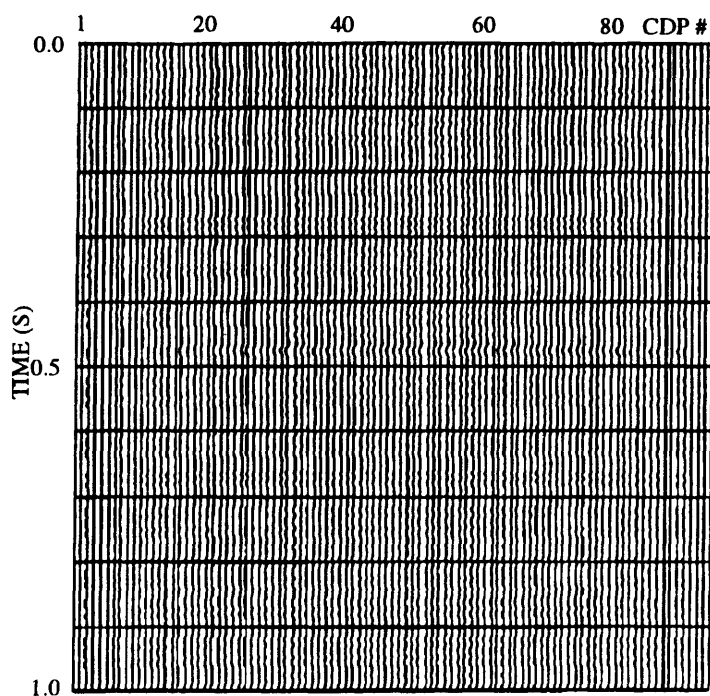


FIGURE 4.20 Pre-stack directional filtered stacked section. The direction window is $115^{\circ} - 125^{\circ}$. There is little signal on the section.

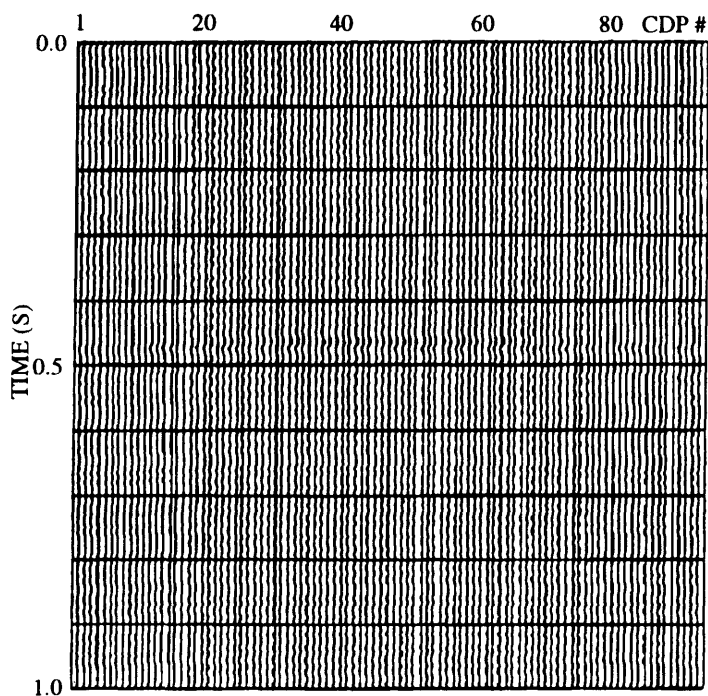


FIGURE 4.21 Pre-stack directional filtered stacked section. The direction window is $125^{\circ} - 130^{\circ}$. There is little signal on the section.

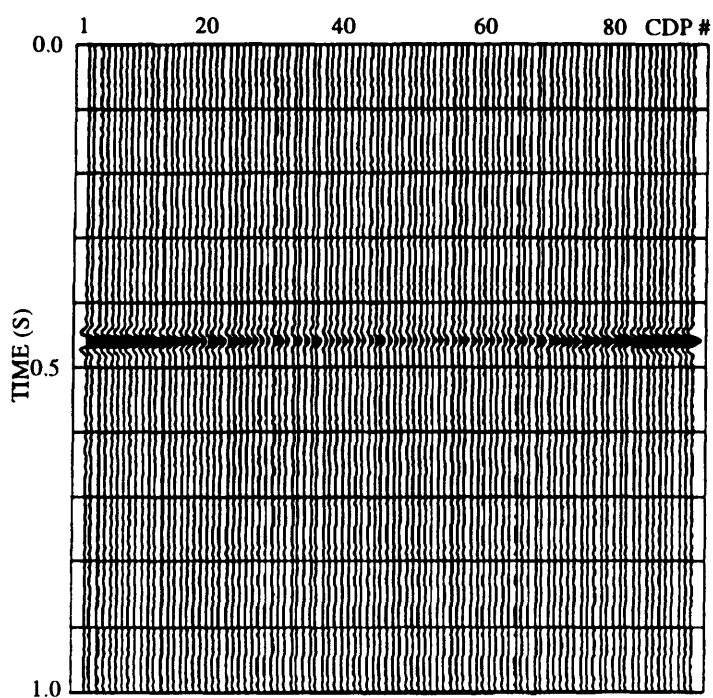


FIGURE 4.22 Pre-stack directional filtered stacked section. The direction window is $130^{\circ} - 140^{\circ}$. There is an event on the section at 0.46 s. It is from the fault plane.

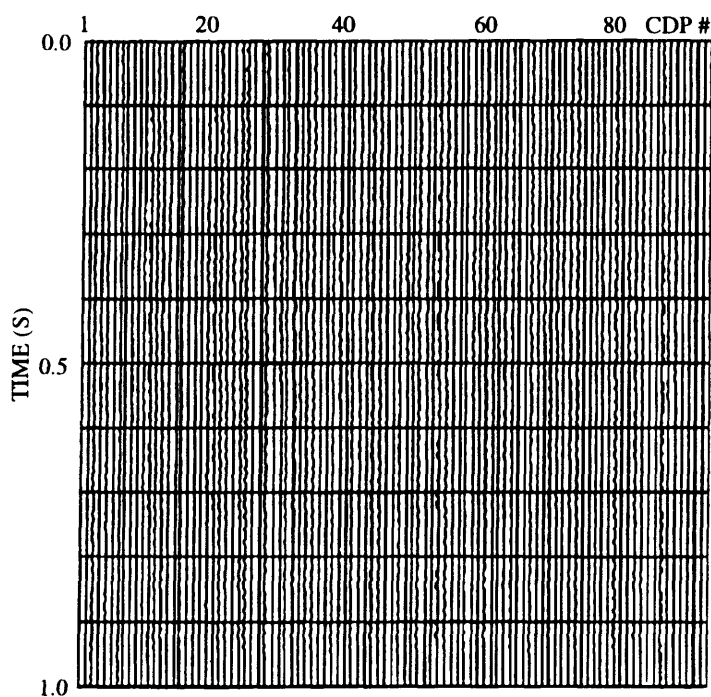


FIGURE 4.23 Pre-stack directional filtered stacked section. The direction window is $140^{\circ} - 145^{\circ}$. There is no signal on the section.

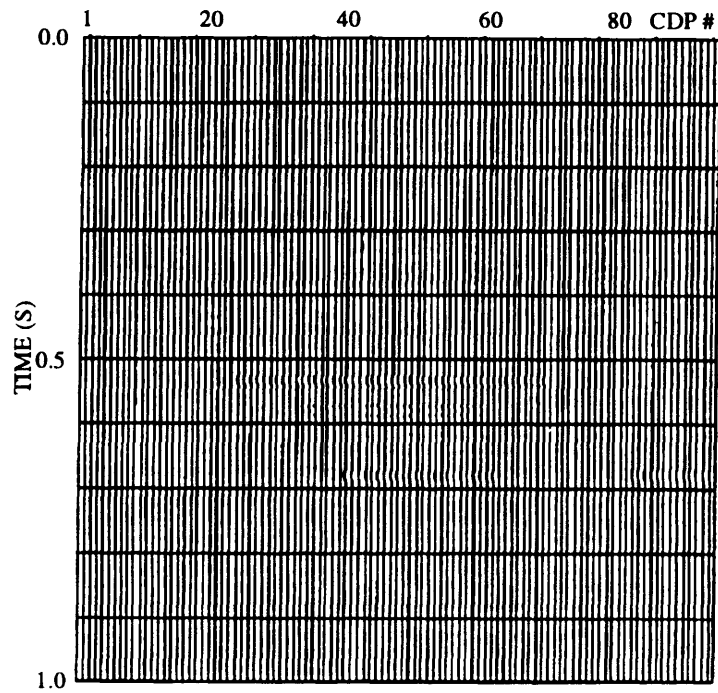


FIGURE 4.24 Post stack directional filtered stacked section. The direction window is $75^{\circ} - 85^{\circ}$. There is little signal on the section.

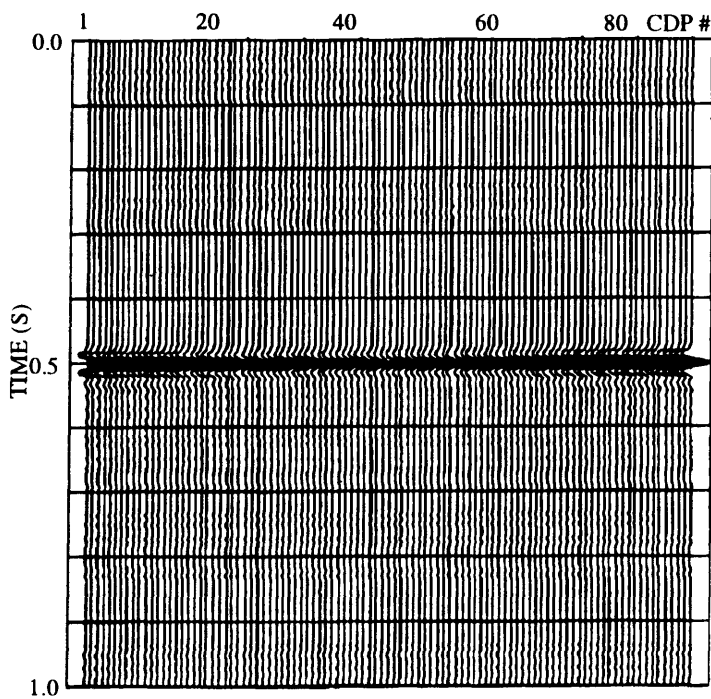


FIGURE 4.25 Post stack directional filtered stacked section. The direction window is $85^{\circ} - 95^{\circ}$. There is an event on the section at 0.5 s. It is from the flat layer.

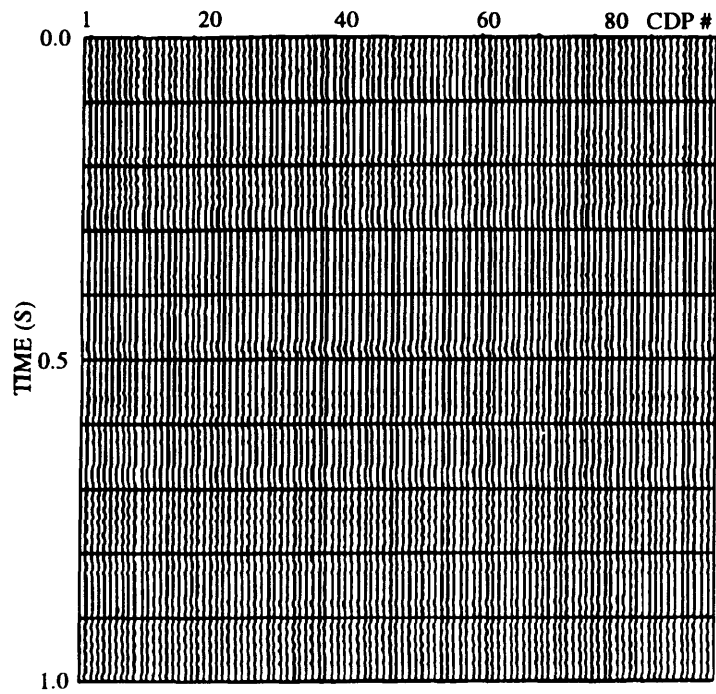


FIGURE 4.26 Post stack directional filtered stacked section. The direction window is $95^{\circ} - 105^{\circ}$. There is little signal on the section.

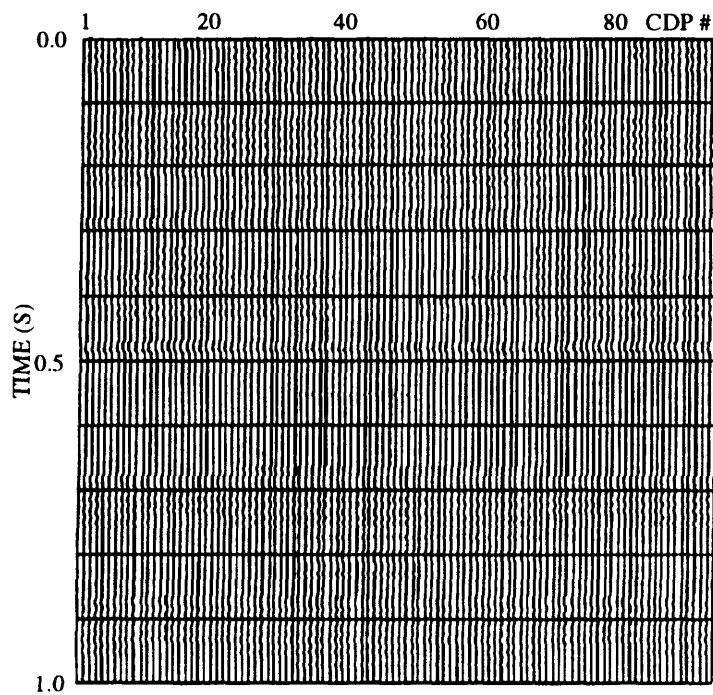


FIGURE 4.27 Post stack directional filtered stacked section. The direction window is $105^{\circ} - 115^{\circ}$. There is little signal on the section.

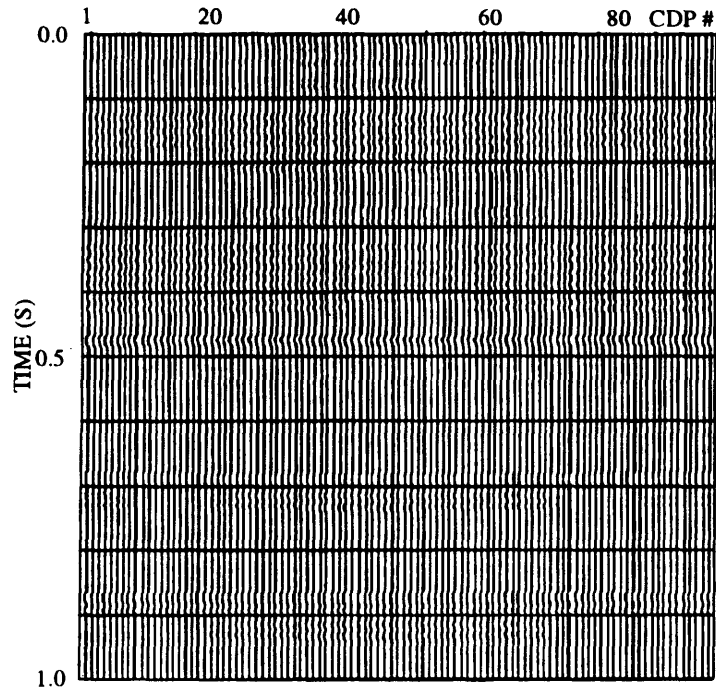


FIGURE 4.28 Post stack directional filtered stacked section. The direction window is $115^{\circ} - 125^{\circ}$. There is no signal on the section.

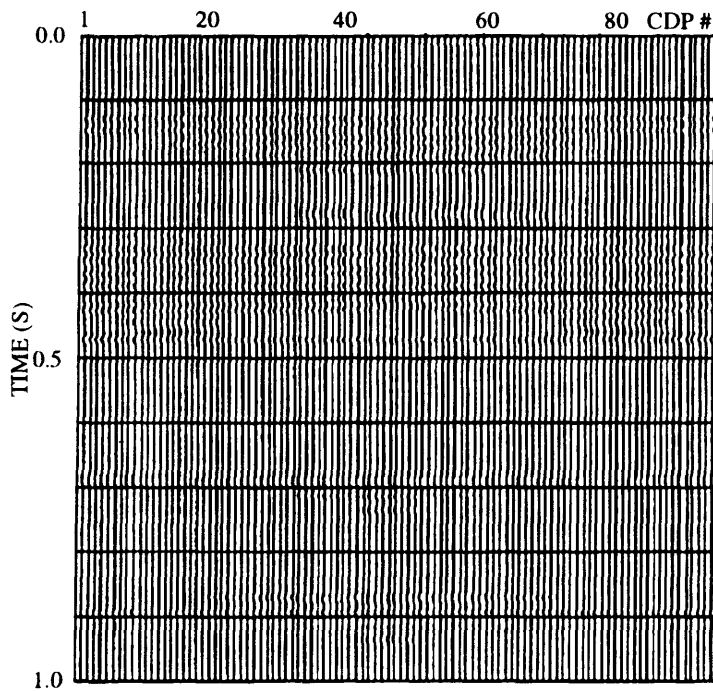


FIGURE 4.29 Post stack directional filtered stacked section. The direction window is $125^{\circ} - 130^{\circ}$. There is little signal on the section.

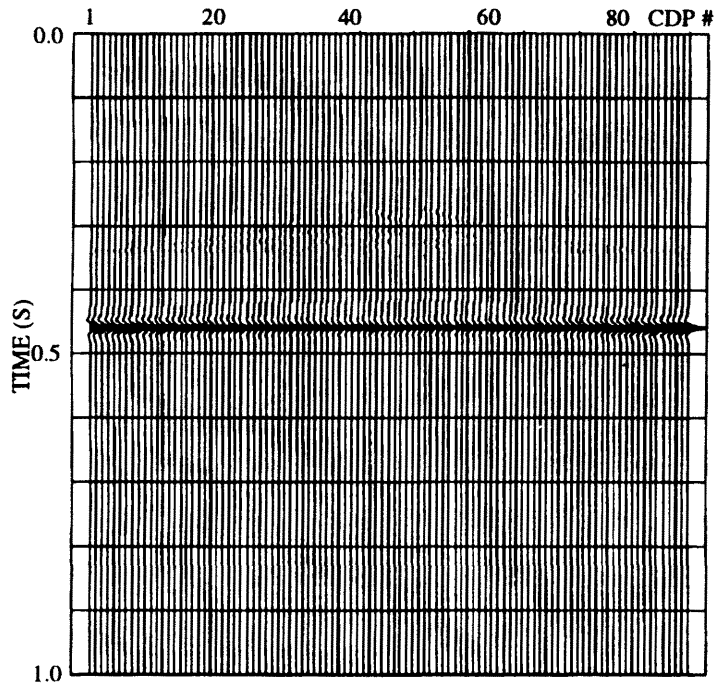


FIGURE 4.30 Post stack directional filtered stacked section. The direction window is $130^{\circ} - 140^{\circ}$. There is one reflection on the section. It is from the fault plane.

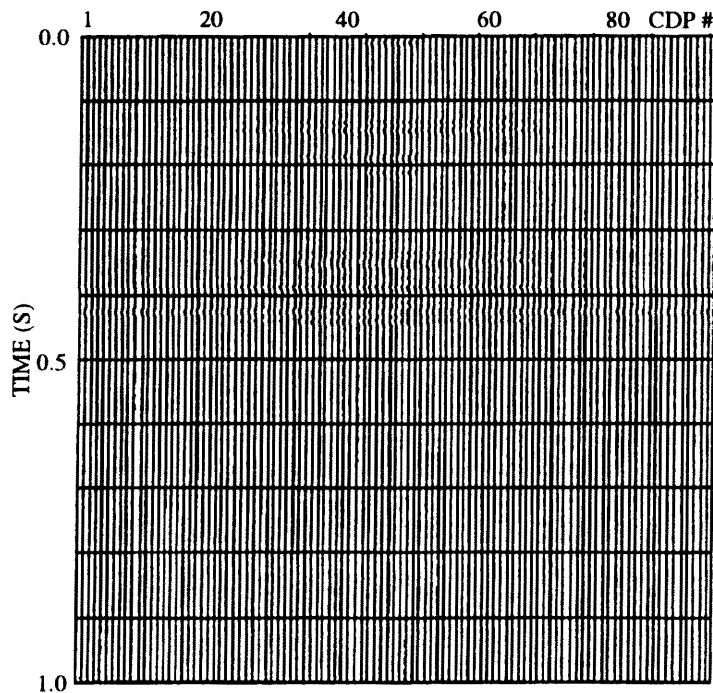


FIGURE 4.31 Post stack directional filtered stacked section. The direction window is $140^{\circ} - 145^{\circ}$. There is no signal on the section.

Chapter 5: Off-line imaging

5.1 Introduction

On a 2-D seismic line, we generally assume that the recorded seismic energy is from directly beneath the seismic line. In other words, the raypaths of the seismic wave are restricted to the vertical plane through the seismic line. In fact, in many 2-D seismic datasets, there are not only the reflections from the geological interfaces beneath the seismic line, but also some reflections and/or scattered energy from structures away from the line. These off-line energies can degrade the quality of the seismic data. Moreover, they can lead to misinterpretation of the seismic data. For example, if there is a reef beside the seismic line, the line records both reflections from the interfaces beneath the line and the reef beside the line. On the processed section, there may be a reef image. One might think the reef is just beneath the seismic line. To eliminate the misinterpretation of conventionally processed 2-D seismic sections, it is necessary to separate the in-line and off-line energies. We can take advantage of 3-component seismic data to: 1) enhance the S/N ratio and improve the quality of the conventionally processed sections by rejecting the off-line energy; 2) build an image of the off-line reflection to get a partial 3-D image from a 2-D seismic line by rejecting in-line energy (Zheng and Stewart, 1993; 1994).

Perelberg and Hornbostel (1994) discussed some applications of polarization analysis. One of these applications is removal of off-line energy. They built a numerical fault and dome model and generated 3-component seismic data. The off-line reflection is removed by the polarization filter using covariance matrix method. We would like to extend the application of the polarization filter from synthetic data to real data in this chapter.

In previous chapters, we discussed the polarization filter and applied it to a simple synthetic data to separate the seismic waves from different directions. In this chapter, we will apply the polarization filter to two more complicated synthetic models and one physical model. In these models, the off-line energy is from a "reef" instead of a fault plane. Therefore, the off-line energy is more like scattered waves rather than a planar

reflection, and it is weaker than that from the fault plane. Moreover, we also tested the polarization filter on real data to reject off-line energy in order to enhance in-line energy. The field data we used is provided by Gulf Canada Resources Ltd. The line is in Rumsey area, Central Alberta, which passes through a pinnacle reef.

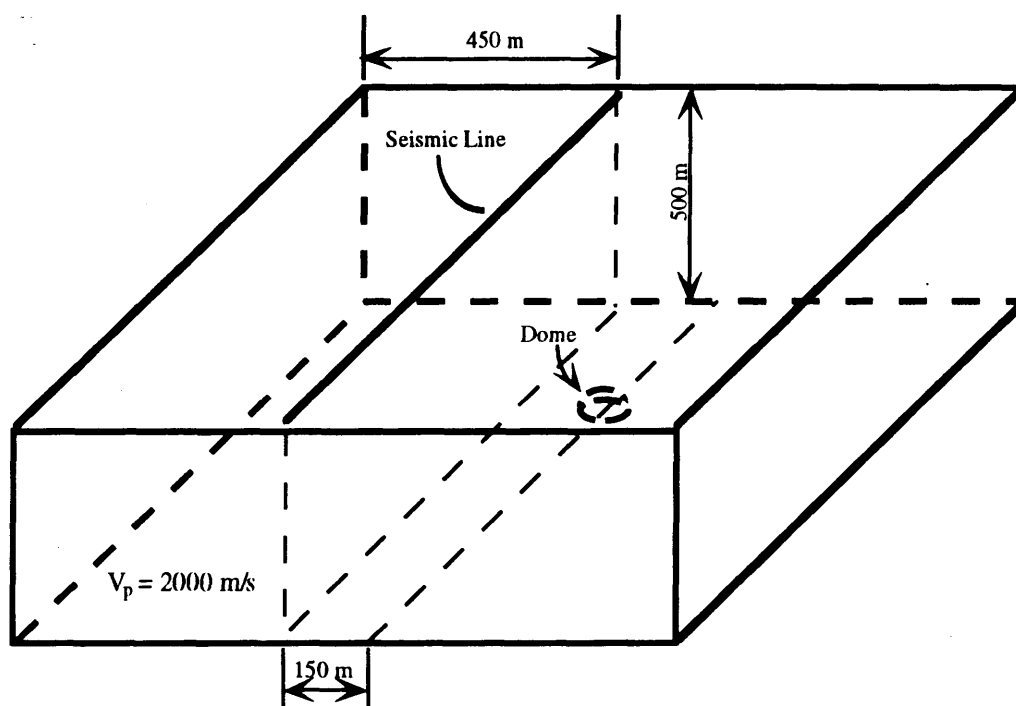


FIGURE 5.1. The single layer numerical model. The thickness of the layer is 500 m. The P-wave velocity is 2000 m/s. There is a dome on the bottom of the layer and the offset from the seismic line to the dome is 150 m. The height of the dome is 100 m. The cross profile of the bottom of the dome is an ellipse with a long axis of 75 m parallel to the seismic line.

5.2 Synthetic modeling data

The first synthetic model used for building the off-line image is shown in Figure 5.1. The model is composed of a layer overlying a half space. The thickness of the layer is 500 m. There is a dome on the bottom of the layer. The bottom of the dome is an ellipse. The long axis is 75 m (parallel to the seismic line) and the short axis is 50 m. The height of the dome is 100 m. It is 150 m away from the seismic line laterally. The

P-wave velocity of the medium is 2000 m/s and the P-wave velocity is 2700 m/s for the half space. There is a seismic line on the surface. The line is 1000 m long. There are total 51 stations on the line and the station interval is 20 m. A total of 11 shots are recorded by all stations except the one on the shot point. The shot interval is 100 m (Figure 4.3).

Figures 5.2 and 5.3 show the vertical and transverse components of two shot records. We added 10% random noise to the records. In the vertical component data, we can see a hyperbolic shaped coherence in the time range of 0.5 - 0.6 s, which is the reflection from the bottom of the layer. We also can see some scattered energy in the middle part of the line at the time of 0.43 s approximately, which is the scattered wave from the top of the dome. In the transverse component data, it is hard to see coherent signal because of the noise.

A conventionally processed migrated section is shown in Figure 5.4. In the section, we can see a flat horizon at the of 0.5 s. It is the bottom of the layer. Also, we can see a very weak image in the middle of the line at time of 0.43 s. It is the image of the dome. Figure 5.5 is the in-line energy enhanced migrated section. We enhanced the waves from the directions of 85° - 95° to produce this section. Figure 5.6 is the off-line energy enhanced migrated section. We enhanced the waves from the direction range from 105° to 115°. In Figure 5.5, we still can see a little bit dome energy left in the in-line energy enhanced section. This is because, as we discussed in Chapter 3, the noise can somewhat effect the polarization direction of a signal. That means there is some energy leaking. Figure 5.6 tells us a new story. It brings us a new point of view of 2-D seismic line. The dome is not directly beneath the seismic line. It comes from a side of the seismic line. Figure 5.6 gives a clear off-line image. From the direction window of the polarization filter and the two-way time on the off-line enhanced section, we can estimate the location and the depth of the dome. As we know the window is from 105° to 115°. The measured two way time from Figure 5.6 is about 0.43 s. In this simple case, we already know that there is only one layer and the P-wave velocity is 2000 m/s. Therefore the distance from the dome to the seismic line is about:

$$D = 0.43 \times 2000 / 2 = 430 \text{ m} \quad (5.1)$$

Now we can get the minimum lateral distance from the dome to the line:

$$S_{\min} = D \cos 105^\circ = -111.3 \text{ m} \quad (5.2)$$

The maximum lateral distance is:

$$S_{\max} = D \cos 115^\circ = -181.7 \text{ m} \quad (5.3)$$

The negative distance means the dome is on the right side of the seismic line, according to the definition of the wave direction in Chapter 4 (Figure 4.9). It gives us an approximate location of the dome that we can see from 2-D seismic line, although it is not very accurate. Comparing with the actual offset of 150 m of the “reef” in Figure 5.1, the polarization filter yields a reasonable and acceptable result. This image of the off-line energy provides more detailed information than the conventionally processed 2-D seismic line, and could help design future exploration programs: what data to buy or where to put further 2-D or 3-D surveys.

In a real situation, there is a weathering layer with low velocity on the surface. This low velocity layer bends the seismic raypath to close to vertical direction. In other words, this low velocity layer makes the difference of the directions of in-line reflection and off-line reflection smaller. It makes the direction separation difficult. To test the polarization filter in the case of low velocity weathering layer, we built another synthetic model. Figure 5.7 is a two-layer model. The thickness of the first layer is 20 m and the P-wave velocity is 1300 m/s. The thickness of the second layer is 480 m and the P-wave velocity is 2000 m. Like the model in Figure 5.1, there is a dome 150 m away from the seismic line. The height of the dome is 50 m. The raypaths in Figure 5.7 show there are three events recorded in the seismic line, two reflections from the bottoms of the two flat layers, respectively, and an off-line scattered wave from the dome. We applied the polarization filter with a direction window of $95^\circ - 105^\circ$ to reject the in-line energy and enhanced the off-line energy. Figure 5.8 is the migrated section of the off-line energy enhanced data. It shows a dome image in the centre of the line and at time of 0.47 s. To estimate the location of the dome in multilayer case, the interval velocities and the thicknesses of all layers above the dome should be used. Taking the low velocity layer into account, the approximate range of the location of the dome is from 79.2 m to 235.3 m on the right side of the seismic line. This example indicates that even with the

existence of the low velocity weathering layer, the polarization filter still can separate the in-line and off-line energies and build an image of the off-line energy.

5.3 Physical modeling data

In moving from synthetic to real data, we consider a physical modeling case. The physical model we used to test the polarization filter is shown in Figure 5.9. The model is made of plexiglas. We built a "reef" on the bottom of the model. The "reef" anomaly in the plexiglas plate is a milled-out hole. The plate is supported by a jig apparatus. Therefore, the top and bottom surfaces of the layer and the surface of the "reef" are free surfaces. A scale factor between the actual dimension of the model and the field size based on the ultrasonic and seismic frequency is 10, 000. The seismic line is then a scaled distance of 200 m away from the reef. The P-wave velocity of the plexiglas is 2750 m/s. An end-on spread of geophone cable is used in the seismic survey. The near offset is 200 m and the far offset is 1100 m. There are total 10 traces per shot. Both station and shot intervals are 100 m. A total of 12 shots were recorded in the survey. The maximum fold is 5.

A shot record of the physical modeling data is shown in Figure 5.10 (vertical component) and Figure 5.11 (transverse component). In both components, we can see some coherence. The strongest one is at time of 0.72 s approximately for trace 1. It is the reflection from the flat bottom of the model. The signal at time of 0.62 s for trace 1 is the reflection from the top of the "reef". There are also some coherent noise in the record. They are multiples and the reflections from the interfaces between plexiglas layers.

We used the conventional technique to process both vertical and transverse components of the physical modeling data. The stacked sections are shown in Figures 5.12 (vertical) and 5.13 (transverse). In both sections, we can see the image of the flat bottom of the model and the reef. The flat interface is at the time of 0.72 s. The reef image is in the middle part of the line and at the time of 0.62 s. We also can see clearly the diffraction at the edge of the "reef". The interesting thing is the amplitude and the phase change of the flat reflection. In the middle part of the line, the reflection is weaker than that at the ends of the line. The wavelet is changing from zero phase on the ends to mixed phase in the central part. It is noticed that this anomaly appears at the same location of the "reef" reflection. It implies that there is some relationship between them.

When we look at Figure 5.9 closely, we can find that the seismic line can not only record the reflections from the flat bottom and the top of the "reef", but also the reflection from the bottom side of the "reef" (point A in Figure 5.9). After a simple calculation, we found the distance from point A to the seismic line is about 200 m. The two-way travel time from A to the seismic line is about 15 ms longer than the two-way travel time from the flat bottom to the line. The dominant frequency of the seismic wave here is about 30 Hz. That means the reflection from point A is delayed about a half cycle compared with the reflection from the flat bottom. Therefore, the energy from the flat bottom was partially canceled by the reflection from point A, and the phase was also changed by the reflection from A.

We applied the polarization filter to the physical modeling data. When we use a direction window of $50^\circ - 85^\circ$, there is no signal left in the final stacked section (Figure 5.14). If we use the direction window of $85^\circ - 93^\circ$, the "reef" reflection is successfully removed from the stacked section (Figure 5.15). Only the reflection from the flat bottom of the model is left in Figure 5.15. When we change the direction window to $95^\circ - 105^\circ$, we removed the reflection from the flat bottom (Figure 5.16). In this stacked section, the only signal is the reflection from the top of the "reef". When we use the direction window of $105^\circ - 150^\circ$, almost all signals are removed from the stacked section (Figure 5.17). We also can calculate the approximate location of the "reef". The two-way travel time of the "reef" reflection measured from Figure 5.16 is 0.615 s. Therefore the distance from the top of the "reef" to the seismic line is:

$$D = 0.615 \times 2750 / 2 = 846 \text{ m} \quad (5.4)$$

The minimum lateral distance from the seismic line is:

$$S_{\min} = D \cos 95^\circ = -74 \text{ m} \quad (5.5)$$

The maximum lateral distance is:

$$S_{\max} = D \cos 105^\circ = -219 \text{ m} \quad (5.6)$$

Similar to the above calculation, the minimum depth of the "reef" is:

$$D_{\min} = D \sin 105^\circ = 817 \text{ m} \quad (5.7)$$

The maximum depth of the “reef” is:

$$D_{\max} = D \sin 95^\circ = 842 \text{ m} \quad (5.8)$$

These figures are close to the figures measured from the model (Figure 5.9). Actually, the distance from the “reef” to the seismic line is 200 m and the angle of the raypath from the “reef” is about 103.5°. We underestimated the location of the “reef” somewhat. It could be caused by the free surface effect.

5.4 Field data of Rumsey area

In 1987, Gulf Canada Resources Ltd. shot a 3-component seismic line (87G53-01) in Rumsey area, Central Alberta (Figure 5.18). This line goes through the Rich D3A Oil Pool, which is a pinnacle reef in Leduc Fm. The Rich field is located in the southern part of the east Ireton Shale basin, southwest of the Fenn-Big Valley reef complex and east of the Bashaw reef complex. The Leduc Fm reefs in the area developed as isolated pinnacles and large atolls. Pinnacles in this area typically attain heights of 200 m and are overlain by Ireton Fm shales (Anderson et al, 1989). The 9-36-34-21W4M well is tied with the seismic line 87G53-01 at field station number 176. It penetrated Leduc Fm and is an oil producer. Figure 5.19 is the Leduc structure map around the well. The major geological interfaces around the line, including Cooking Lake, Calmar, Wabamun and Banff, are almost flat with a slight dip to west. For the Cooking Lake, the maximum dip angle is 14°. For Calmar, Wabamun and Banff, the dip angle is less than 5° (Anderson et al, 1989). There is no major structure beside the line. Therefore we cannot expect to build an off-line structure image from this line. We applied polarization filter to this line to reject off-line scattered noise and to enhance the in-line image.

Line 87G53-01, which was acquired by Airborne Geophysical Surveys Ltd. for Gulf Canada Resources Ltd., runs from north to south from station 101 to station 257 with station interval of 30 m. OYO 3-component geophones and Gus Bus I recording system were used to record the seismic waves. The source is 2 kg dynamite at a depth of 18 m. All 157 stations recorded for all shots. There are a total of 38 shots. The best shot record is shown in Figure 5.20 (vertical component) and Figure 5.21 (transverse

component). We can see that the raw data are very noisy. There is strong ground roll at near offsets and high frequency noise all over the record.

The sonic log and synthetic seismogram with a 20 Hz Ricker wavelet for the well 9-36-34-21W4M which ties the seismic line is shown in Figure 5.22. The conventionally processed vertical component section is shown in Figure 5.23 and an enlarged section of Figure 5.23 with the synthetic seismogram inserted at the proper location is shown in Figure 5.25. In Figure 5.25, the reverse polarity of the synthetic seismogram is used, because it ties the seismic section better. Although the frequency of the synthetic seismogram is lower than the frequency of the seismic section, major features tied very well. We can see the overlying interfaces, Wabamun, Banff and Mannville, are bumping above the reef. We also can see the velocity pull-up on the underlying interfaces. Figure 5.24 is the stacked section the transverse component. There is little coherent signal on the transverse component section. As we described before, the line passes over the top of the reef and there is no off-line structure around the line so that the off-line energy on the seismic section is scattered noise. We used the polarization filter to reject the off-line energy to enhance the S/N ratio of the seismic section instead of building an off-line image. One thing that should be mentioned is that based on the information we collected, we do not know the geophone and instrument responses. Therefore the seismic signal has not been calibrated. This means the direction we measured from the seismic data may not be the true wave direction. In the following discussion, the value of direction is the value we measured from the seismic data. In any case we are trying to reject the off-line energy. So we do not have to estimate the location of the off-line sources. Figures 5.26, 5.27 and 5.28 are the polarization filtered sections using different direction windows. It appears that the 20° - 160° window is best choice for this line. Comparing Figures 5.26 and 5.25, all coherent signals are preserved and the noise is reduced. Figure 5.26 is somewhat clearer than the original section Figure 5.25. For example, at time of 1.33 s, there is a weak and discontinuous event cross the section. In Figure 5.25, the amplitude of this event is almost the same as the amplitude of the noise around the event. In Figure 5.26, it is easier to distinguish the event from the background noise, because the background noise was reduced by the polarization filter. Windows 50° - 130° and 80° - 100° are too harsh. In Figures 5.27 and Figure 5.28, it is too clean on the part below 1.1 s and also some signals were removed at 1.34 s and 1.48 s. Although Figures 5.27 and 5.28 are too clean to be true, the horizons above the Nisku were preserved. It indicates that the horizons above Nisku are almost flat or only have a very small dip angle.

5.5 Polarization processing procedures

From three-component seismic data, we can take the vertical and transverse components to enhance in-line image and build an off-line image. The polarization filter can be applied on the raw data, if the data have reasonable high S/N ratio to separate the in-line and off-line energy. Then we can use the filtered in-line data to create a better stacked section and the filtered off-line data to build an off-line image using conventional processing flow (choice I). If the data have low S/N ratio, an alternative way is to process the vertical and transverse components using conventional processing techniques separately, then to apply the polarization filter to the stacked sections of the vertical and transverse components to enhance in-line image and build off-line image (choice II). The processing flow charts are shown in Figures 5.29 and 5.30.

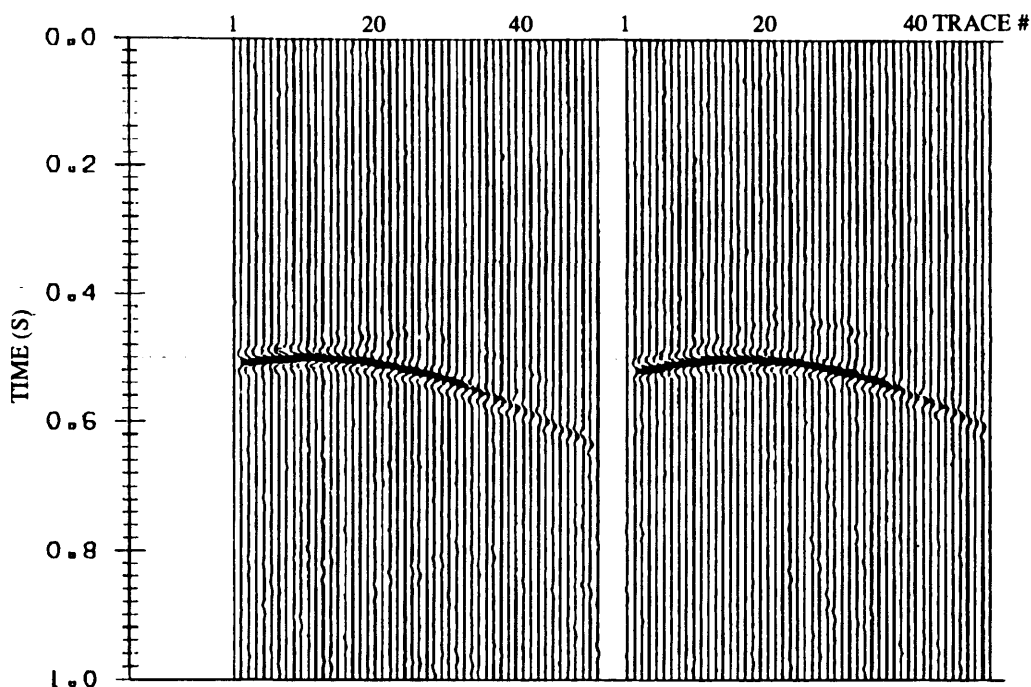


FIGURE 5.2. Two shots of the vertical component data recorded on the seismic line in Figure 5.1. There is strong reflection from the bottom of the layer and weak scattered wave from the dome that is 150 m away from the seismic line. Ten percent of random noise was added to the recordings.

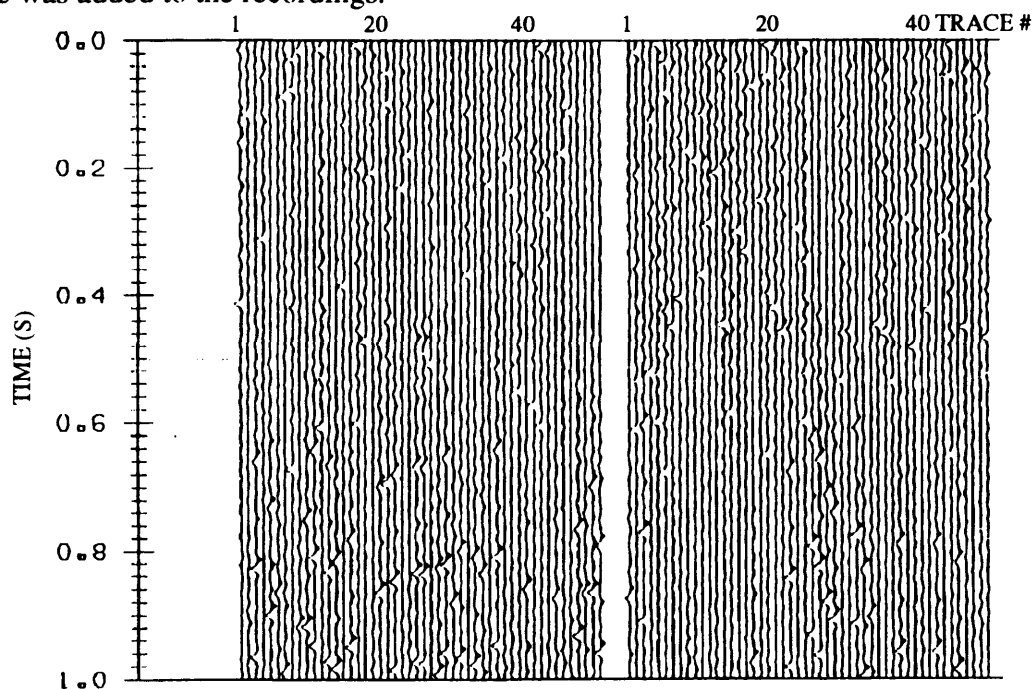


FIGURE 5.3. The transverse component of the same shots in Figure 5.2. Because of the noise, it is very difficult to locate the scattered wave.

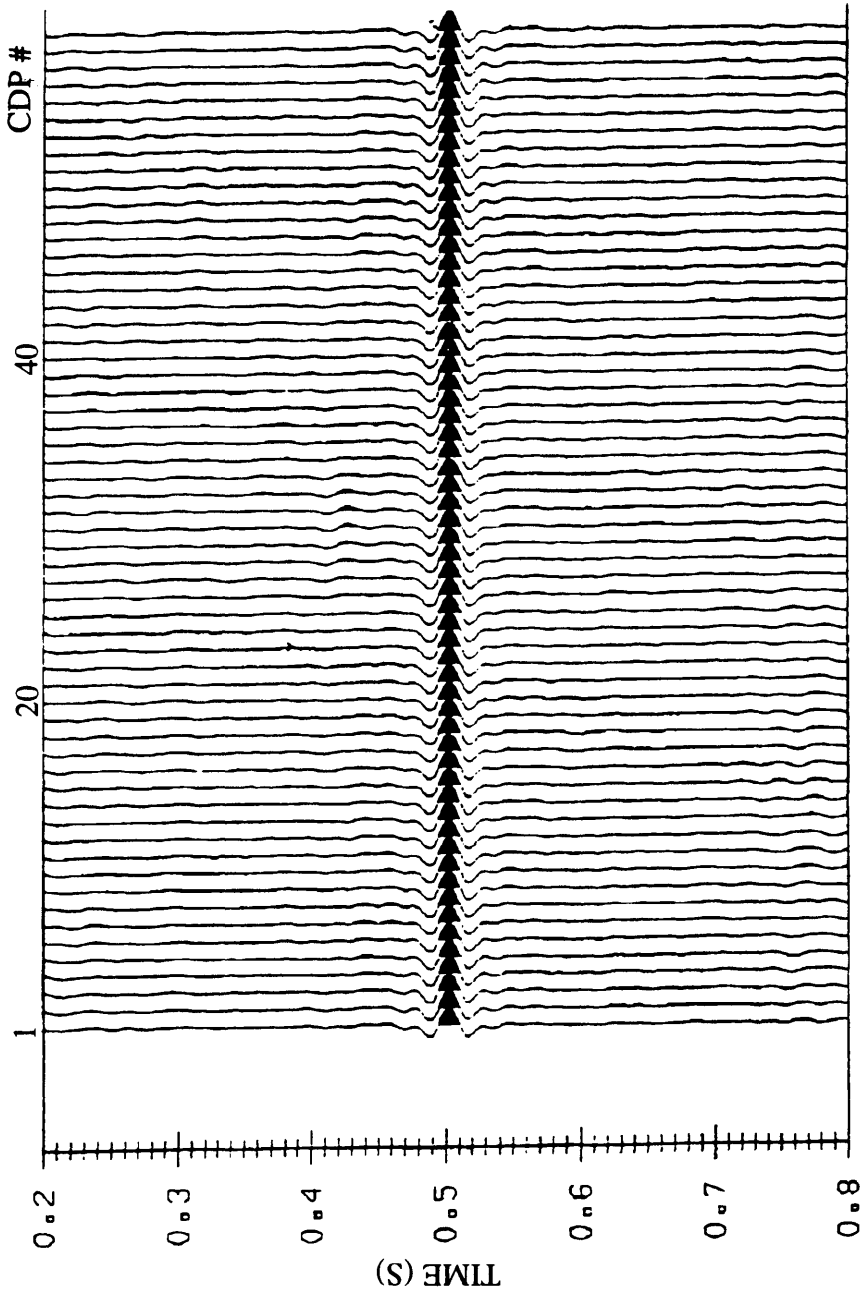


FIGURE 5.4. The migrated section of the vertical component. There is a flat layer at time of 0.5 s and also a weak dome image on the centre of the section and at time of about 0.42 s.

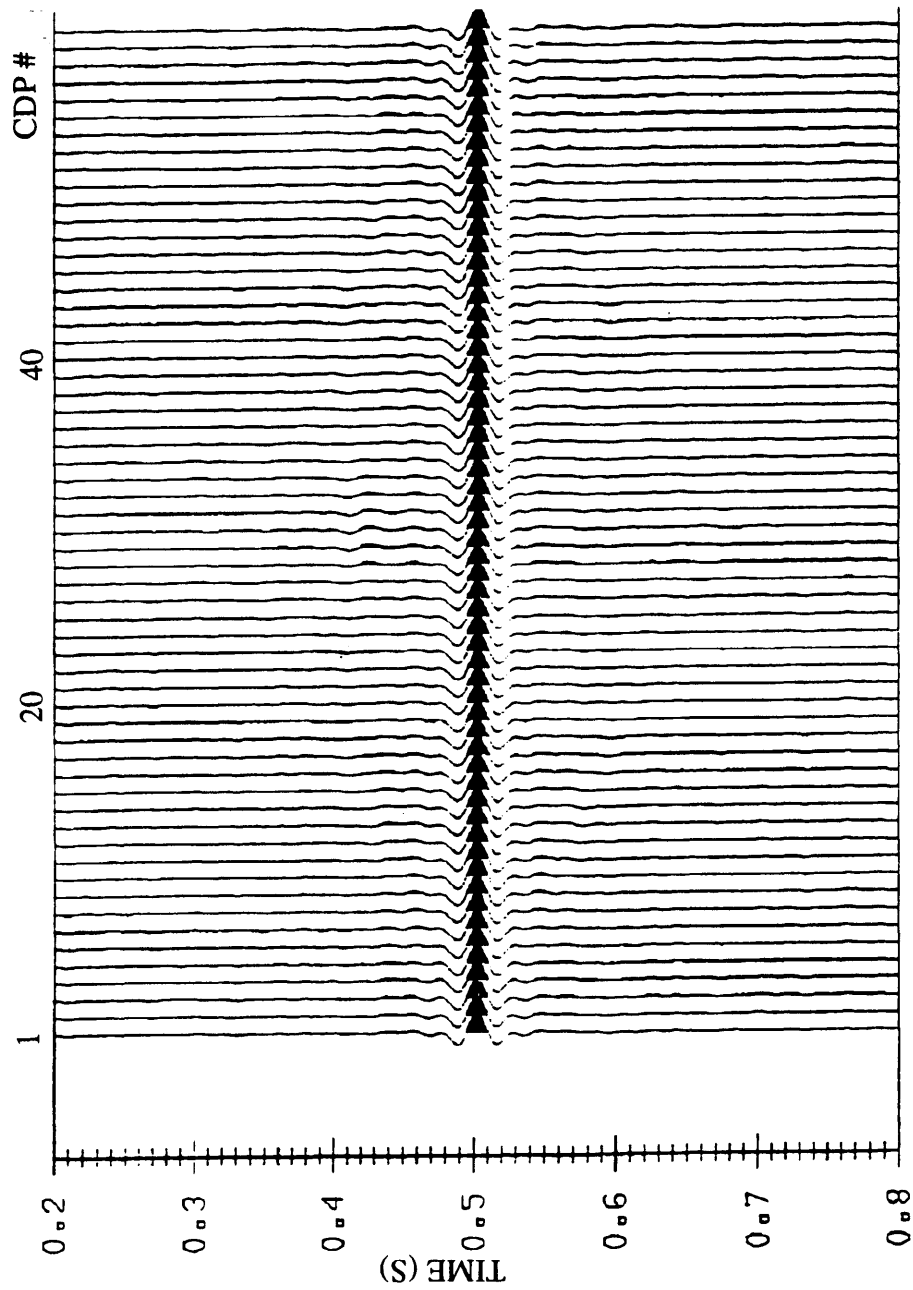


FIGURE 5.5. The in-line energy enhanced migrated section. There is a little bit energy leaking from the scattered wave.

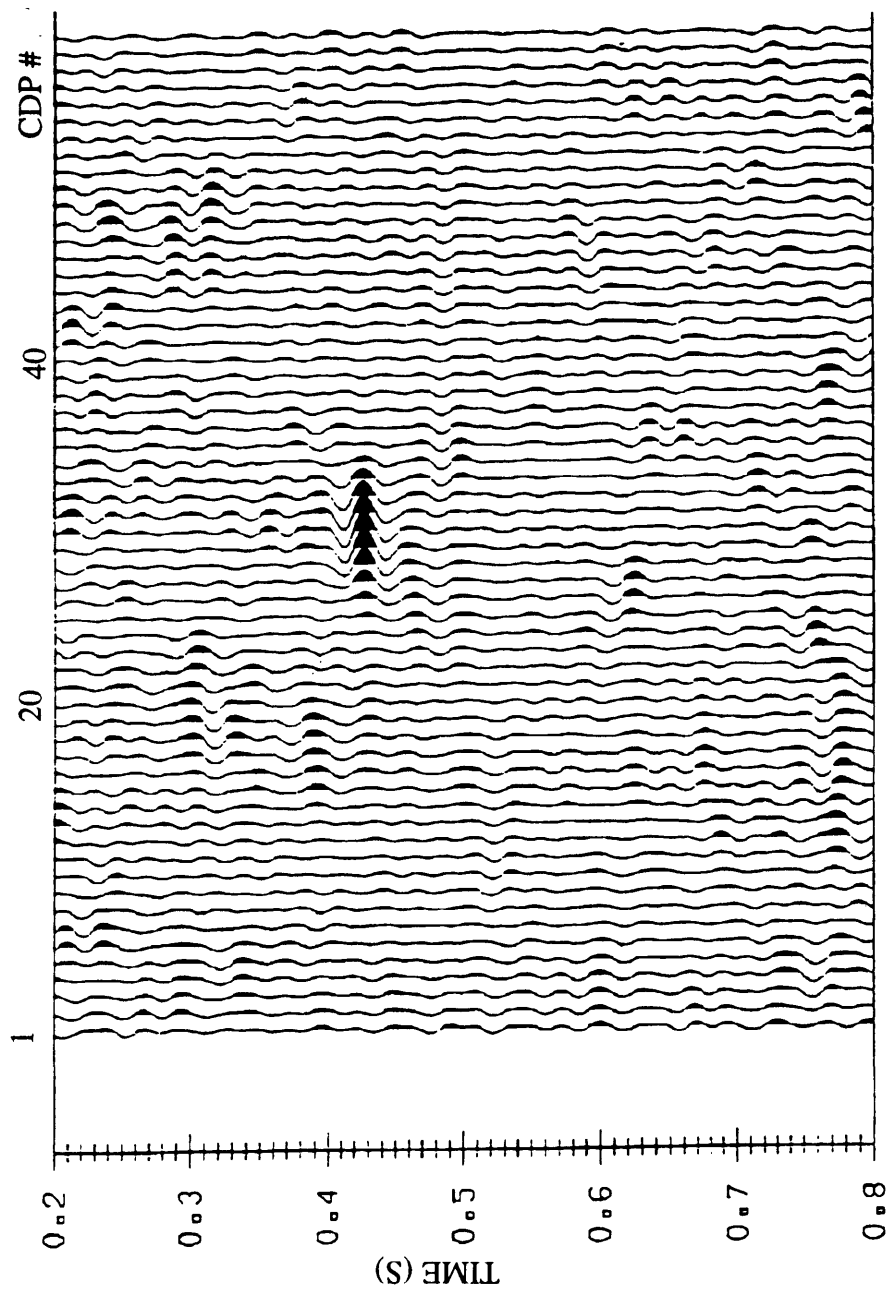


FIGURE 5.6. The off-line energy enhanced (105° - 115°) migrated section. The reflection from the flat layer no longer exists on the section. The dome image is enhanced.

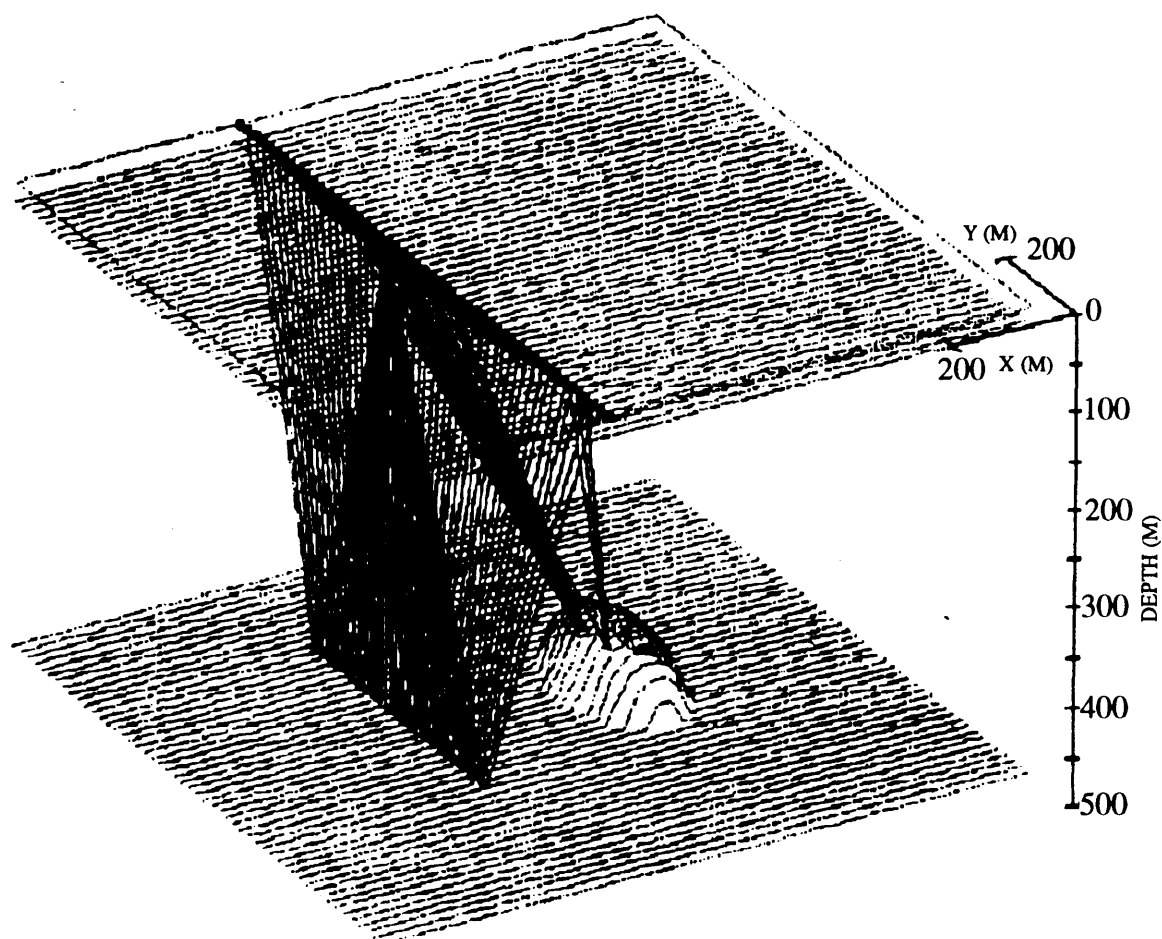


FIGURE 5.7. The two-layer synthetic model. The first layer is 20 m thick and its velocity is 1300 m/s. The second layer is 480 m thick and its velocity is 2000 m/s. There is a dome on the bottom of the second layer with the height of 50 m. The dome is 150 m away from the seismic line. From the raypaths of the seismic waves, we can see that there are three events recorded in the seismic line, two reflections from the bottom of the two layers, respectively, and the scattered wave from the dome.

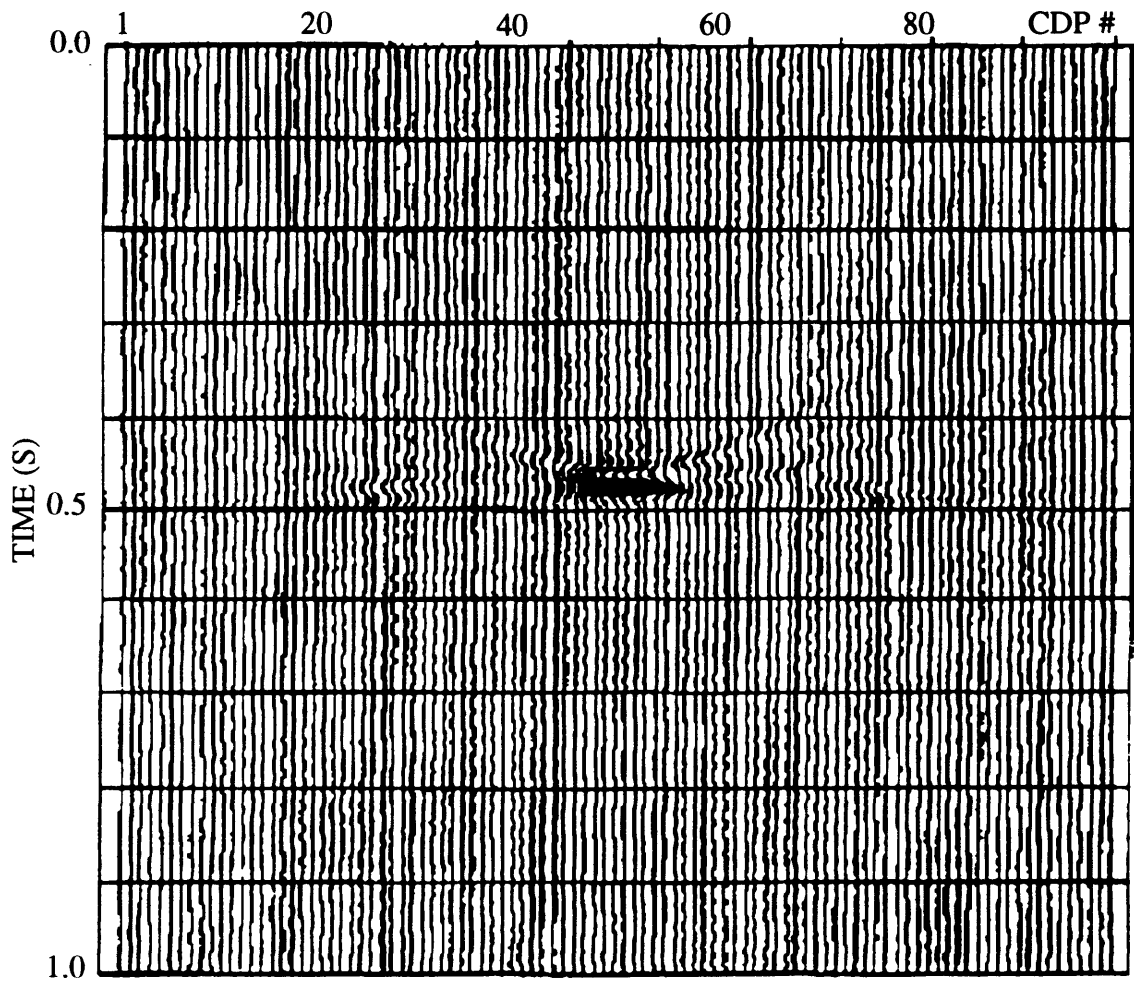
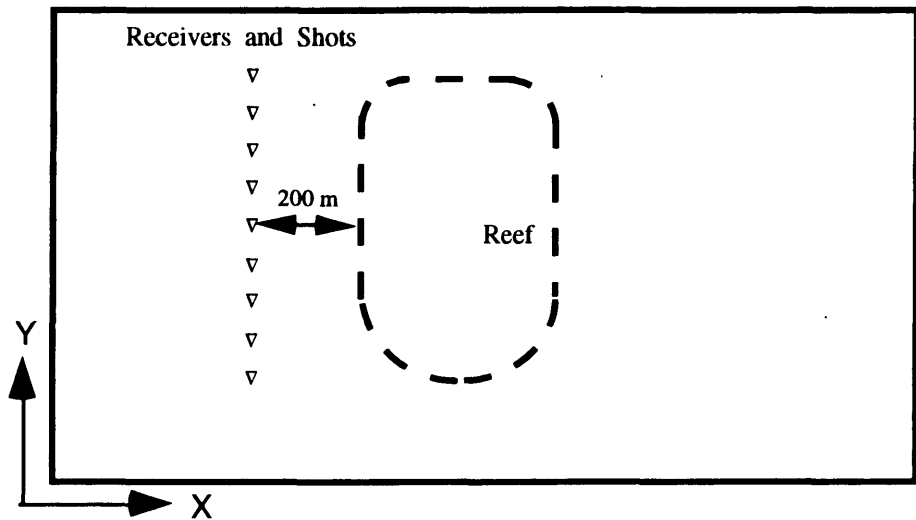
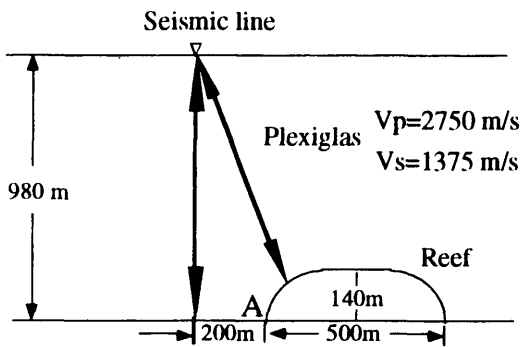


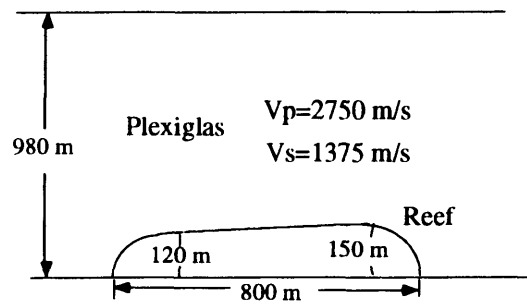
FIGURE 5.8. A polarization filter with a direction window of $95^{\circ} - 105^{\circ}$ was applied to the data recorded by the seismic line in Figure 5.7 to reject the in-line energy and enhance the off-line energy. This figure is a migrated section of the off-line energy enhanced data. We can see a clear image of the dome without the interference of the reflections from the flat layers.



a) Plan view



b) X-direction cross-section



c) Y-direction cross-section

FIGURE 5.9. The physical model used for testing polarization filter. The model is made of plexiglas. There is a milled-out hole on the bottom of the model. The P-wave velocity of plexiglas is about 2750 m/s. (not scaled)

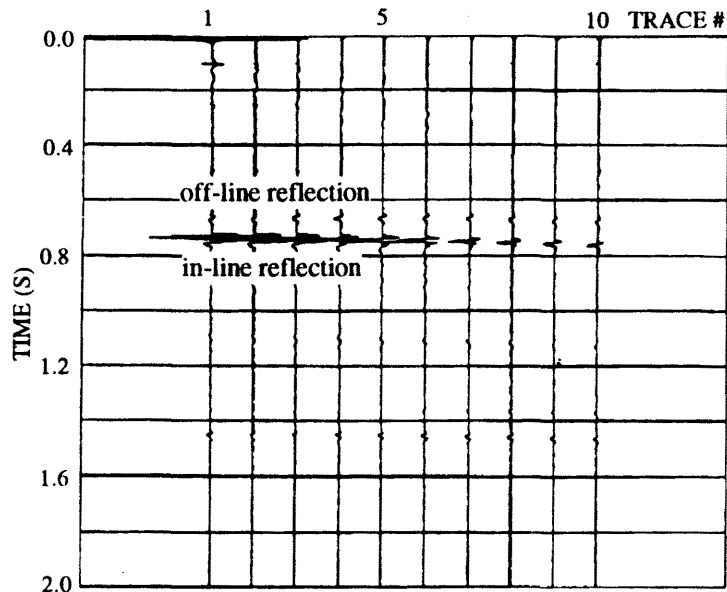


FIGURE 5.10. A vertical component shot record of the physical modeling data. There are some coherence in the record. The strongest one is at time of 0.72 s for trace 1. It is the reflection from the flat bottom of the model. The signal at time of 0.62 s for trace 1 is the reflection from the top of the "reef".

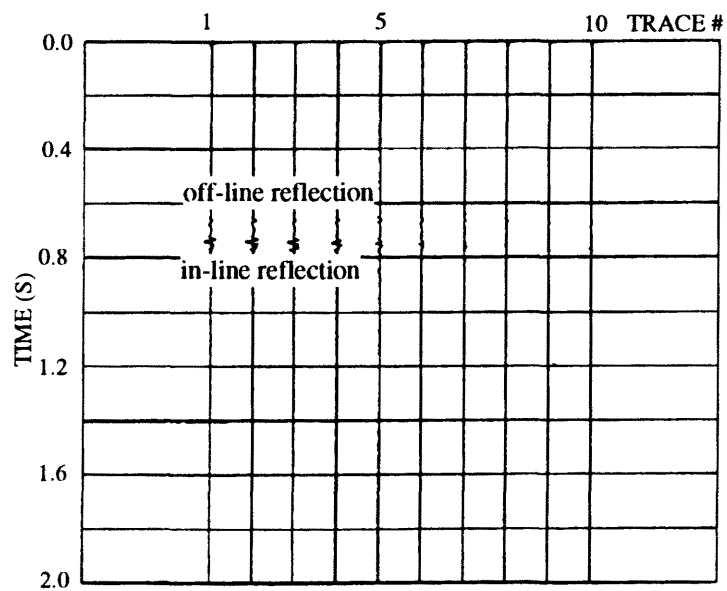


FIGURE 5.11. A transverse component shot record of the physical modeling data. We also can see the reflection from the flat bottom of the model and the top of the "reef".

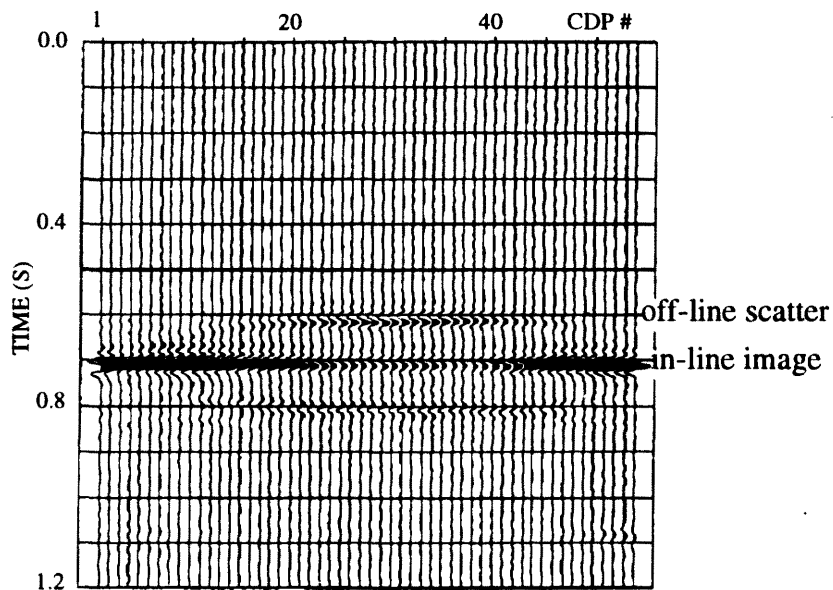


FIGURE 5.12. Conventional processed stacked section of the vertical component of the physical modeling data. We can see the images of the flat bottom of the model and the top of the "reef". The amplitude and phase change of the flat event. We will discuss it in the text.

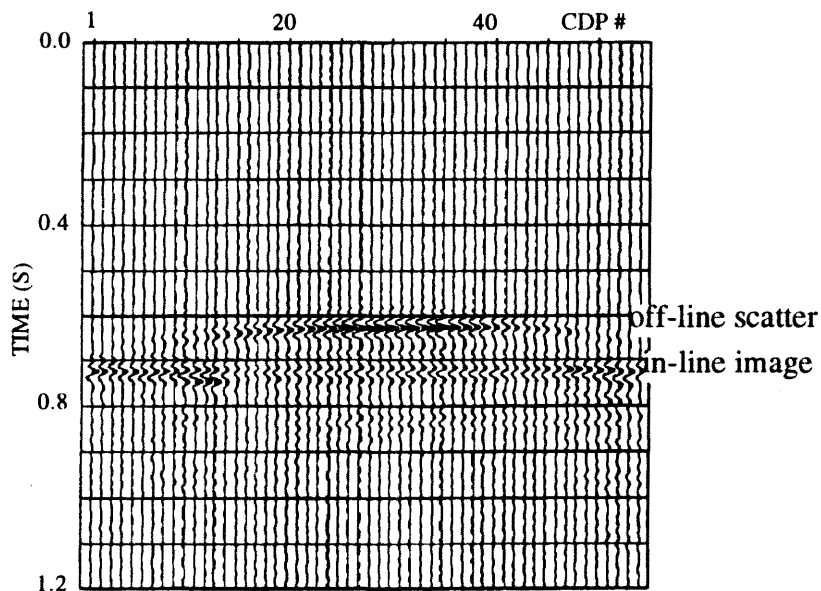


FIGURE 5.13. Conventional processed transverse component of the physical modeling data. We also can see same two events as the vertical component. However, the flat event is relatively weaker comparing with Figure 5.12

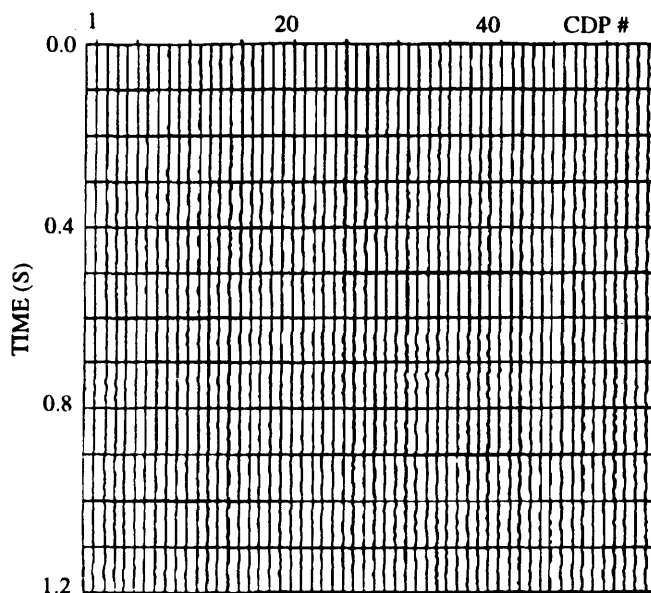


FIGURE 5.14. Polarization filtered section (direction window is 50° - 85°). There is no signal on the section.

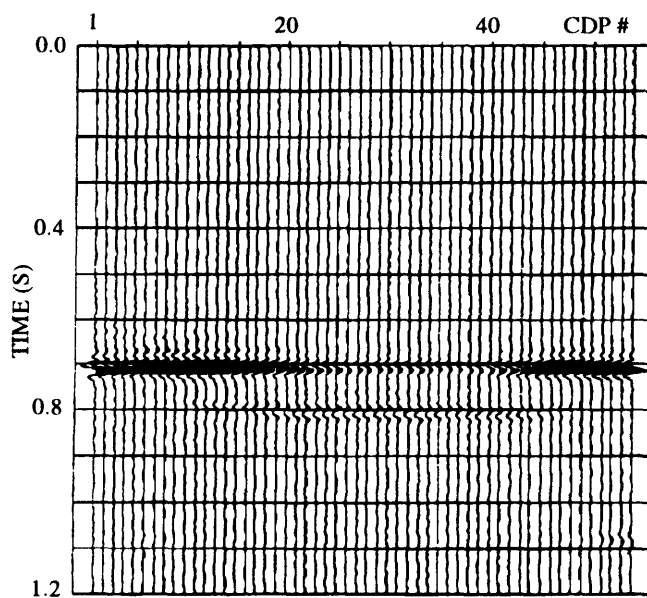


FIGURE 5.15. Polarization filtered section (direction window is 85° - 95°). The reflection from the top of the "reef" is removed.

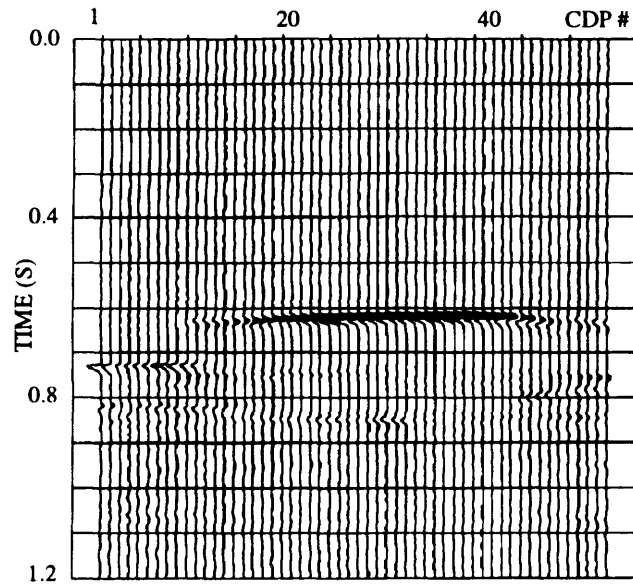


FIGURE 5.16. Polarization filtered section (direction window is 95° - 105°). We remove the flat reflection. There is only the reflection from the top of the "reef" and a little bit leaked energy of the flat layer on the section.

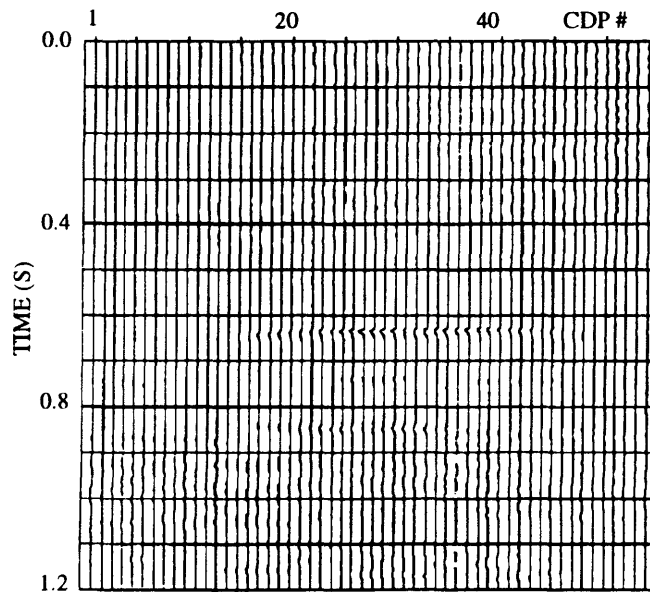


FIGURE 5.17. Polarization filtered section (direction window is 105° - 150°). There is less energy on the section.

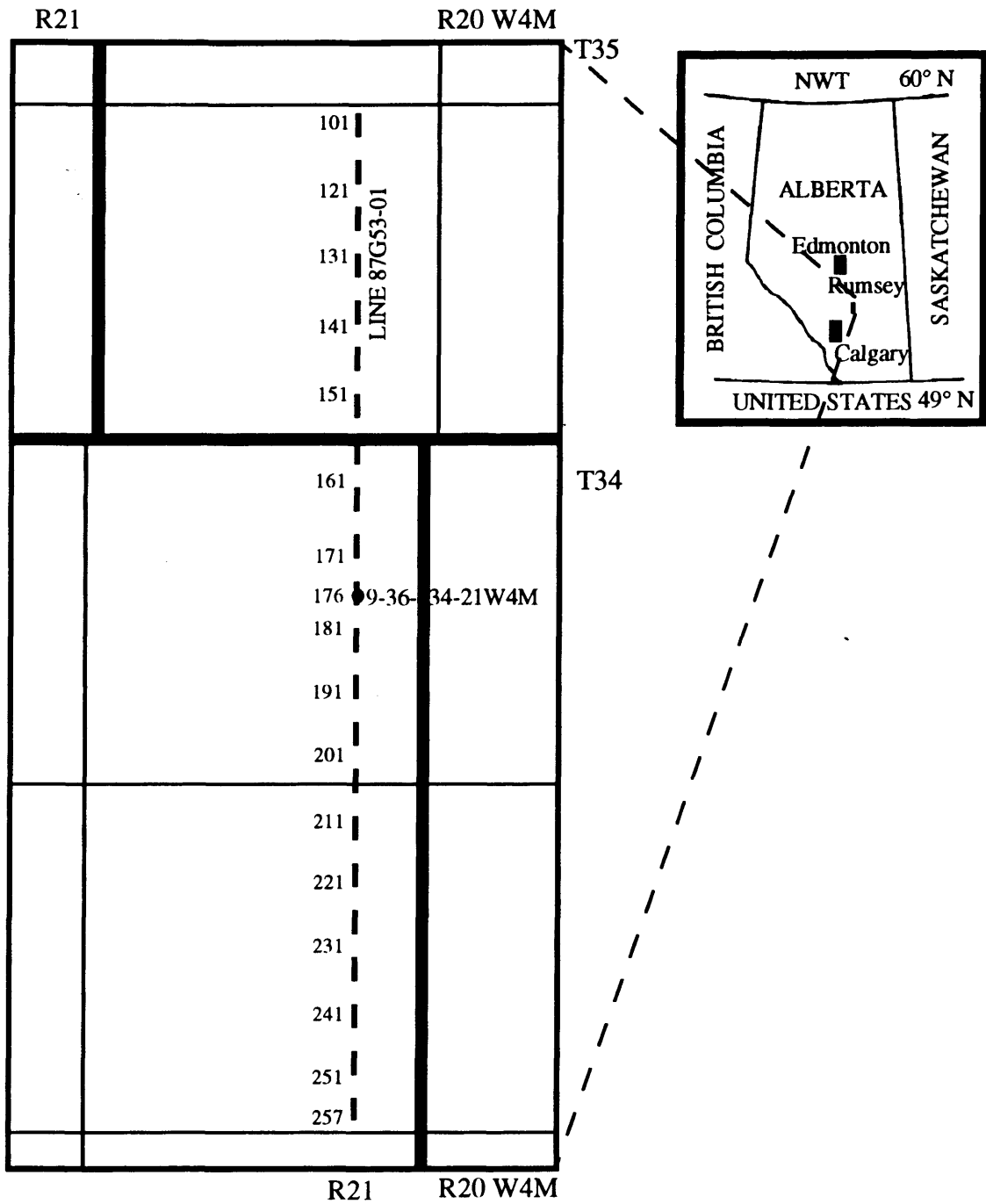


FIGURE 5.18 The study area and the approximate location of the seismic line and the well.

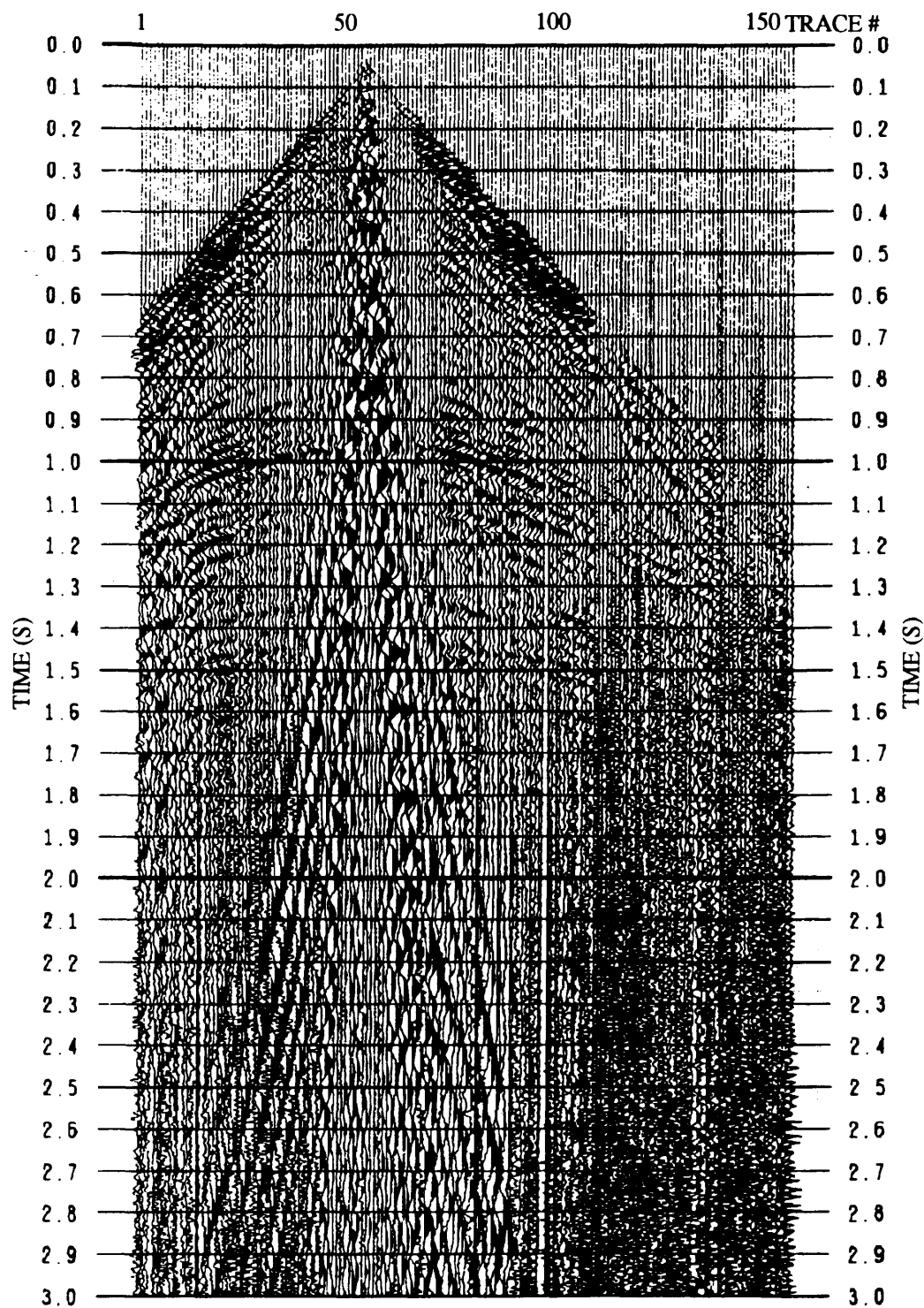


FIGURE 5.20 The vertical component of a shot record of the seismic line 87G53-01. It is the best shot of this line. There is ground roll at the near offsets and some high frequency noise.

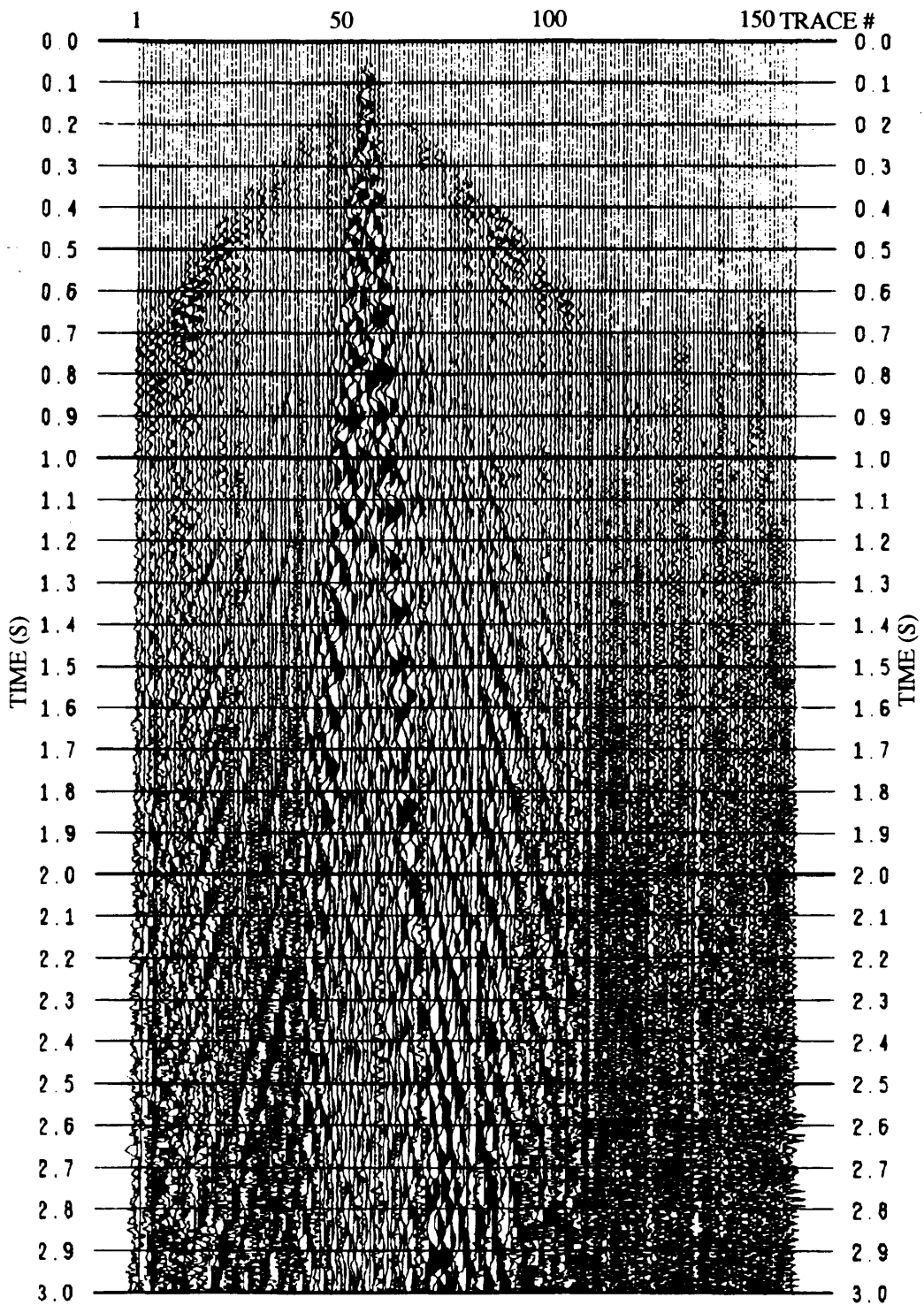


FIGURE 5.21 The transverse component of the same shot record as that in Figure 5.20.

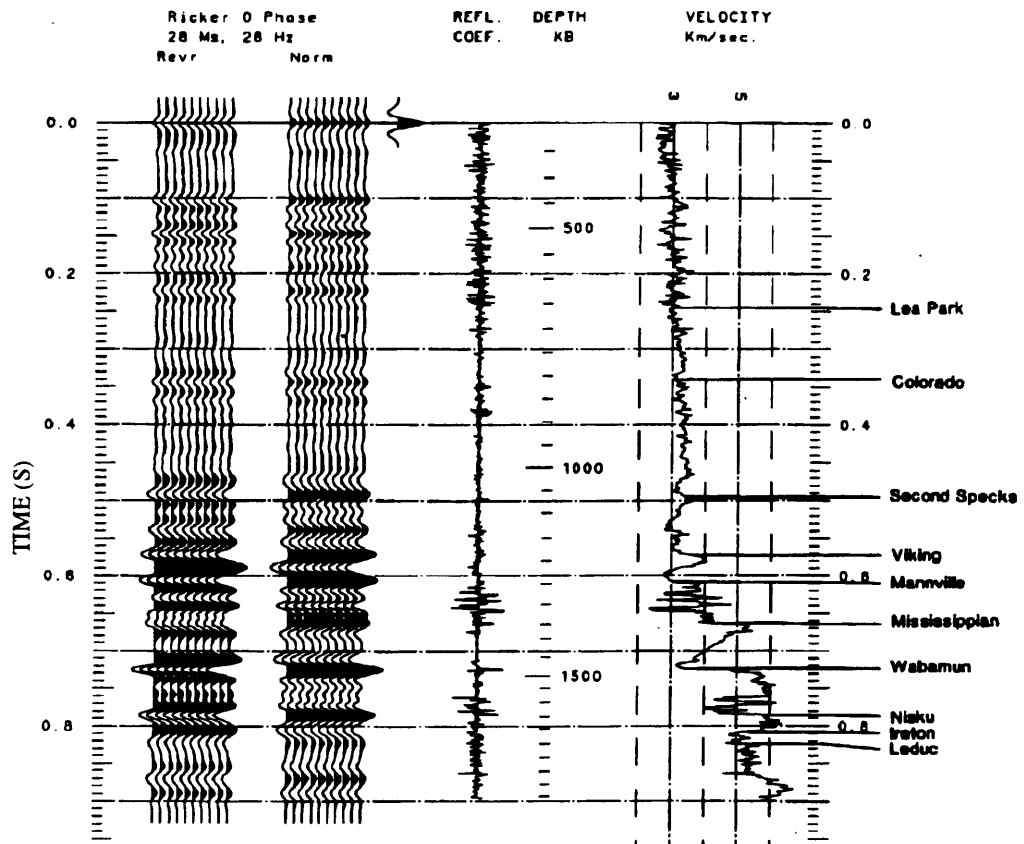


FIGURE 5.22 The synthetic seismogram and sonic log for the well 9-36-34-21W4M. (from Anderson et al., 1989)

9-36-034-21W4M

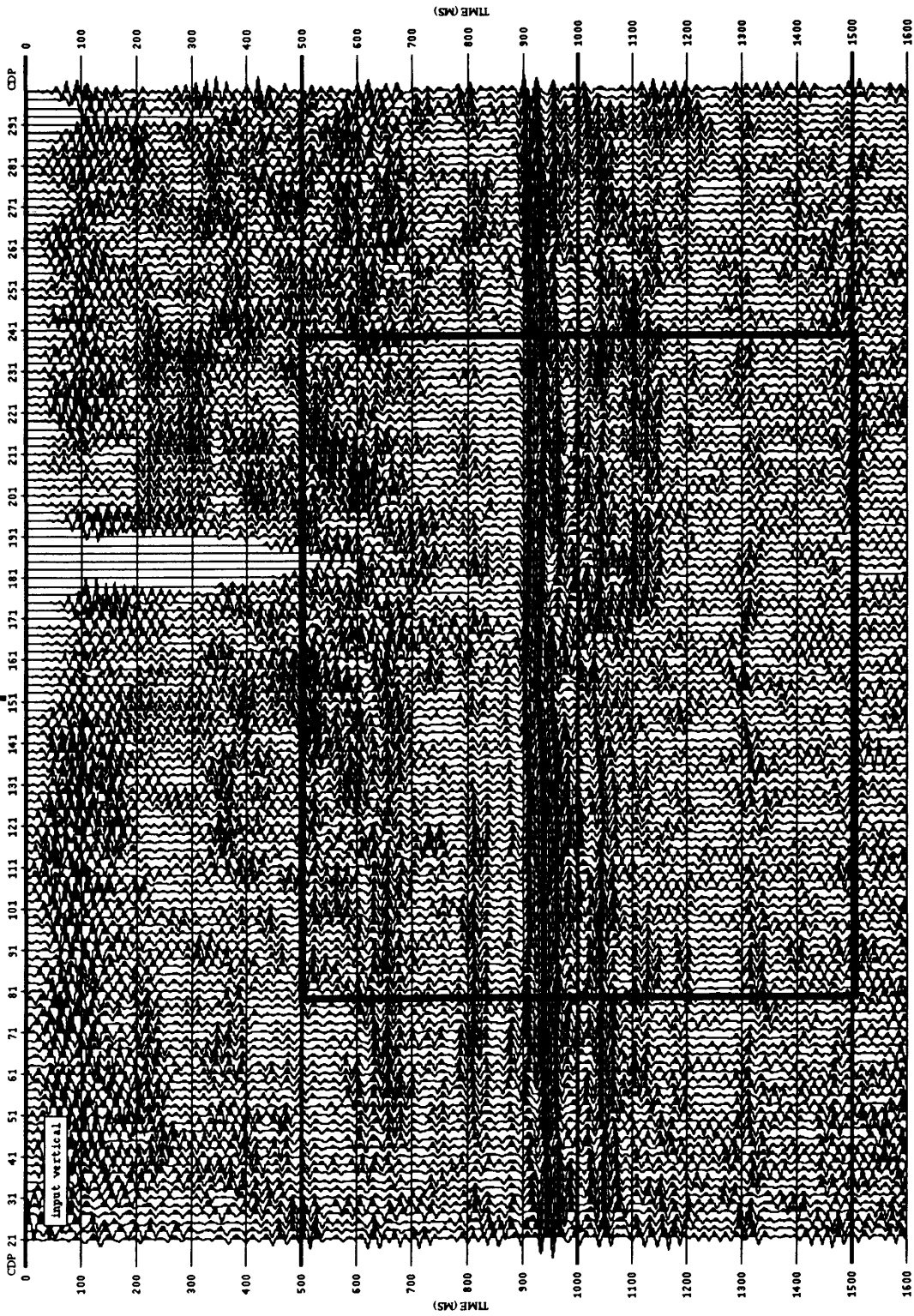


FIGURE 5.23 The stacked section of the vertical component data. (see Figure 5.25 for the boxed part)

9-36-034-21W4M

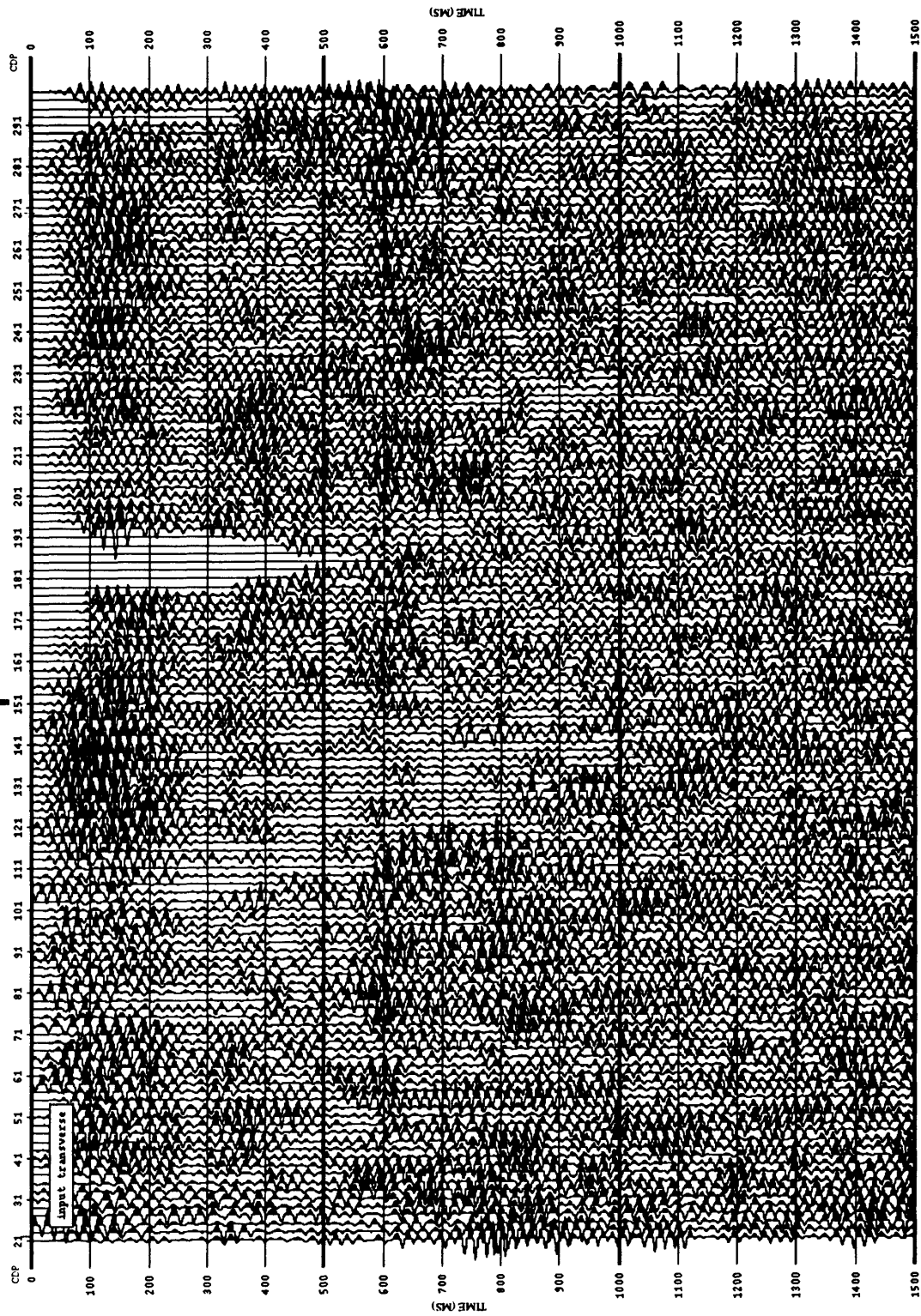


FIGURE 5.24 The stacked section of the transverse component data.

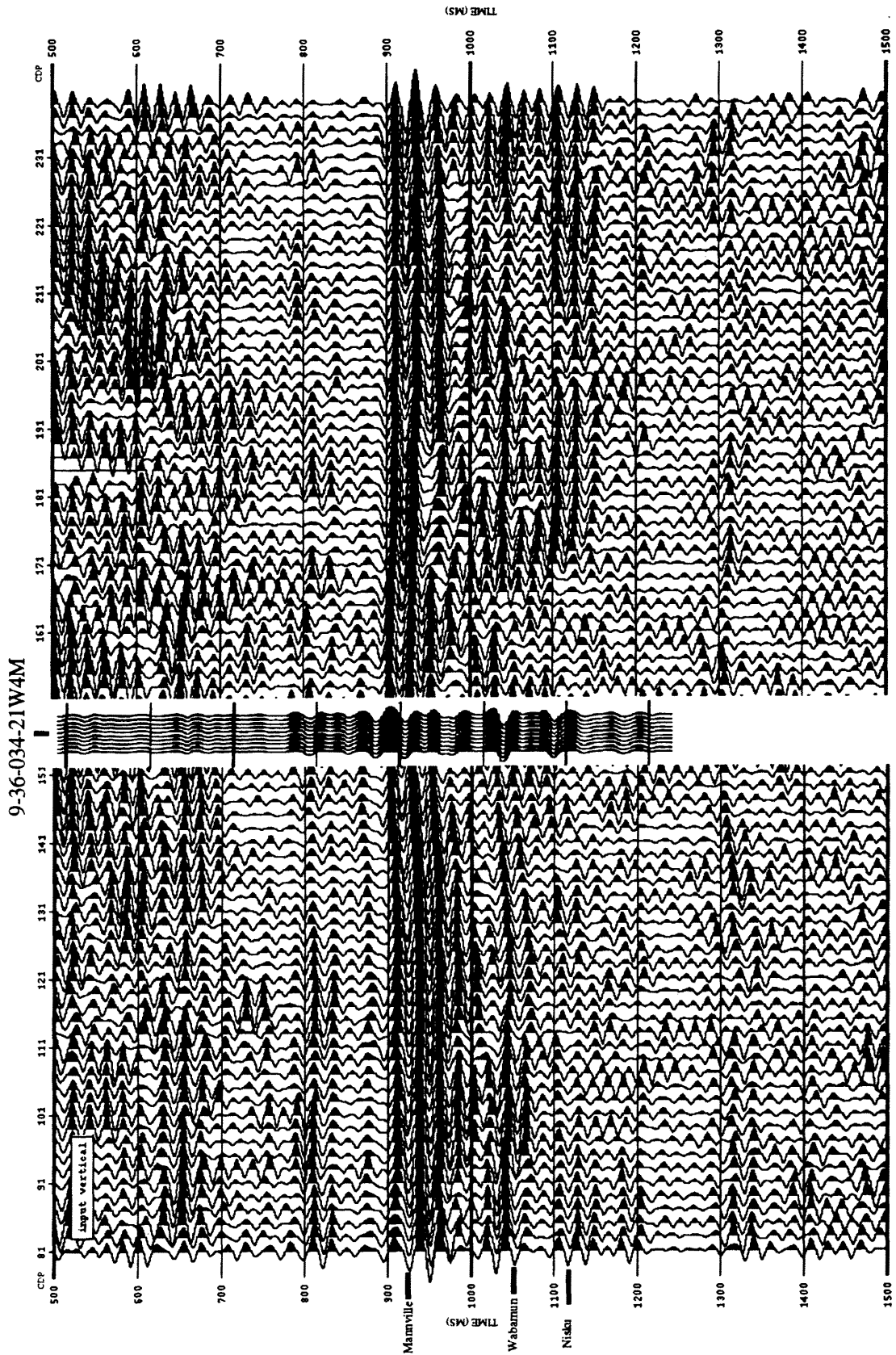


FIGURE 5.25 The enlarged stacked section of the vertical component with the synthetic seismogram (reverse polarity).

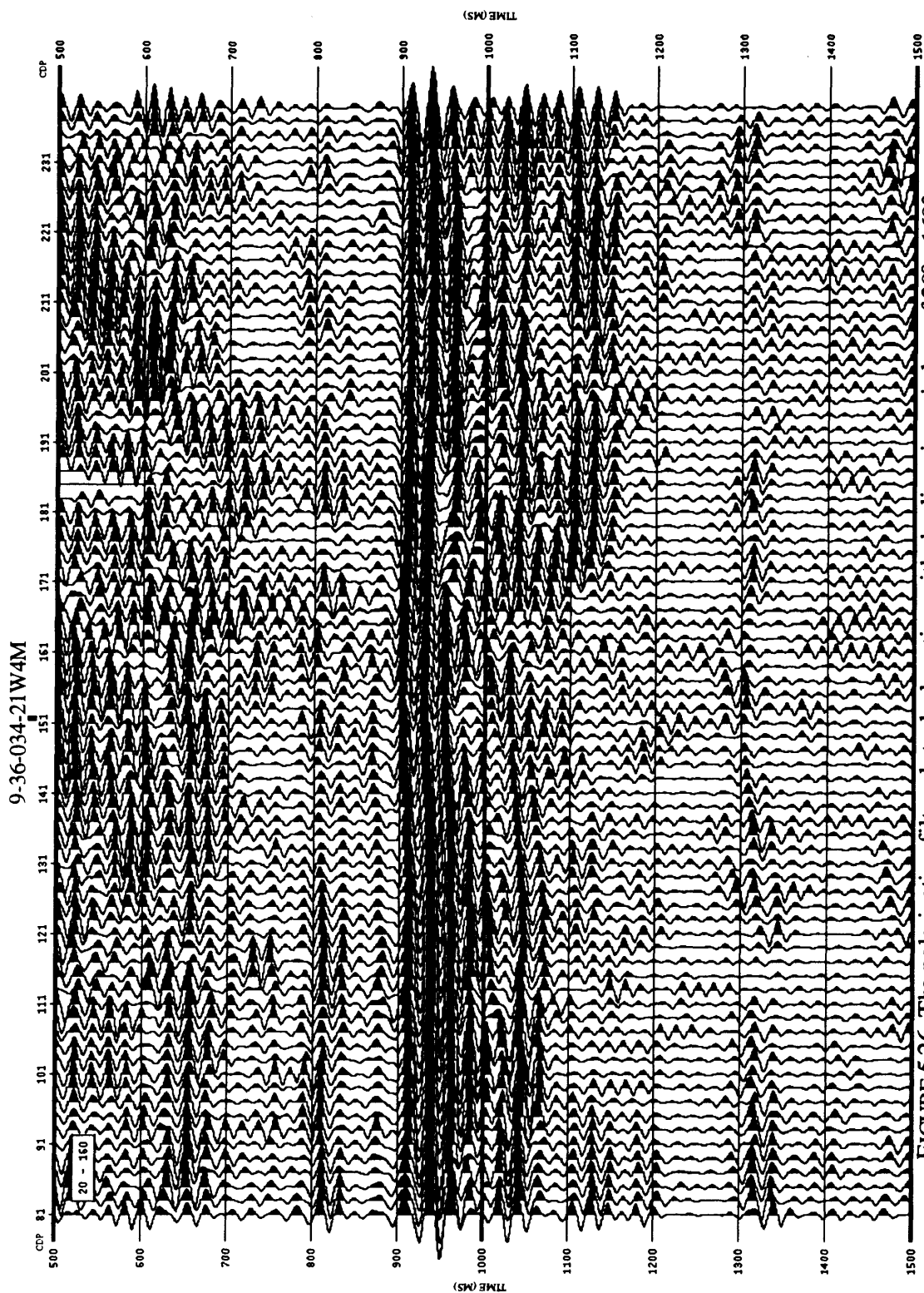


FIGURE 5.26 The polarization filtered stacked section with the direction window of 20° - 160°.

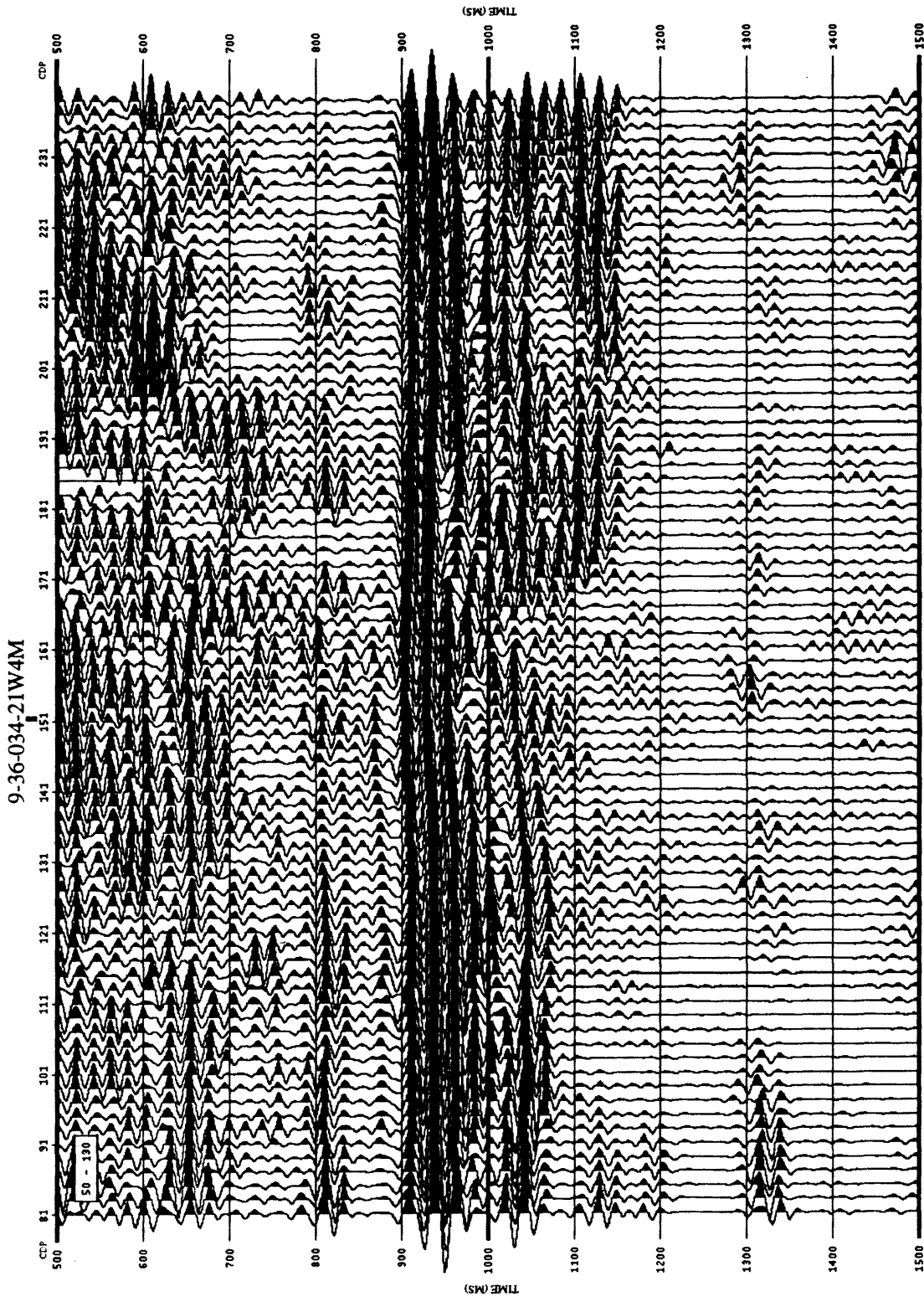


FIGURE 5.27 The polarization filtered stacked section with the direction window of 50° - 130°.

9-36-034-21W4M



FIGURE 5.28 The polarization filtered stacked section with the direction window of 80° - 100°

CHOICE I

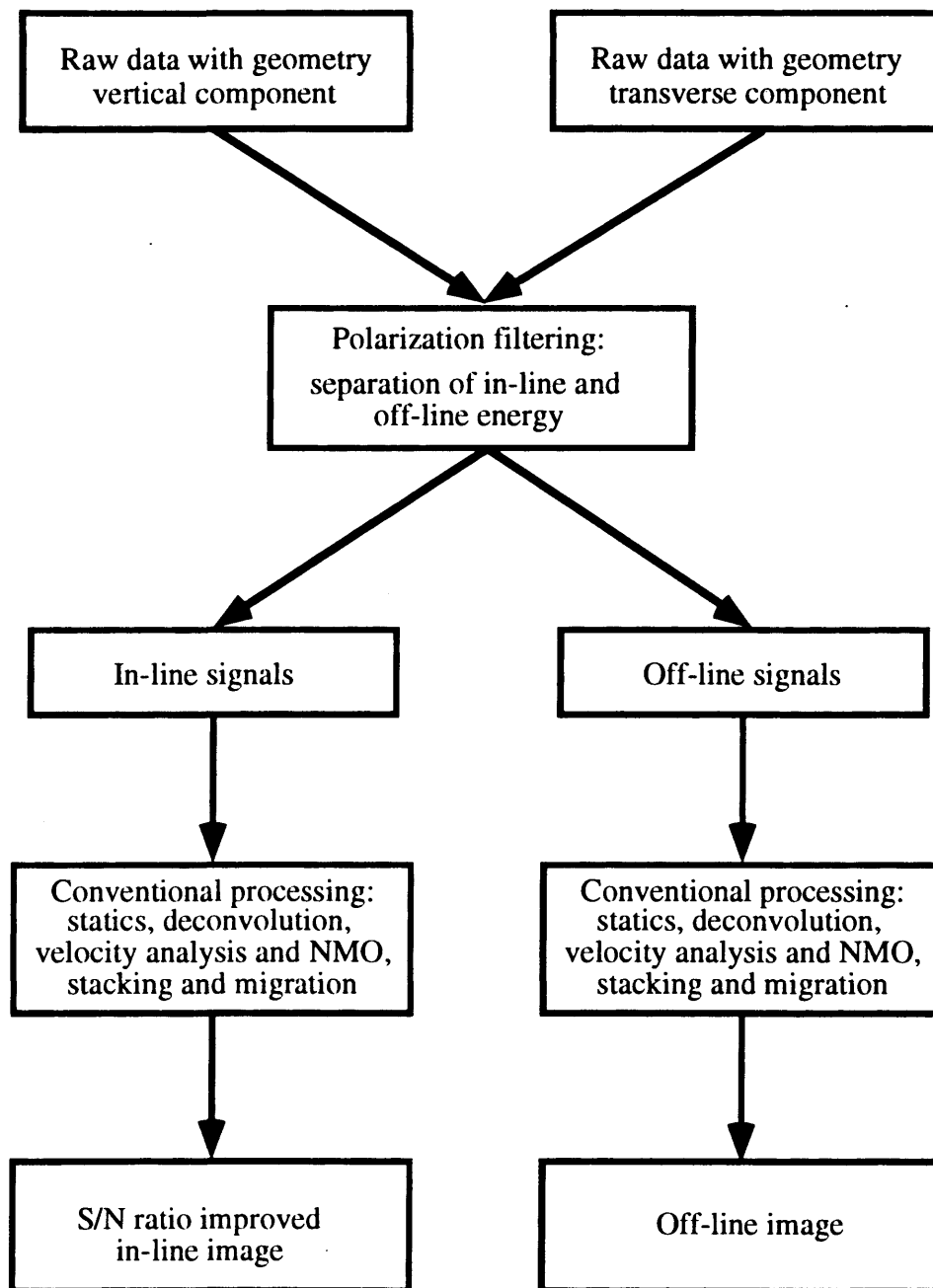


FIGURE 5.29 Flow chart: pre-stack polarization filtering.

CHOICE II

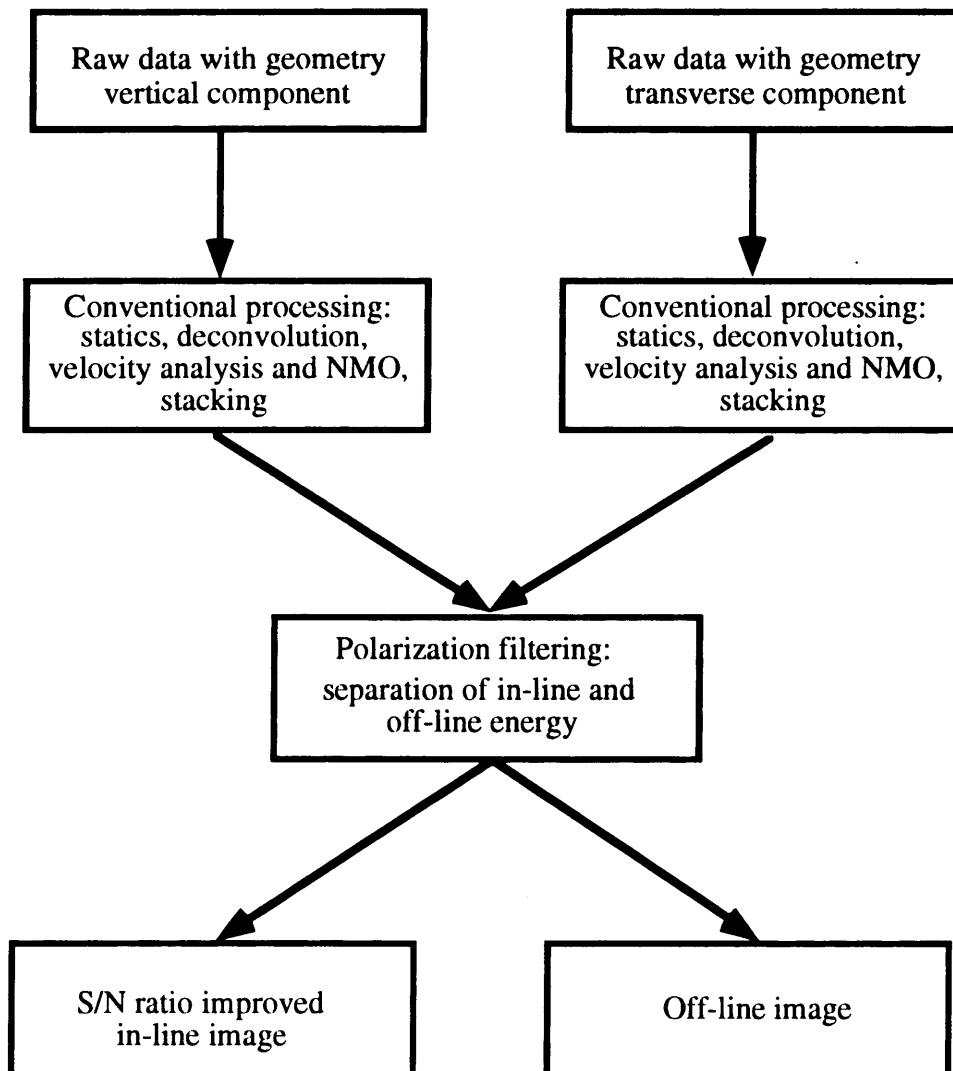


FIGURE 5.30 Flow chart: post-stack polarization filtering.

Chapter 6: Conclusions

The polarization direction of a P wave is generally in the propagation direction of the wave. Most previous polarization analysis relies on the eigenvalue method of analysing the covariance matrix of the observed data. This is an effective method. We use a direct least-squares method that is similar but faster than to directly solve for eigenvalues. This time-domain method finds the direction in which the sum of the projections of the particle motion of the seismic data is maximum.

Polarization filtering, as discussed in the previous chapters, can be used to detect and separate seismic waves from different directions. If we have three-component seismic data, we can use the polarization filter to: 1) reject the in-line energy and extract the off-line to build an off-line image; 2) reject the off-line energy to enhance the signal-to-noise (S/N) ratio of the conventionally processed sections. Although existing noise can effect the polarization direction, some S/N ratio enhancement techniques can be used to effectively suppress this effect. In this thesis, numerical modeling data, physical modeling data and field data were used to test the polarization filter and successful results are yielded.

In this thesis, the covariance method and the least-squares method of polarization analysis are discussed and applied to synthetic and real data on the shot record bases. The noise effect on the polarization direction is studied with analytic formulae and synthetic data. The noise has a significant effect on the polarization direction. Therefore, if seismic data have low S/N ratio, some S/N ratio enhancement techniques are necessary to be applied before the polarization filtering. CMP stacking is a typical method to improve S/N ratio in seismic data processing. This technique does not change the polarization direction of seismic waves, which is verified in Chapter 4. In Chapter 5, synthetic data and physical modeling data are used to separate in-line and off-line seismic energy and build off-line image using the polarization filter. The polarization filter is also applied to the real seismic data of Rumsey area to enhance in-line energy. But, because that line is just over a reef and there is little apparent off-line reflection.

Computer code for the polarization filter was developed to build an off-line image and improve the in-line image using 3-component seismic data. The main procedures for

making an off-line picture are: 1) apply conventional processing (statics, NMO, deconvolution, and stacking) to both vertical and transverse components, 2) apply the directional filter to the vertical and transverse stacked sections to separate in-line and off-line signals and create in-line and off-line sections, 3) migration can be applied to the off-line section and in-line proved section, if necessary. For rejecting off-line energy, we can use similar procedures. We tested this processing flow on numerical and physical modeling data. The physical model consists of a plexiglas plate with an embedded "reef". Ultrasonic transducers in vertical and horizontal directions surveyed the reef from an offset of 200 m scaled distance. A reasonable off-line image was reconstructed.

The polarization filter is also applied to the field data from the Rumsey area of central Alberta to reject the off-line energy to enhance S/N ratio of the conventionally processed section. The seismic line goes through the Rich D3A Oil Pool, which is a pinnacle reef in Leduc Fm located in the southern part of the east Ireton Shale basin, southwest of the Fenn-Big Valley reef complex and east of Bashaw reef complex. The major geological interfaces around the line are almost flat with a slight dip to west. There is no major structure beside the line. The polarization filter was applied to the stacked sections of vertical and transverse components with a direction window centered vertically downward. The output of the polarization filter has a better S/N ratio comparing with the original section of the vertical component. The coherent reflections remain in the filtered section and the noise is reduced.

The polarization filter can be used to enhance the seismic wave from a certain direction, if the data have a reasonable signal-to-noise ratio. If the data have low signal-to-noise ratio, some techniques like CMP stacking should be used to enhance signal before polarization filtering. We can use the polarization filter to build an off-line image and enhance the signal-to-noise ratio of the in-line image, if a three-component seismic dataset is available.

Chapter 7: Future work

The application of the polarization filter can be extended by applying it to data from structurally complex areas. We consider a case here from the Alberta Foothills. We can use it to enhance the seismic waves from certain direction, in-line or off-line, to get a better image of complicated structure. A shot record of 3-component seismic data acquired in the Foothills area is shown in Figures 7.1, 7.2 and 7.3. The polarization filter may help to build a clear image of steep structure and clear up in-line image by rejecting off-line noise.

In plains area, it is expected to get a better off-line image of reefs, if a seismic line in a suitable geological area is available. This means we can build a partial 3-D image along a 2-D line by using 3-component dataset and polarization filter.

Some quality control should be done in the acquisition phase. The amplitudes of vertical and horizontal component should be calibrated. The geophone orientation in field should be controlled properly, otherwise the direction of waves detected by the polarization filter will not be correct and this effect may be not recoverable.

In the processing phase, it is necessary to develop multi-station processing techniques to eliminate noise and to improve the effectiveness and accuracy of the filtering. If such pre-stack noise attenuation techniques can be created, then the polarization filter may be applied to effectively reduce ground roll.

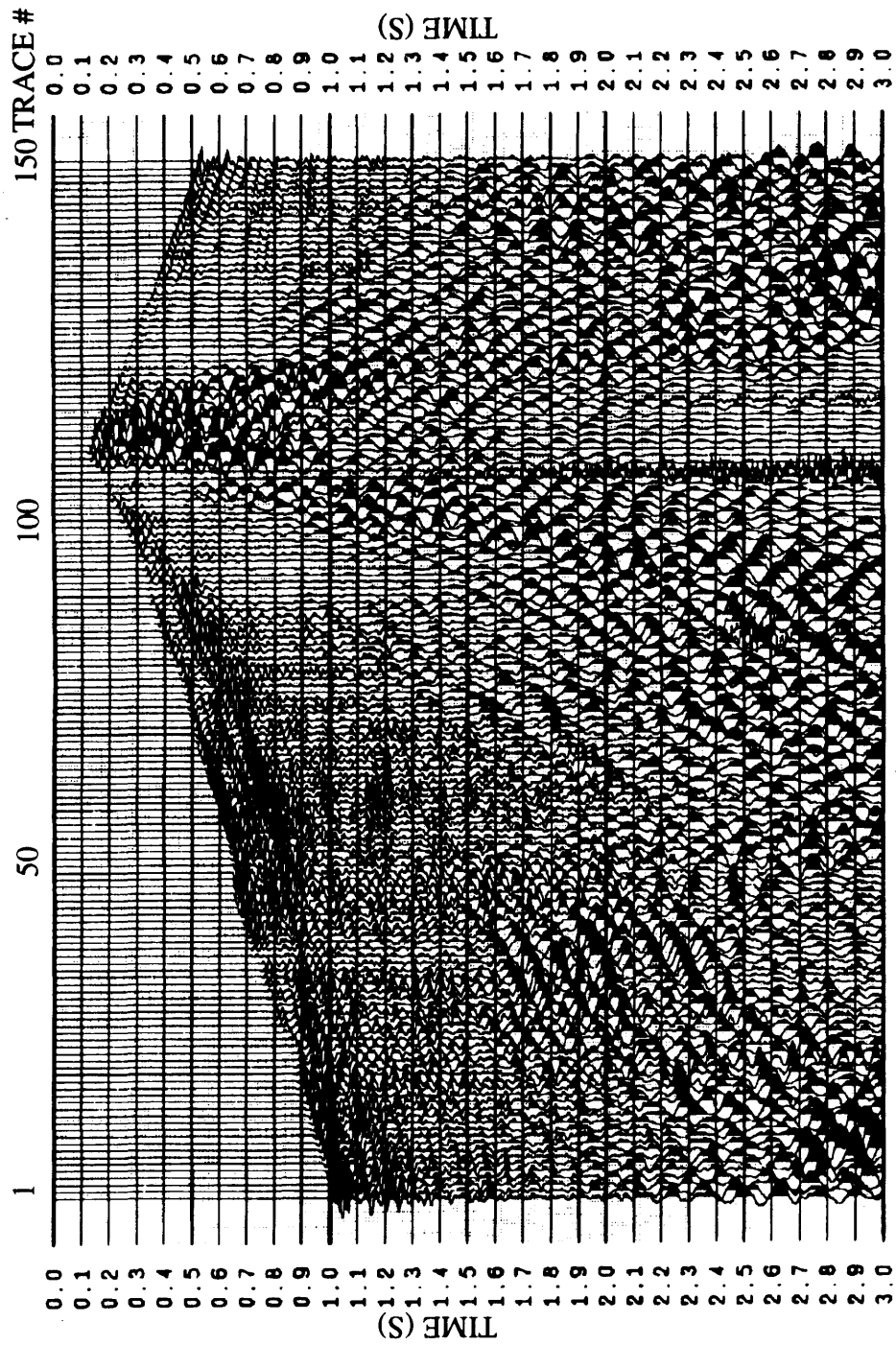


FIGURE 7.1 A shot record from the Alberta Foothills area (vertical component).

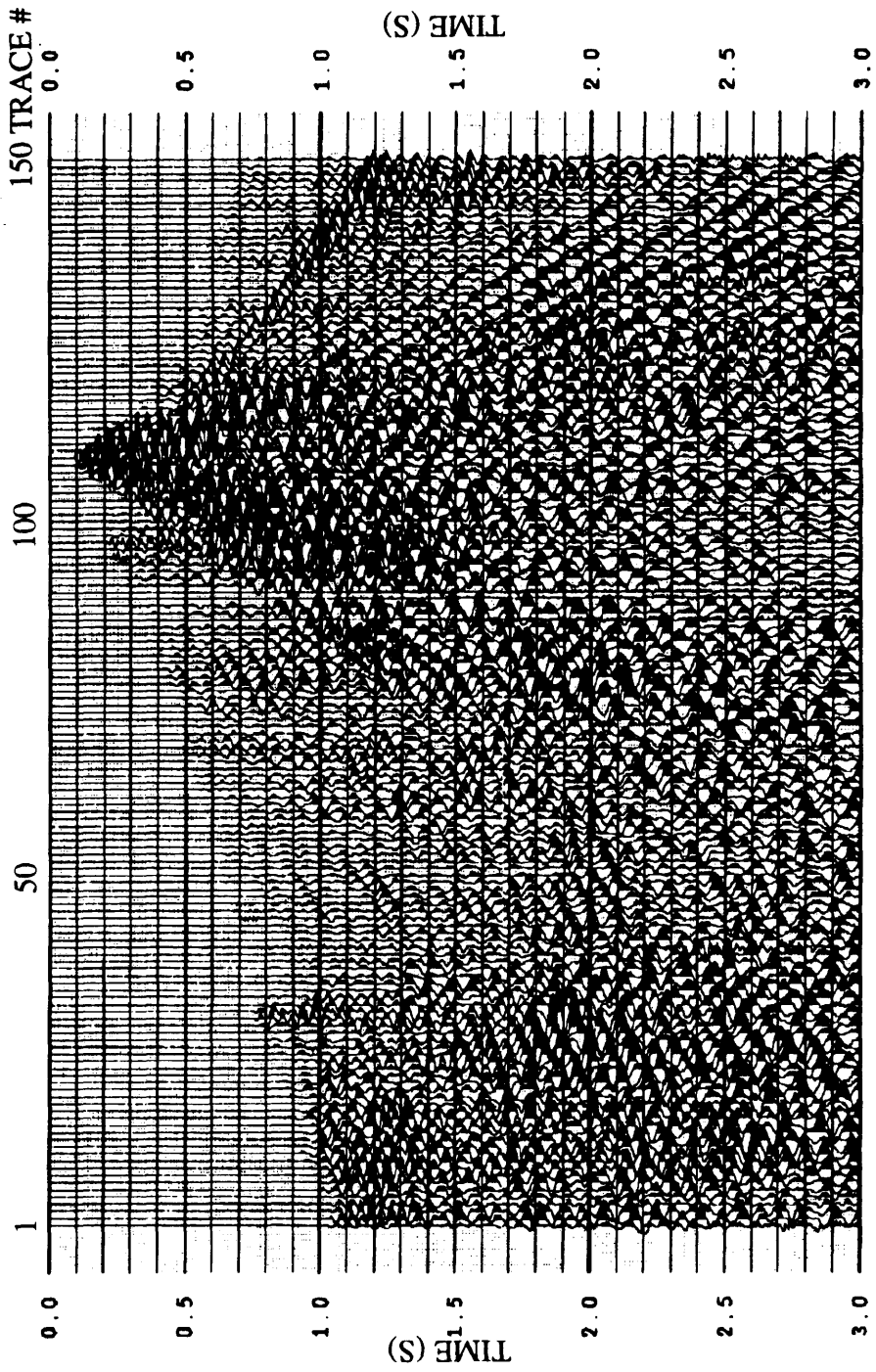


FIGURE 7.2 A shot record from the Alberta Foothills area (radial component)

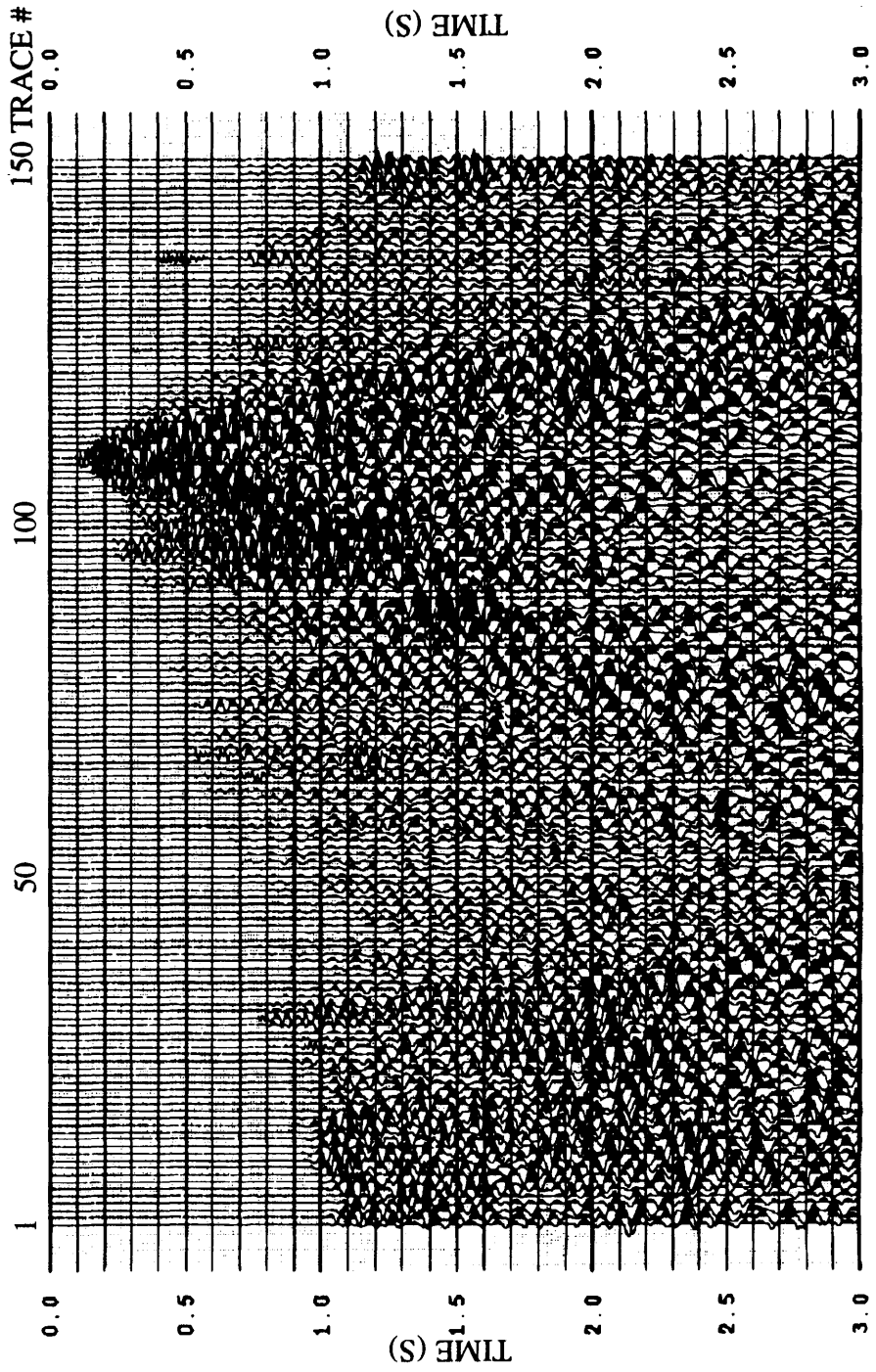


FIGURE 7.3 A shot record from the Alberta Foothills area (transverse component).

References

- Anderson, N.L., White, D. and Hinds, R., 1989, Woodbend group reservoirs: In Anderson, N.L., Hills, L.V. and Cederwall, D.A., Eds., *The CSEG/CSPG geophysical atlas of Western Canadian hydrocarbon pools*,: Can. Soc. Expl. Geophys./Can. Soc. Petrol. Geol.
- Bataille, K. and Chiu, J.M., 1991, Polarization analysis of high-frequency, three-component seismic data: *Bull. Seis. Soc. Am.*, **81**, 622 - 642.
- Cho, W.H. and T.W. Spencer, 1992, Estimation of polarization and slowness in mixed wavefields: *Geophysics*, **57**, 805 - 814.
- Davis, R.E., Foote, F.S., Anderson, J.M., and Mikhail, E.M., 1981, *Surveying - theory and practice*: McMray Hill.
- DiSiena, J.P., Gaiser, J.E., and Corrigan, D., 1984, Horizontal components and shear wave analysis of three-component VSP data: In Toksoz, M.N. and Stewart, R.R., Eds., *Vertical Seismic Profiling, Part B: Advanced Concepts*: Geophysical Press.
- Eaton, W.S., 1989, The free surface effect: implications for amplitude-versus-offset inversion: *Can. J. Expl. Geophys.*, **25**, 97 - 103.
- Ebrom, D.A., Tatham, R.H., Sekheren, K.K., McDonald, J.A. and Gardner, G.H.F., 1989, Nine-component data collection over a reflection dome: A physical modeling study: presented at the 59th Ann. Internat. Mtg., Soc. Expl. Geophys.
- Flinn, E.A., 1965, Signal analysis using rectilinearity and direction of particle motion: *Proc. I.E.E.E.*, **53**, 1874 - 1876.
- French, W.S., 1974, Two-dimensional and three-dimensional migration of model-experiment reflection profiles: *Geophysics*, **39**, 265 - 277.
- Gal'perin, E.I., 1984, *The polarization method of seismic exploration*, D. Reidel Publishing Company.
- Hospers, J., 1985, Sideswipe reflections and other external and internal reflections from salt plugs in the Norwegian-Danish basin: *Geophys. Prosp.*, **33**, 52 - 71.
- Jurkevics, A., 1988, Polarization analysis of three-component array data: *Bull. Seis. Soc. Am.*, **78**, 1725 - 1743.
- Kanasewich, E.R., 1981, *Time sequence analysis in geophysics*: The University of Alberta Press.

- Lucas, E., 1989, Polarisation analysis of seismic data: M.Sc. Thesis, Flinders University of South Australia.
- Mayne, W.H., 1962, Common reflection point horizontal data stacking techniques: *Geophysica*, **27**, 927 - 938.
- Montalbetti, J.F., and Kanasewich, E.R., 1970, Enhancement of teleseismic body phases with a polarization filter: *Geophys. J.R. Astro. Soc.*, **21**, 119 - 129.
- Perelberg, A.I. and Hornbostel, S.C., 1994, Applications of seismic polarization analysis: *Geophysics*, **59**, 119 - 130.
- Samson, J.C., and Olson, J.V., 1980, Some comments on the descriptions of the polarization states of waves: *Geophys. J.R. Astro. Soc.*, **61**, 115 - 129.
- Samson, J.C., and Olson, J.V., 1981, Data-adaptive polarization filters for multichannel geophysical data: *Geophysics*, **46**, 1423 - 1431.
- Sheriff, R.E., 1984, Encyclopedic dictionary of exploration geophysics: *Soc. Expl. Geophys.*
- Stewart, R.R. and Marchisio, G., 1991, Side-scanning seismic: Analysis and a physical modeling study: Presented at the 1991 Ann. Nat. Mtg., *Can. Soc. Expl. Geophys.*,
- Yilmaz, O., 1987, Seismic data processing: *Soc. Expl. Geophys.*
- Zheng, Y. and Stewart, R.R., 1993, Polarization filtering of three-component seismic data: Presented at the 1993 Ann. Nat. Mtg., *Can. Soc. Expl. Geophys.*, Calgary, Canada.
- and --, 1994, Off-line imaging using 3-component seismic data: Presented at the 64th Ann. Internat. Mtg., *Soc. Expl. Geophys.*